University of Alberta

Towards a unified cellular role for the Axenfeld-Rieger malformation genes PITX2 and FOXC1

by

Matthew Alexander Lines ©

A thesis submitted to the Faculty of Graduate Studies and Research in
partial fulfillment of the

requirements for the degree of Master of Science

Medical Sciences - Medical Genetics

Edmonton, Alberta
Fall 2004

Library and
Archives Canada

Published Heritage
Branch

395 Wellington Street
Ottawa ON K1A 0N4
Canada

Bibliothèque et
Archives Canada

Direction du
Patrimoine de l'édition

395, rue Wellington
Ottawa ON K1A 0N4
Canada

Your file Votre référence
ISBN: 0-612-95800-0
Our file Notre référence
ISBN: 0-612-95800-0

The author has granted a non-exclusive license allowing the Library and Archives Canada to reproduce, loan, distribute or sell copies of this thesis in microform, paper or electronic formats.

The author retains ownership of the copyright in this thesis. Neither the thesis nor substantial extracts from it may be printed or otherwise reproduced without the author's permission.

L'auteur a accordé une licence non exclusive permettant à la Bibliothèque et Archives Canada de reproduire, prêter, distribuer ou vendre des copies de cette thèse sous la forme de microfiche/film, de reproduction sur papier ou sur format électronique.

L'auteur conserve la propriété du droit d'auteur qui protège cette thèse. Ni la thèse ni des extraits substantiels de celle-ci ne doivent être imprimés ou aturement reproduits sans son autorisation.

In compliance with the Canadian Privacy Act some supporting forms may have been removed from this thesis.

While these forms may be included in the document page count, their removal does not represent any loss of content from the thesis.

Conformément à la loi canadienne sur la protection de la vie privée, quelques formulaires secondaires ont été enlevés de cette thèse.

Bien que ces formulaires aient inclus dans la pagination, il n'y aura aucun contenu manquant.

Canadä

Acknowledgements

I would firstly like to thank my graduate committee and supervisor for guidance in this project, both past and present. Research is a team effort, and I would also like to acknowledge many other individuals who contributed to this work directly. Kathy Kozlowski provided a number of wild-type and mutant *PITX2* expression constructs used in chapter two. Patient *PITX2* sequencing in the cohort studied in chapter one was partly performed by Kathy Kozlowski and Steven Kulak, and partly in the laboratory of Dr. Elise Héon at U. Toronto. Most instrumental to this work was Dr. Fred Berry, who has been a gracious and perpetual source of help for the last three years. Thanks to Vincent Biron and Dr. Alan Underhill for sharing their expertise in microscopy. Special thanks to Farideh, who keeps track of all our orders and somehow keeps the chaos in the lab at an optimum. Lastly, it has been a pleasure to work alongside all of the members of the ocular genetics lab, both past and present, during the past three years. I wish everyone the absolute best.

My fondest thanks are reserved for those who lend me their support, and occasionally their food -- my parents and Rosie, as well as the Kowand and Nguyen families. I honestly couldn't get by without you. To Angela: You're a kind person who has always been there for me, and I'm glad you keep me around. You'll be in the grad school kettle soon enough ('mwah ha ha').

So yeah, thanks once again to all of you - you all do more than you know. Ciao.

Table of Contents

Subject **Page**

Chapter one: General Introduction **1**
- Glaucoma 2
- Axenfeld-Reiger malformations 5
- Embryology of AR malformation 9
- Genetics of AR - Pituitary Homeobox 2 (*PITX2*) 12
  - Mouse model and expression profile of *PITX2* 13
  - Domain structure of PITX2a 17
  - PITX2a self-interaction 27
  - Recruitment of coactivators by PITX2 28
- Forkhead box transcription factor C1 (*FOXC1*) 29
  - FOXC1 mouse model and expression 30
  - Domain structure of FOXC1 31
- Criteria for a joint model for PITX2 and FOXC1 in AR 32

Chapter two: Characterisation and prevalence of *PITX2* microdeletions in the aetiology of AR malformations **33**
- Introduction 34
  - Genetic aetiology of *PITX2* mutations and deletions in AR 34
  - Rates of PITX2 and FOXC1 involvement in AR 34
  - Methods 37
    - Human subjects 37
    - Real-time quantitative PCR (qPCR) 37
    - Microsatellite markers 38
  - Results 40
    - Real-time qPCR and microsatellite studies of PITX2 dosage 40
  - Discussion 49
    - Phenotype of *PITX2* mutations versus deletions 49
    - Estimates of prevalence 50

Chapter three: Physical interaction, colocalisation, and subnuclear distribution of PITX2 and FOXC1 **51**
- Introduction 52
  - Possible importance of the PITX2 HD in protein interactions 52
  - Studied patient alleles of PITX2 53
- Methods 56
  - Expression constructs 56
  - Cell culture and transfection 57
  - Lysate preparation 57
  - Immunoprecipitation (IP) 58
  - Immunoblot analysis 58

Immunofluorescence 59
Microscopy and cell imaging 60
Results 61
Dimerisation properties of wild-type and mutant PITX2a 61
PITX2a physically interacts with FOXC1 64
Subnuclear localization of PITX2 and FOXC1 70
Immunofluorescence of PITX2a versus nuclear landmarks 80
Discussion 86
PITX2-PITX2 interactions 86
FOXC1-PITX2a interactions 87

Chapter four: General Discussion and Conclusions **91**
Extracellular signals involved in mesenchymal immigration 92
Outstanding questions regarding dosage sensitivity and protein interactions 98
Future Prospects 99

Bibliography **101**

Appendices

A: Composition of reagents used 115
B: Peptide sequence expressed by pCI-HA-PITX2a 116
C: Antibody information and suppliers 117
D: Explanation of 65kDa PITX2a immunoblot species 118
E: Expression of *FOXC1* in human TM cell line total RNA 119

List of figures

Figure **Page**

Chapter 1

1-1: Eye anatomy and aqueous circulation 3
1-2: Axenfeld-Rieger malformations 6
1-3: Periocular mesenchyme and anterior segment development 10
1-4: Genomic structure of human *PITX2* 14
1-5: Coexpression of PITX2 and FOXC1 in the developing mouse eye 18
1-6: Conserved domains in PITX2 and comparison with other homeoproteins 21
1-7: Comparison of the human PITX2 and *Drosophila* Q50 Paired HDs 25

Chapter 2

2-1: Real-time qPCR analysis of *PITX2* dosage 41
2-2: Microsatellite hemizygosity mapping of *PITX2*-containing deletions 44
2-3: Haplotype analysis illustrating cosegregation of del(PITX2) and AR in the kindred of patient 6 46

Chapter 3

3-1: Reciprocal immunoprecipitation (IP) of wild-type and mutant PITX2a 62
3-2: Physical interaction of PITX2 and FOXC1 66
3-3: Transactivation and PITX2-binding domains of FOXC1 overlap 68
3-4: Immunoprecipitation of wildtype and mutant PITX2a by FOXC1 71
3-5: Colocalisation of FOXC1 and PITX2 within a subdomain of the cell nucleus 73
3-6: Mutant PITX2a does not affect the subnuclear localisation of wild-type PITX2a or FOXC1 76
3-7: Detailed analysis of PITX2a-PITX2a-FOXC1 triple localisation 78
3-8: Subnuclear localisation of PITX2a versus HP1 α and trimethyllysyl-20 histone H4 [(Me)$_3$K20H4] 81
3-9: Subnuclear localisation of PITX2 versus SC35 and p300 84

Chapter 4

4-1: Possible circuit for integration of soluble and mechanical signals by a PITX2-FOXC1 complex 96

List of tables

Table		Page
2-1:	Novel microsatellite markers near *PITX2*	39
3-1:	Patient alleles of PITX2a studied	54

List of symbols and abbreviations

Δ	null allele (deletion)
ΔF	change in fluorescence emission
AD	transactivation domain
AD1	N-terminal activation domain of FOXC1; residues 1-50
AD2	C-terminal activation domain of FOXC1; residues 436-553
Al	Aristaless
Alx3	Aristaless-like homeoprotein
Antp	Antennapaedia
AR	Axenfeld-Rieger malformations
ASD	anterior segment dysgenesis
Bcd	Bicoid
BLAST	basic local alignment search tool
BLASTp	peptide BLAST search
BMP4	bone morphogenetic protein 4
bp	base-pairs
BSA	bovine serum albumin
C39	39 C-terminal residues of PITX2
Cart1	cartilage Paired-class homeoprotein 1
CBP	(cAMP-response element binding protein)-binding protein
cDNA	complementary (reverse transcription-derived) DNA
C/EBPα	CCAAT/enhancer-binding protein α
Ch	congenital hyrocephalus
ChIP	chromatin immunoprecipitation
CLIM-1	coactivator of LIM proteins 1
C_T	threshold cycle (qPCR amplification)
CycD1, CycD2	cyclins D1 and D2
Cx40	connexin 40
DLX2	Distal-less homeobox 2
DMEM	Dulbecco's modified Eagle's medium
DNA	deoxyribonucleic acid
E	embryonic day (example: E11 = 11 days post-coitum)
EGF	epidermal growth factor
EGF	epidermal growth factor receptor
eGFP	enhanced green fluorescent protein
EMSA	electrophoretic mobility shift assay
ENPEP	glutamyl aminopeptidase
ERK	extracellularly-regulated kinase
EST	expressed sequence tag
FGF8	fibroblast growth factor 8
FAM	6-carboxyfluorescein
FHD	Forkhead domain; residues 69-178 in FOXC1
FOXC1	Forkead box C1
FREAC3	Forkhead-related activator 3 (see FOXC1)
GAL4	galactose auxotrophy complementation group 4
GH	pituitary growth hormone
HA	influenza A haemagglutinin epitope
HD	homeodomain
HDAC1	histone deacetylase 1
HOXD3	homeobox D3

HP1α, HP1β	heterochromatin proteins 1α and 1β
HRP	horseradish peroxidase
HTM	human trabecular meshwork cell line
IGD	iridogoniodysgenesis
IH	iris hypoplasia
Ig	immunoglobulin
IgG	immunoglobulin γ
IOP	intraocular pressure
IP	immunoprecipitation
K50	homeodomain type defined by a lysine at position 50
kb	kilobase-pairs
LacZ	β-galactosidase
LCE	long-chain fatty-acyl elongase
MAP kinase	mitogen-activated protein kinase
Mb	megabase-pairs
$(Me)_3$K20H4	lysine 20-trimethylated histone H4
MGB	minor groove-binder
MIM	Mendelian Inheritance in [hu]Man
Mix-1	mesoderm-induced homeobox 1
mRNA	messenger ribonucleic acid
OAR	Otp, Aristaless, Rax C-terminal motif
Otp	orthopaedia
P2	TAATNNATTA (palindromic TAAT site, 2bp spacing)
P3	TAATNNNATTA (palindromic TAAT site, 3bp spacing)
PAGE	polyacrylamide gel electrophoresis
PAX6	Paired-box factor 6
PBP	PPAR-binding protein
PBS	phosphate-buffered saline
PBSA	PBS plus BSA (1% w/v)
PBS-PI	PBS plus protease inhibitors
PCR	polymerase chain reaction
pG	streptococcal protein G-agarose resin
PIT-1	pituitary homeoprotein 1
PITX1, PITX2, PITX3	pituitary homeobox genes 1, 2, and 3
PITX2BD	PITX2-binding domain
PLOD1, PLOD2	procollagen lysyl hyroxylases 1 and 2
PM	periocular mesenchyme
Prd	Paired
PRL	Prolactin
Prx2	Paired-like homeobox 2
Q50	homeodomain type defined by a glutamine at position 50
qPCR	real-time quantitative PCR
Rac1	Ras-related C3 botulinum toxin substrate 1
RhoA	Ras homologue A
RIPA	radioimmunoprotection assay buffer
RIPA-PI	RIPA plus protease inhibitors
ROCK	Rho-associated coiled-coil protein kinase
ROX	6-carboxy-X-rhodamine
RPM	rotations per minute (microfuge)
Rx	retina and anterior neural fold homeobox (Rax)
SC35	splicing factor, arginine/serine-rich, 30kDa

SDS	sodium dodecyl sulphate
SDS 2.0	sequence detection software (Applied Biosystems)
SHORT	syndrome; short stature, joint hyperextensibility, ocular depression, Rieger anomaly, and teething delay
T	threshold emission level
T_A	primer pair annealing temperature
TAMRA	6-carboxytetramethylrhodamine
TBS	Tris-buffered saline
TBST	TBS plus Tween (0.05%)
TGFα	transforming growth factor α
TGFβ	transforming growth factor β family
TGFβR1, TGFβR2	transforming growth factor β receptors 1 and 2
TIP60	HIV-1 TAT-interacting protein, 60kDa
TM	trabecular meshwork
TRAP	thyroid hormone receptor-associated protein
TRD	transcriptional regulatory domain of FOXC1; residues 215-366
VEGFR	vascular endothelial growth factor receptor
VIC	VIC-2 amidite
Wnt	Wingless-type ligand family

Chapter one:

General Introduction

This chapter contains arguments and text presented in:

Lines MA, Kozlowski K, Walter MA. 2002. Molecular genetics of Axenfeld-Rieger malformations (Review). *Human Molecular Genetics* 11(10): 1177-1184.

Glaucoma

Glaucoma is a leading cause of visual impairment, affecting an estimated 66 million persons, at least six to eight million of whom are bilaterally blind (1). Glaucoma is characterised by the gradual demise of retinal ganglia, causing progressive narrowing of the visual field and eventual blindness. Intraocular pressure (IOP) is the single most important risk factor for progression of glaucoma, as well as a good predictor of the rate of visual field loss in patients (2). Elevated IOP is thought to damage retinal ganglion cell axons via gradual excavation of the optic nerve head, which is the least resistive point in the ocular globe's tough outer sclera and cornea. While the large majority of glaucoma is attributable to increased IOP, a minority of patients are apparently normotensive, and it is unclear what differences in mechanism distinguish the similar optic neuropathies seen in both disorders (3).

Intraocular pressure homeostasis in humans is governed by the circulation of aqueous humour from its site of secretion at the ciliary body, past the lens and iris, and into the anterior chamber, from which it is drained via structures situated at the apex of the iridocorneal angle (figure 1-1) (4, 5). Aqueous is actively synthesised at the ciliary body, by a mechanism involving active transport of plasma Na^+, and is returned to the lymphatic system via Schlemm's canal, a circular vessel underlying the corneoscleral limbus. Before draining into Schlemm's canal, aqueous passes through a filtering matrix of endothelium-covered collagenous beams, referred to as the trabecular meshwork (TM). The aqueous humour is then transported across the endothelium of Schlemm's canal by pressure-dependent transport in giant vacuoles and is removed from the eye. Both the rate of aqueous extrusion and removal contribute to the maintenance of a normally small IOP of about +12-22mmHg relative to the outside atmosphere. Ocular hypertension, then, can result from increased secretion or decreased drainage of aqueous humour, and typical glaucoma therapy hinges on medical or surgical abatement of either effect.

The glaucomas, rather than a single disorder, are a family of related diseases that can be further subdivided according to various etiologic features. One common clinical distinction in glaucoma is between open- or closed-angle forms, based on the angular width of the anterior chamber as assessed with a goniolens. The width of the anterior chamber is determined by the convexity of the iris, the anterior-posterior placement of the iris root, and the degree to which the iris is pushed forwards by the

Figure 1-1: Eye anatomy and aqueous circulation

Bottom left: Schematic of gross anatomy of the eye, adapted from (7).
Top left: Meridional section of the human anterior segment, adapted from (8). The major flow of aqueous humour, from secretion at the ciliary body to drainage at the trabecular meshwork, is indicated with a dashed arrow. A small proportion of aqueous (about 0.2μL/min) does not pass into Schlemm's canal, but instead follows a distinct uveoscleral route which is not illustrated (9).
Top right: Schematic of the limbus and iridocorneal angle drainage pathway in meridional section, adapted from (8).
Bottom right: Immunohistochemical stain for enolase $\gamma\gamma$ (neuronal enolase) illustrating neural crest-derived structures in the adult human iridocorneal angle, adapted from (10). This panel shows a similar section to the one illustrated at top right. Neural crest derivation of aqueous drainage pathway structures is discussed on page 12.

Structures indicated:

AC: anterior chamber
C: cornea
CB: ciliary body
CE: corneal endothelium
Cj: conjunctiva
CS: corneal stroma
I: iris
IPE: iris pigmented epithelium
IS: iris stroma
L: lens
ON: optic nerve
ONH: optic nerve head
P: pupil
R: retina
RPE: retinal pigment epithelium
S: sclera
SC: Schlemm's canal
SL: Schwalbe's line
TM: trabecular meshwork

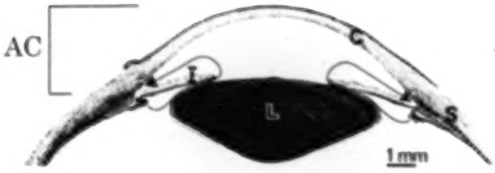
AC
C
I
L
S
1mm

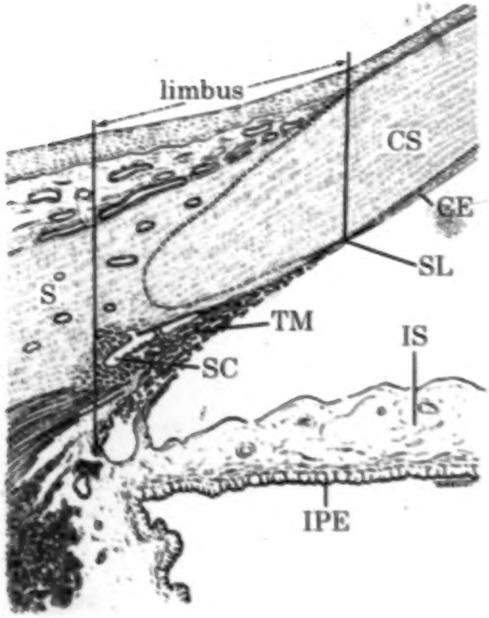
limbus
CS
CE
SL
S
TM
IS
SC
IPE

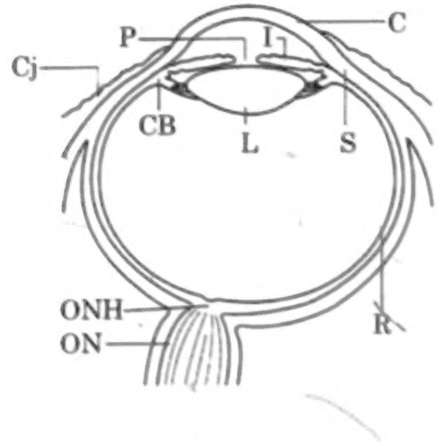
P
I
C
Cj
CB
L
S
ONH
ON
R

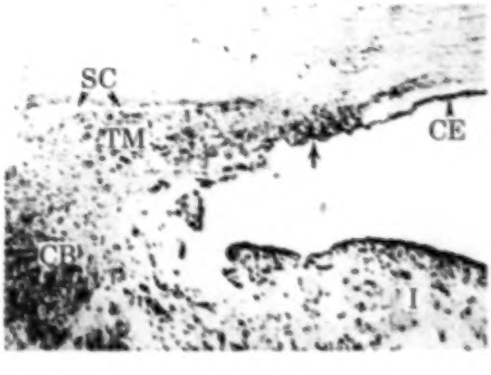
SC
TM
CE
CB
I

lens, all properties which vary in the general population (6). Depth of the anterior chamber, rather than a fixed measurement, varies in a given eye over time, and narrowing of the angle can result in 'angle-closure' glaucoma. Congenital forms of closed-angle glaucoma can result from occlusion of the TM by an abnormally high iris root insertion, or less commonly by extraneous tissue in the angle or dysgenesis of the TM and/or Schlemm's canal themselves. The Axenfeld-Rieger phenotype, discussed below, is one of several hereditary anterior segment dysgeneses associated with morphological abnormalities of the iridocorneal angle and closed-angle glaucoma.

Axenfeld-Rieger malformations

The heritability of various ocular dysgeneses in humans was a subject of interest since the inception of human genetics itself as a formal field of study. Darwin, for instance, reviewed some of the (limited) clinical literature on this subject in 1875:

> *Amaurosis, either congenital or coming on late in life, and causing total blindness, is often inherited; it has been observed in three successive generations. Congenital absence of the iris has likewise been transmitted for three generations, a cleft-iris for four generations, being limited in this latter case to the males of the family. Opacity of the cornea and congenital smallness of the eyes have been inherited. Portal records a curious case, in which a father and two sons were rendered blind, whenever the head was bent downwards, apparently owing to the crystalline lens, with its capsule, slipping through an unusually large pupil into the anterior chamber of the eye* (11).

The above account was roughly contemporary with key developments in early genetics, such as the discovery of nucleic acids by Friedrich Miescher in 1869, and the original publication of Gregor Mendel's work in 1866. Incidentally, this period also produced the first clinical descriptions of what we now term the Axenfeld-Rieger (AR) phenotype (depicted in figure I-2).

In 1883, The German pathologist Adolph Vossius (1855-1925) published a report of a patient with hypoplasia of the iris, full-thickness iris holes (polycoria) and several absent teeth (12). Later, in 1920, the ophthalmologist K Theodor Axenfeld (1867-1930) identified a patient with a *ringlinie*, or prominent white line in the peripheral cornea, to which anterior synechiae (strands of abnormal iris tissue) were adherent (13).

Figure 1-2: Axenfeld-Rieger malformations

Top panel: Externally visible features of Axenfeld-Rieger malformations as previously published in (14). Panels A through C were generously provided courtesy of Dr. Elise Héon.

A: Slate grey, hypoplastic iris revealing the underlying pupillary sphincter muscle. Note posterior embryotoxon (white line anterior of the scleral-corneal limbus, particularly visible at four o'clock). A surgical drainage bleb is visible at nine o'clock.

B: More severely hypoplastic, chocolate-coloured iris, nasally displaced, with large full-thickness tear in the opposite (temporal) side of the pupil.

C: Excessive periumbilical skin.

D: Small, malformed, and absent teeth

Bottom panel: Gonioscopic view of Axenfeld Anomaly as published in (15). Arrow indicates one of several large synechiae between the posterior embryotoxon and iris. Towards the right of this image, these adhesions become more broad and sheetlike, occluding a large portion of the trabecular meshwork.

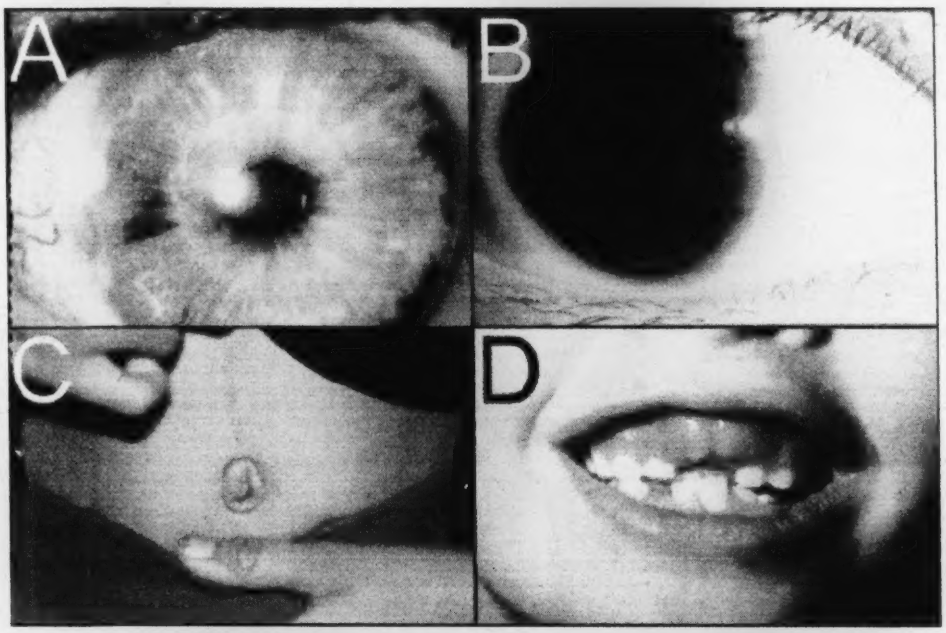
A
B
C
D

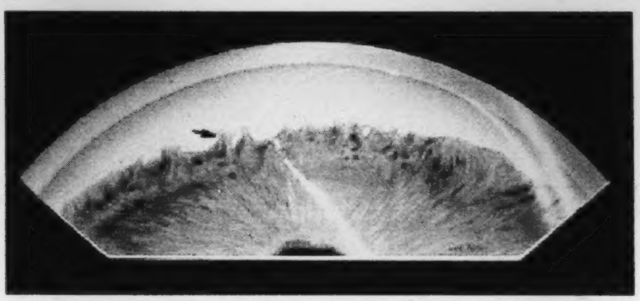

Axenfeld's anomaly was described as *embryotoxon cornea posterius*, a thickening and central displacement of Schwalbe's line, which is the rim of the corneal endothelium's basement membrane at its peripheral boundary. Another German ophthalmologist, Herwigh Rieger (1898-1986), produced a detailed report of anterior synechiae and marked iris defects in conjunction with elevated intraocular pressure and abnormal tissue in the iridocorneal angle in a mother and two children, constituting the first recognition of inheritance in this disorder (16). Rieger's anomaly, which represented a heritable developmental defect involving the iris stroma, corneal endothelium, and iridocorneal angle, was described as 'mesodermal dysgenesis of the cornea and iris'.

While Axenfeld anomaly and Rieger anomaly were long considered to be distinct clinical disorders, the similar iridocorneal angle dysgenesis observed in both disorders led ophthalmologists to the gradual recognition that both diseases were part of the same phenotypic continuum (17-19). These suspicions were confirmed by a detailed account of twenty-four patients in five families, in which the same pattern of posterior embyrotoxon, iris defects, and/or anterior synechiae was confirmed in patients variously diagnosed with Axenfeld or Rieger ocular anomalies (20). All patients examined had some degree of posterior embryotoxon, and more than half developed glaucoma. Occasionally observed systemic features of the disease included small, missing, or malformed teeth in six affecteds, redundant periumbilical skin in four patients, or pituitary abnormalities (empty sella or parasellar cyst) in two cases. It was suggested, based on clinical and histological evidence, that both Axenfeld and Rieger anomalies, with and without dental or umbilical findings be considered a single, clinically variable disorder, Axenfeld-Rieger (AR) syndrome. AR is also now known to coincide with a variety of other, variably expressive or comorbid traits, such as atrial and ventricular cardiac septal defects, outflow tract abnormalities, hydrocephalus, sensorineural deafness, short stature and pituitary insufficiency, as well as a characteristic facial appearance (21-25).

Arguably, the most deleterious manifestation of the Axenfeld-Rieger phenotype is secondary high-tension glaucoma, the incidence of which is estimated at approximately fifty percent in affected individuals (20, 26). Management of glaucoma in AR is similar to that of nonsyndromic forms the disease, and hinges on reduction of intraocular pressure to protect the optic nerve head from mechanical damage. The common occurence of glaucoma in AR is a key element of our laboratory's interest in this disorder, as rare Mendelian phenotypes such as AR may afford a window on the molecular pathways governing ocular development and IOP homeostasis.

Embryology of AR Malformation

The mature eye is a composite structure derived from four cell lineages representing the ectodermal and mesodermal germ layers of the embryo (figure 1-3). At about E11 in mouse (day 33 in humans), when the anterior chamber is beginning to develop, the eye is bounded by the optic cup, which is a two-layered neurectodermal bowl derived from an outgrowth of the telencephalon (8). Contained within the optic cup is a spherical lens vesicle newly formed by cavitation of the overlying surface ectoderm. The inner layer of the optic cup is fated to develop into the neuroretina, while the outer layer will differentiate into the retinal pigment epithelium. The optic cup retains a connecting stalk bridging it and the forebrain, which will eventually develop into the optic nerve. The rim of the optic cup at this stage demarcates the future position of the iris root and limbus, which have yet to develop.

Surrounding the optic cup and lens vesicle at E11 is a loosely packed mass of stellate, migratory, multipotent cells -- the periocular mesenchyme, which will give rise to many of the anterior segment structures shown in figure 1-1 (8, 27). This population, following chemoattractive signals secreted by the lens vesicle, insinuates itself between the lens vesicle and the overlying surface ectoderm in three successive waves of immigration. The first wave, beginning at E12 in mouse, or six weeks of human gestation, generates the presumptive corneal endothelium. Signals issued by the adjacent lens vesicle cause the presumptive corneal endothelium to flatten, polarise, and express cell-adhesion molecules such as N-cadherin (28). Establishment of a continuous corneal endothelium is essential for formation of an anterior chamber, and local disruption of this process results in patent adhesion of the lens vesicle and cornea (29, 30).

Two other migratory movements of the periocular mesenchyme are important in development of the anterior chamber. Beginning at E15.5 in the mouse and about day 43 of human gestation, the rim of the optic cup itself grows inwardly (anteriomedially) to produce the pigmented epithelia of the iris and ciliary body (8, 27). Concomitantly, the periocular mesenchyme crawls inwardly along this advancing epithelial surface and populates the ciliary muscle and the anterior two-thirds of the iris. The presumptive corneal stroma appears at about 47 to 52 days of human gestation as a result of a third wave of mesenchymal immigration, completing the gross patterning of the anterior segment. The entire interior surface of the anterior chamber, including the corneal endothelium and stroma, iris stroma, and angle, is occupied by a continuous layer of

Figure 1-3: Periocular mesenchyme and anterior segment development

Top panel: Morphogenetic movements of the periocular mesenchyme in mouse as presented in (27). Abbreviations used are the same as those in figure 1-1. A: First wave of invasion circa E13; mesenchyme (shown in red) insinuates itself between the lens vesicle and surface ectoderm to produce the future corneal endothelium.

B: Circa E14, the mesenchyme anterior to the lens is composed of several layers in direct contact with the lens vesicle

C: Circa E15, the presumptive corneal endothelium is induced to form an occluding monolayer by signals from the adjacent lens, and the anterior chamber is formed. A second wave of mesenchymal immigration along the advancing optic cup rim will produce the anterior iris (yellow) and ciliary body.

D: By E15.5 the anterior chamber is well elaborated and the primordia of the cornea, iris, and ciliary body are in place.

Bottom: Simplified diagram of mesenchymal movements adapted from (8).

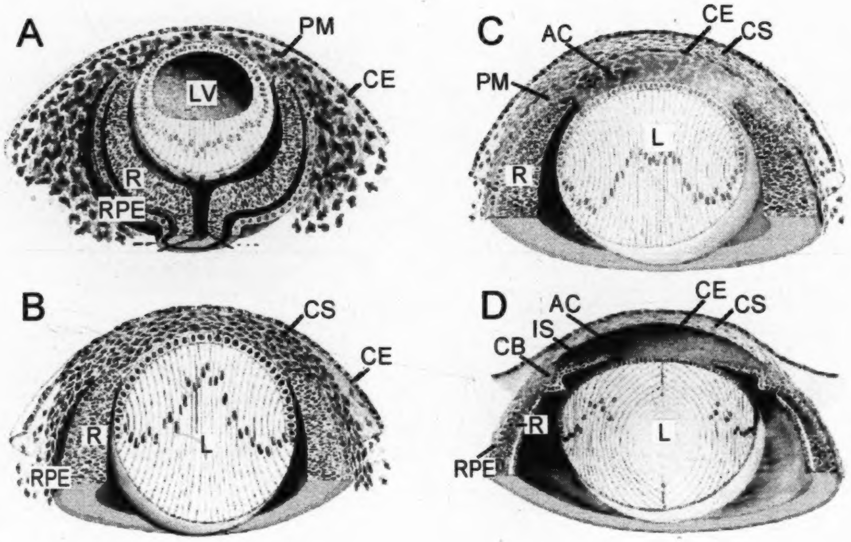
A
PM
LV
CE
R
RPE
B
CS
CE
R
L
RPE
C
AC
CE
CS
PM
L
R
D
AC
CE
CS
IS
CB
R
L
RPE

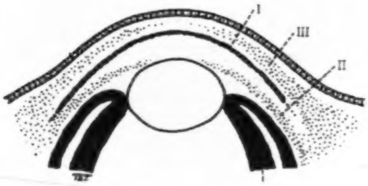
I
III
II

mesenchyme-derived tissue (8, 20, 27). The TM forms by reorganisation of an undifferentiated wedge of angle mesenchyme, which begins to form a proper reticular network at about 15 weeks, but remodeling of this tissue continues until after birth (8, 10).

The embryological model for AR has evolved somewhat since Rieger's description of this disorder as mesodermal in origin. The periocular mesenchyme was historically thought to be descended from paraxial mesoderm, although it has more contemporarily been established in chick, mouse, and primate embryos that the cranial neural crest is an important contributor to the iridocorneal angle (8, 10, 31-33). Cell lineage tracing experiments using quail-chick hybrids first revealed the TM and Schlemm's canal to be at least largely descended from the neural crest (31). In human and primate eyes, the endothelial cells lining the trabecular beams of the TM express a neurectoderm-specific marker (enolase $\gamma\gamma$), as do cultured cells isolated from the mature human TM (10, 32). More recently, careful grafting experiments in the mouse have shown that the periocular mesenchyme actually contains descendents of both the (anterior) cranial neural crest and the underlying paraxial mesoderm from somitomere one (33). While both germ layers may therefore be important in the formation of the anterior segment, the aberrant ocular morphology seen in AR is presently attributed primarily to the neural crest. Neuronal enolase staining reveals that the corneal endothelium, anterior iris epithelium, ciliary musculature, and trabecular cells of the anterior TM are largely or entirely neurectodermal in origin (figure 1-1, lower right) (10). Additionally, AR has been described as a consequence of a more generalised systemic neurocristopathy, likely representing an earlier developmental block specific to this same lineage (34).

Genetics of AR - Pituitary homeobox 2 (PITX2)

There are four known genetic loci for diseases belonging to the AR spectrum of anterior segment dysgenesis (AR, iridogoniodysgenesis, or autosomal dominant iris hypoplasia), situated on human chromosomes 4q25 (35-39), 6p25 (40, 41), 13q14 (42), and 16q (43). While genes at the 13q14 and 16q loci remain uncloned, two causative factors have been positionally identified. These two genes, *PITX2* and *FOXC1*, will occupy the remainder of this introduction.

The *PITX2* homeobox transcription factor was cloned in 1996 as the gene mutated in six of ten pedigrees with 4q25-linked AR (44). Mutations were subsequently identified in autosomal dominant iris hypoplasia and iridogoniodysgenesis syndrome, substantively proving these three disorders to be allelic (45, 46). The cloning of *PITX2* was achieved by four independent groups, two of whom noted that this gene is alternatively spliced (44, 47-49). *PITX2* produces three transcripts, (*PITX2a, PITX2b,* and *PITX2c*) representing distinct combinations of the four 5' exons but sharing the majority of the open reading frame, which is contained within exons V and VI (figure 1-4). A fourth isoform, *PITX2d*, has been described in a single report (50). This transcript has been suggested to be translated from an internal methionine, but a proper Kozak consensus (CCARCCAUGG) is absent at this position in *PITX2* (CGGGACAUGU) (50, 51). The translation product of this isoform has never been detected, and would, in any case, lack a complete homeobox (the function of which is described on page 17). Of the three generally accepted *PITX2* isoforms, *PITX2a* encodes the smallest polypeptide (32kDa), but was the first characterised as well as the first shown to be expressed in the developing eye (44). It has consequently been the best-studied within the context of AR malformations.

Mouse model and expression profile of *PITX2*

Cloning of the human and mouse *PITX2* genes revealed a high level of peptide sequence conservation, with only two predicted amino acid substitutions throughout PITX2a (44, 47). In order to recapitulate the AR malformation phenotype in an animal model, several gene-targeting efforts have disrupted the murine *Pitx2* gene, yielding null, hypomorphic, and conditional (floxed) alleles (52, 53). Like human *PITX2* mutations, *Pitx2* knockouts have pleiotropic effects in heterozygotes (52, 53). *Pitx2*$^{+/-}$ mice have AR-like anterior ocular defects, such as full-thickness iris tears and irregular, displaced pupillae, although these findings manifest at a relatively low penetrance (approximately ten percent) (52). A number of other ocular features, such as cataract and microophthalmia, are also seen in a minority of affected mice, as are maloccluded incisors, mirroring the dental phenotype of AR patients. A minority of severely affected heterozygotes are small bodied, potentially corresponding with rare reports of pituitary insufficiency in association with AR (21, 52, 54).

While *Pitx2*$^{+/-}$ mice are a provisional model for AR, stronger deficiencies in murine *Pitx2* cause a relatively severe phenotype which is lethal in mid-to-late gestation. Mice homozygous for null or hypomorphic alleles of *Pitx2* succumb between E10.5 and E18.5, with features including incomplete neural tube or ventral body wall closure, failed heart

Figure 1-4: Genomic structure of human *PITX2*

This figure illustrates the exon/intron structure of the *PITX2* gene on human chromosome 4q25. Exons (numbered boxes) are shown to scale, with lengths (basepairs) indicated below. Introns are not shown to scale, with lengths (kilobasepairs) indicated in parentheses. Exon composition of each of the *PITX2a*, *PITX2b*, and *PITX2c* transcripts is illustrated; outspliced exons are shown with dashed lines. 5' and 3' untranslated regions are shown in light grey, while the initiator (ATG) codon and stop (TGA) codon of each transcript are also illustrated. Regions encoding the conserved homeodomain (HD, exons V and VI) and Aristaless-like OAR tail motif, discussed on page 24, are shown in black. The reported sizes of each transcript as determined by Northern analysis in (47) are also indicated.

This figure is based on (49) and (50), and updated with curated transcript information from the EnsEMBL genome browser (www.ensembl.org). A fourth *PITX2* transcript, *PITX2d*, has been described in a single report but is not illustrated (50).

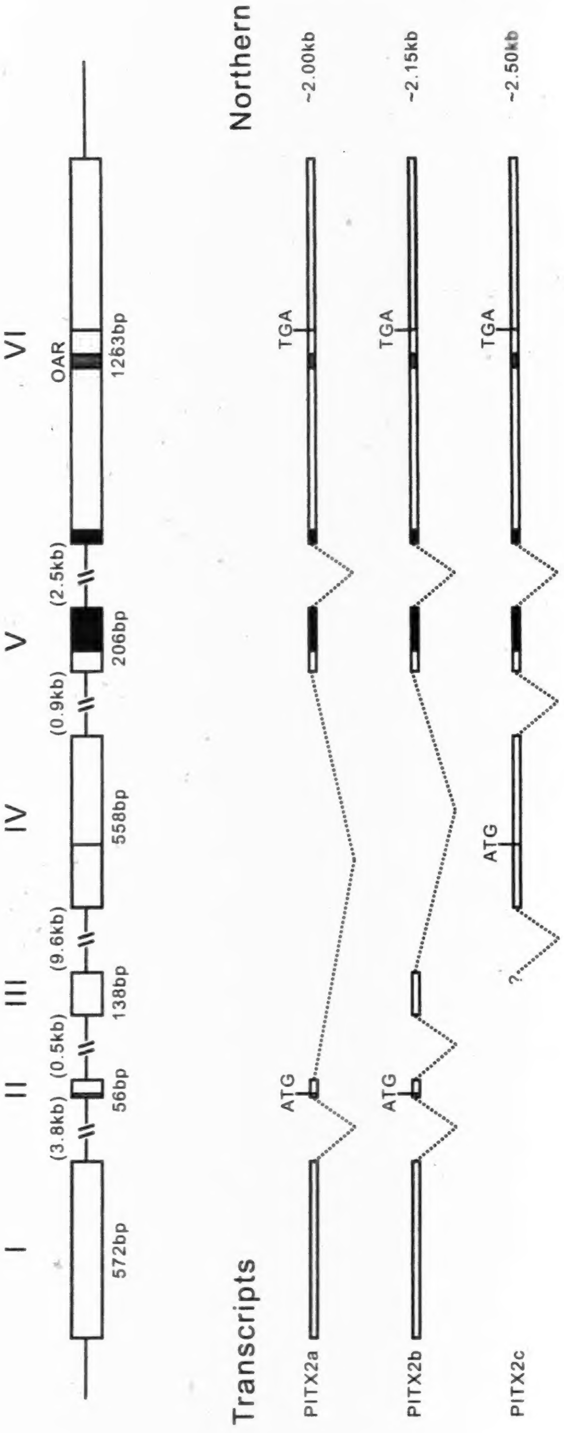
I
II
III
IV
V
VI
572bp
(3.8kb)
56bp
(0.5kb)
138bp
(9.6kb)
558bp
(0.9kb)
206bp
(2.5kb)
OAR
1263bp
Transcripts
Northern
PITX2a
ATG
TGA
~2.00kb
PITX2b
ATG
TGA
~2.15kb
PITX2c
?
ATG
TGA
~2.50kb

septation, and right lung isomerism (52, 53). *Pitx2*$^{-/-}$ mice have a number of ocular features absent in *Pitx2*$^{+/-}$ heterozygotes, including the absence of extraocular muscles, persistent lens pit, optic nerve coloboma, and, interestingly, aberrant placement of the eye itself. By E12.5, the globes of *Pitx2*$^{-/-}$ mice are small, oriented nasally, and submerged beneath a hyperplasic mesenchyme which intrudes between the surface ectoderm and eye. These findings implicate *Pitx2* broadly in the development of the eye, although homozygous *PITX2* defects are not likely to be clinically relevant due to the lethality of this phenotype. It is, however, worth noting that the absent extraocular muscles, like the anterior iris, corneal stroma, and trabecular meshwork, are normally derived by mesenchymal condensation (55, 56).

Development of the anterior pituitary is also compromised in *Pitx2*$^{-/-}$ mice, in which the ectodermal primordium (Rathke's pouch) is properly committed but does not expand post-E10.5, and the adjacent mesenchyme is again observed to be markedly hypoplasic (52, 57). Reverse transcriptase polymerase chain reaction (RT-PCR) demonstrates that all three isoforms of *Pitx2* are expressed in Rathke's pouch from E13.5, as well in all five secretory cell types of the mature gland (47, 52). In reporter assays, PITX2 can drive the expression of several pituitary hormone promotors, including growth hormone, the beta subunit of follicle stimulating hormone, and prolactin (58-60). The arrested pituitary development of *Pitx2*-null mice is not noted heterozygotes, so this phenotype can be rescued by even moderate levels of Pitx2 activity (52).

The expression of *Pitx2* during mouse development correlates well with organs affected in AR, and is detectable in the periocular mesenchyme, dental epithelium, first branchial arch, umbilicus, pituitary primordium, and limb buds (44, 47-49, 61). During ocular development, Pitx2 is expressed in mesenchyme surrounding the optic eminence as early as E8.5, in anticipation of the arrival of the optic cup and lens vesicle (62). By E11.5, when these latter two structures have formed, and mesenchymal immigration commences, Pitx2 is highly expressed in the periocular mesenchyme (44, 47, 63). Expression is retained in mesenchymal derivatives such as the corneal endothelium and trabecular meshwork thereafter, gradually becoming restricted to the angle by E18.5 (Figure 1-5) (44, 47, 63). This pattern in which *PITX2* expression is extinguished in the eye is correspondent with the arrest and differentiation of mesenchymes arriving at each of these tissue primordia, so expression of ocular fates may involve *PITX2* downregulation. However, transcripts of *PITX2* are also well-represented in cDNA libraries derived from the mature trabecular meshwork, suggesting a maintenance role in this tissue (64, 65). The ocular expression pattern of *PITX2* is depicted in figure 1-5, which also shows that of a second AR gene (*FOXC1*). The latter is discussed beginning on page 29.

Nonocular expession of *PITX2* may shed some light on the systemic phenotypes of *PITX2* gene-targeted mice and AR patients. For instance, in the developing molar teeth, stimulatory (FGF8) and repressive (BMP4) signals define a restricted zone of PITX2 expression (66). Recently, the procollagen lysyl hydroxylases *PLOD1* and *PLOD2* have been identified as *PITX2* targets, as have at least one *Distal-less* homeobox gene (*DLX2*) (67, 68). Each of these three genes may be plausibly involved in the microdontia and oligodontia found in AR. The cardiac septal and valve defects sometimes seen in AR patients, in contrast, may specifically involve the *c* isoform of *PITX2*. Exon-specific *in situ* hybridisation demonstrates differences in expression between *PITX2a/b* and *PITX2c* due to their use of different promotors (53, 69, 70). While *PITX2a/b* and *PITX2c* are present together in the periocular mesenchyme, *Pitx2c* exclusively is laterally expressed under the control of Nodal and Sonic hedgehog in the left lateral plate mesoderm, as well as in the heart tube prior to looping (69-72). Complete loss of *PITX2c* function randomises heart looping and leads to left molecular isomerism of cardiac atria, ventricles, and outflow tract (73, 74).

Domain structure of PITX2a

The most obvious conserved sequence element within PITX2 is a sixty amino-acid homeodomain (HD), which spans residues 38 through 97 of PITX2a and is present in all three isoforms. The HD is a DNA-binding module first identified in a number of *Drosophila* homeotic and segmentation genes that function as crucial directors of the overall body plan (75). The HD itself is a compact bundle of three α-helices, of which helices one and two form a cross-brace hydrophobically packed against the third, C-terminal helix (76, 77). Upon binding of DNA, the homeodomain's third ('recognition') helix is inserted into the target's DNA's major groove and makes sequence-specific contacts with the bases therein. The sequence specificity of HD binding has been studied *in vitro* by selection of preferred sites from pools of random oligonucleotides, and the majority of HDs preferentially bind elements of the sequence TAATNN in this (highly artificial) system (78, 79). The last two nucleotides of this short consensus are influenced largely by the amino acid sidechain at position 50 of the HD, which is on the

Figure 1-5: Coexpression of PITX2 and FOXC1 in the developing mouse eye

Left panel: Tissue immunofluorescence of endogenous PITX2 in the eye from embryonic days 11.5 through 18.5 as published in (63). PITX2 is widely expressed in the periocular mesenchyme from E11.5 (A), in the hyaloid plexus at E13.5 (B), and in the presumptive cornea at E13.5 and E15.5 (B, C). PITX2 expression is gradually restricted to the angle of the mature eye; the final pattern at E18.5 is described in the original manuscript as iris-restricted (D), although it is unclear whether angle structures might also be stained. *PITX2* is a well-represented clone in cDNA libraries derived from the mature trabecular meshwork (64, 65).

Right panel: Galactosidase staining in the eyes of mice heterozygous (+/-) or homozygous (-/-) for a LacZ-insertion knockout of FOXC1 as published in (80) and (29) respectively. FOXC1::LacZ, like PITX2, is expressed in the periocular mesenchyme post-E11.5 (E), in the hyaloid plexus at E11.5 and E12.5 (F, H), and in the presumptive corneal stroma at E12.5 (F, G). FOXC1::LacZ is also expressed in the trabecular meshwork from E16.5 on, as well as in the conjunctiva (I, J).

Abbreviations: Periocular mesenchyme (PM), hyaloid plexus (HP), presumptive corneal stroma (CS), conjunctiva (con), trabecular meshwork (TM).

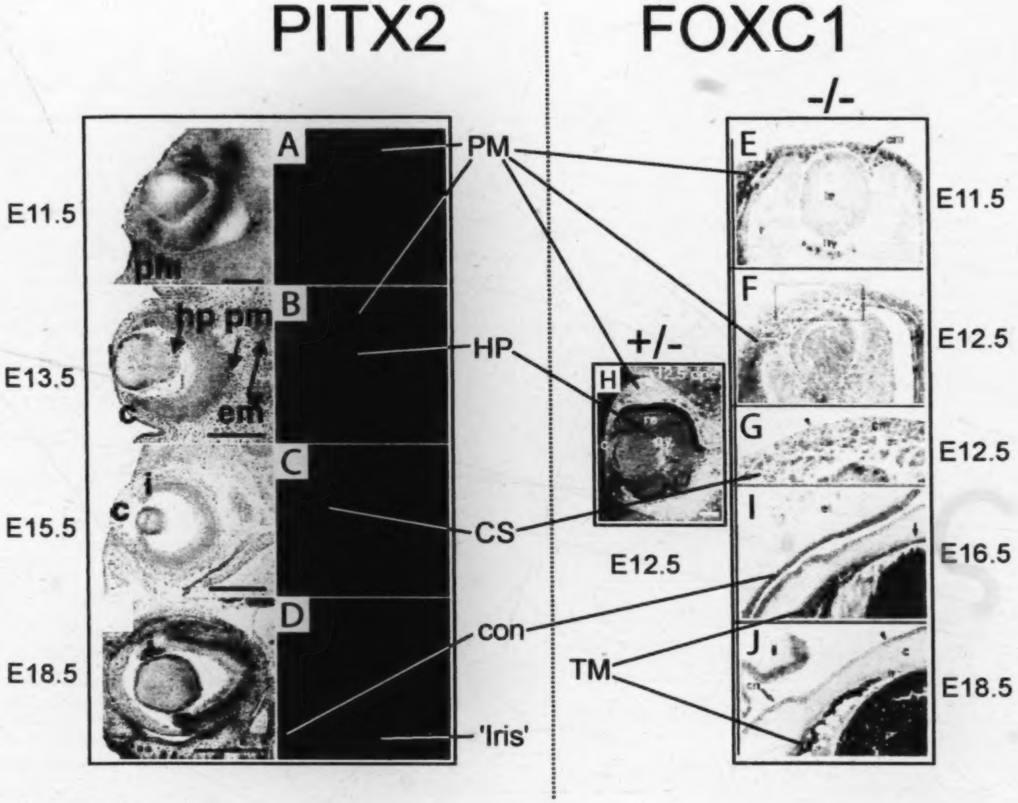
PITX2
FOXC1
-/-
+/-
E11.5
E13.5
E15.5
E18.5
A
B
C
D
pm
hp
pm
c
em
c
i
PM
HP
CS
con
'Iris'
TM
H
E12.5
E
F
G
I
J
E11.5
E12.5
E12.5
E16.5
E18.5

hydrophilic face of the recognition helix C-terminus (76, 81-83). Position 50, a lysine in the HD of PITX2, has been shown to confer an *in vitro* predilection for TAATCC elements to other homeoproteins, and PITX2 can indeed bind this motif (84). Apart from its ability to bind this site, the *in vitro* and *in vivo* DNA-binding specificity of PITX2 has not been examined.

HDs of disparate transcription factors are far from invariant, and phylogenetic efforts divide the known HDs into a variety of subfamilies on the basis of conservation (85). BLASTp alignment to the GenBank 'nr' database reveals the HD of PITX2, in particular, to be most similar to those of the related transcription factors PITX1 and PITX3, which are 97 and 100 percent identical respectively (figure 1-6) (86-88). The mammalian PITX proteins, when compared to the established HD subfamilies, are determined to belong to a grouping named after the *Drosophila* morphogen Paired (47). Because the PITX2 HD has a lysine at the specificity-ruling fiftieth position, PITX2 is also sometimes discussed in terms of a second *Drosophila* factor, Bicoid, which is a K50 homeoprotein with a similar preference for TAATCC sites *in vitro* (44, 89). The Paired HD, despite greater overall paralogy with PITX2, has a serine at position fifty and hence a different *in vitro* binding specificity (81, 82). The HDs of Paired and Bicoid themselves are more divergent with respect to each other than to PITX2, bearing only thirty-eight percent peptide identity and sixty-one percent similarity.

The distinction between Paired-like and Bicoid-like aspects of PITX2, while subtle, is an important one in light of the DNA-binding and protein-protein interactions of these two classical activators. Paired and Bicoid can both bind DNA cooperatively, meaning that in *in vitro* DNA-binding assays, linear increases in the concentration of either factor cause the fraction of bound target DNA to increase exponentially (82, 90). Paired and Bicoid also share an additional ability to self-interact via homophilic protein interactions (83, 91). While both HDs can self-interact and bind cooperatively, structural and functional analyses of these two proteins surprisingly reveal that they do so via very different mechanisms.

Unlike full-length Bicoid, the isolated Bicoid HD does not bind DNA cooperatively, nor does it self-interact in pull-down experiments (91). These activities can be reconstituted by the addition of flanking sequences either N-terminal or C-terminal of the HD. Moreover, multiple mutations of the recognition helix of the bicoid HD, including mutations of K50, have no effect on self-interaction despite drastically altered DNA binding. Together, these data indicate that Bicoid's cooperativity is achieved via a

Figure 1-6: Conserved domains in PITX2 and comparison with other homeoproteins

Peptide sequences of human PITX2 and selected homeoproteins of the Paired and Hox subclasses were compared by CLUSTALW analysis (www.ebi.ac.uk/CLUSTALW). Residues identical in PITX2 are represented as white text on a black background, conservatively substituted residues are shown as black text on a grey background, and nonconservatively substituted residues are depicted as black text on a white background. The amino acid positions comprising the three α-helices identified in the Engrailed crystal structure are shown at top (76). Bicoid itself can be considered a moderately divergent HOX protein (92, 93). On the basis of sequence conservation, Paired and related HDs are a better model for PITX2 than are Bicoid and the HOX proteins. Also implicating PITX2 as a Paired-like homeoprotein is the presence of a C-terminal motif (the OAR domain) named for Orthopedia, Aristaless, and Rax, and found exclusively in the Paired-like HD subfamily (94).

Sequences shown: (from top) human PITX2, mouse PITX2, human PITX3 and PITX1, *Drosophila* Paired, mouse Orthopedia, *Drosophila* Aristaless, Rax, Bicoid, and Antennapedia, and human HOXD3.

%ID: Percentage homeodomain sequence identity with PITX2.

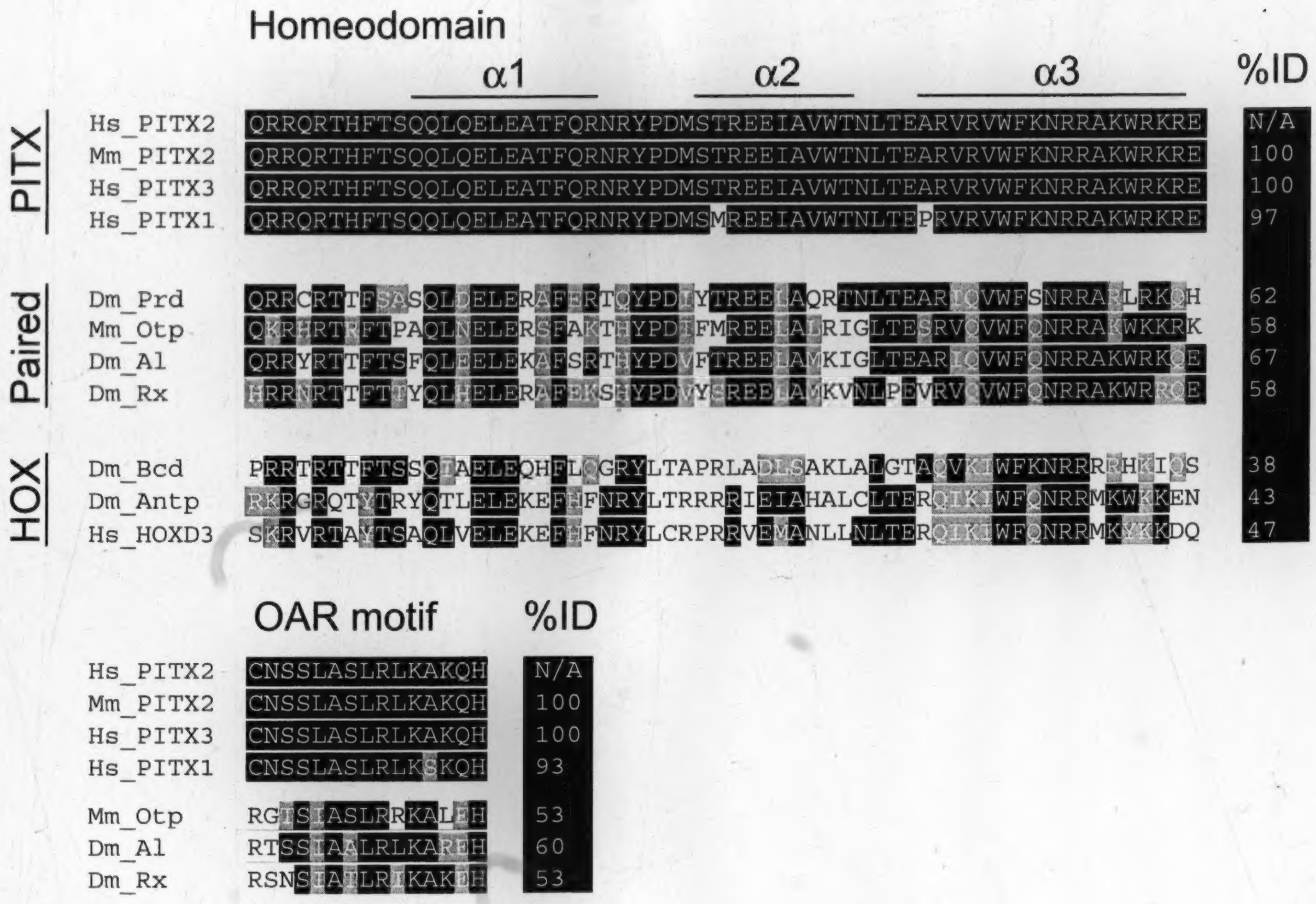
Homeodomain
α1
α2
α3
%ID
PITX
Hs_PITX2 QRRQRTHFTSQQLQELEATFQRNRYPDMSTREEIAVWTNLTEARVRVWFKNRRAKWRKRE N/A
Mm_PITX2 QRRQRTHFTSQQLQELEATFQRNRYPDMSTREEIAVWTNLTEARVRVWFKNRRAKWRKRE 100
Hs_PITX3 QRRQRTHFTSQQLQELEATFQRNRYPDMSTREEIAVWTNLTEARVRVWFKNRRAKWRKRE 100
Hs_PITX1 QRRQRTHFTSQQLQELEATFQRNRYPDMSMREEIAVWTNLTEPRVRVWFKNRRAKWRKRE 97
Paired
Dm_Prd QRRCRTTFSASQLDELERAFERTQYPDIYTREELAQRTNLTEARIQVWFSNRRARLRKQH 62
Mm_Otp QKRHRTRFTPAQLNELERSFAKTHYPDIFMREELALRIGLTESRVQVWFQNRRAKWKKRK 58
Dm_Al QRRYRTTFTSFQLEELEKAFSRTHYPDVFTREELAMKIGLTEARIQVWFQNRRAKWRKQE 67
Dm_Rx HRRNRTTFTTYQLHELERAFEKSHYPDVYSREELAMKVNLPEVRVQVWFQNRRAKWRRQE 58
HOX
Dm_Bcd PRRTRTTFTSSQIAELEQHFLQGRYLTAPRLADLSAKLALGTAQVKIWFKNRRRRHKIQS 38
Dm_Antp RKRGRQTYTRYQTLELEKEFHFNRYLTRRRRIEIAHALCLTERQIKIWFQNRRMKWKKEN 43
Hs_HOXD3 SKRVRTAYTSAQLVELEKEFHFNRYLCRPRRVEMANLLNLTERQIKIWFQNRRMKYKKDQ 47
OAR motif
%ID
Hs_PITX2 CNSSLASLRLKAKQH N/A
Mm_PITX2 CNSSLASLRLKAKQH 100
Hs_PITX3 CNSSLASLRLKAKQH 100
Hs_PITX1 CNSSLASLRLKSKQH 93
Mm_Otp RGTSIASLRRKALEH 53
Dm_Al RTSSIAALRLKAREH 60
Dm_Rx RSNSIATLRIKAKEH 53

homeodomain-extrinsic, self-specific protein-protein interaction. One functional consequence of this activity is that Bicoid's activation of multi-site enhancers can be 'switched on' over a less than fourfold increase in Bicoid concentration, allowing the firm establishment of sharp zones of target gene expression in the embryo (95, 96).

In contrast to the mechanism described above, the homodimerisation and cooperative binding activities of many Paired-like homeoproteins are actually intrinsic to the HD. This feature of Paired-like HDs was first identified because of an interesting consequence on binding specificity of these factors *in vitro*, namely the tendency to prefer palindromic substrates in cyclic binding-site selection experiments (82). The *Drosophila* proteins Paired, Gooseberry, and Goosecoid, as well as *Xenopus laevis* Mix-1, can each bind sites of the sequences TAATNNATTA ("P2") or TAATNNNATTA ("P3") as dimers in electrophoretic mobility shift assays (EMSAs) (82). While all four homeoproteins bind cooperatively to P2 and/or P3 substrates, the preferred sequence between TAAT half-sites is influenced by the position 50 sidechain (generally serine, glutamine, or lysine in Paired-like HDs), consistent with the previously stated importance of this residue for monomeric binding (81, 83, 89). Electromobility shift assays (EMSAs) of the K50 HD of Goosecoid, as well as on a K50 mutant of Paired, have shown that both HDs bind to the expected P3 TAATCCGATTA consensus with twenty-fold or greater cooperativity, such that the monomerically-bound probe is much less abundant than the dimer-DNA complex (82). Both K50 Paired and Goosecoid are similar to PITX2 in terms of both overall resemblance to Paired and the presence of a lysine rather than serine or glutamine at position 50.

Structural studies have yielded some insight into the mechanism of Paired homodimer formation and cooperativity. The crystal structure of a mutant (Q50) Paired HD dimerically bound to a P3 element has been determined to a resolution of two angstroms (83). As expected, the two Q50-Paired monomers are opposed head-to-tail on the adjacent TAAT half-sites of the P3 element. Crucially, complementary surfaces on each HD form an extensive network of intersubunit contacts which stabilize the dimer and bury greater than 1000Å^2 of surface area. The N-terminal arm of each HD forms both hydrophobic contacts and hydrogen bonds with helix II of the opposing subunit, forming a nearly continuous interface between the two monomers. Eighteen ordered water molecules are enclosed within this cavity, and mediate numerous indirect contacts between recognition helices and major groove. The Q50-Paired dimer induces a distortion of the occupied DNA by twenty degrees, which is necessary for the observed inter-HD contacts. While DNA bending should represent a substantial energetic barrier to dimeric binding of the P3 site, monomeric binding of *Drosophila* Engrailed appears to cause a similar topological distortion (76). Binding of one Paired HD may therefore favour cooperative binding of a second monomer through both extensive intersubunit contacts and steric preparation of the occupied site (83). While the PITX2 HD structure has not been determined, it may be reasonable to predict on the basis of paralogy that some or all of the above mechanisms are conserved from *Drosophila* to *Homo sapiens*. Mapping the primary sequence of PITX2's HD onto that of Q50-Paired reveals that residues forming the dimerisation and DNA-binding surfaces are entirely identical, with the exception of two conservative substitutions at positions 28 and 50 (Figure 1-7).

In addition to its DNA-binding domain, PITX2 has a second conserved region which is tentatively thought to be involved in protein interactions and/or autoregulation of transactivity. The OAR domain is a fifteen residue conserved motif first identified as a region conserved between the Paired-like activators Orthopedia, Aristaless, and Rax, and is found, invariably near the extreme C-terminus in a subset of such homeoproteins (97, 98). By BLAST analysis, the OAR of PITX2 in particular found to most resemble those of PITX1, PITX3, and RAX (figure 1-6). Like PITX2, other metazoan homeoproteins bearing an OAR tend to be expressed in mesenchymes which give rise to both anterior craniofacial structures and limb buds (99). While the function of the OAR motif has not been clearly defined, this domain appears to be an autoinhibitory module which suppresses target gene transactivation *in cis*. In reporter assays, removal of the OAR domains of two *aristaless*-like homeoproteins (Cart1 and Prx2) increases reporter activity by approximately threefold and twentyfold respectively, and derepression is accompanied by increased DNA binding of a palindromic target element (94, 100). This effect of the OAR has been recapitulated *in vivo*, as ectopic expression of full-length Cart1 produces no phenotype, while expression of Cart1 lacking an OAR is markedly teratogenic (94). Like many domains of transcription factors, the OAR also appears to be modular, albeit in a limited sense. For instance, autoinhibition of transactivity can be conferred to the Aristaless-like homeoprotein Alx3 by replacing its divergent (vestigal) OAR with that of Cart1 in transgenic mice (94). However, the OAR does not function as a proper repressor in heterologous fusions with the GAL4 activator, suggesting that its function may require the specific structural context of *prd*-related homeoproteins (100).

Figure 1-7: Comparison of the human PITX2 and *Drosophila* Q50 Paired HDs

Top panel: stereoimages of the Q50 Paired dimer structure reported in (83)
Upper stereoimage: Space-filling model with color code representing sequence comparison versus human PITX2. Residues that are identical in PITX2 are depicted in red, conservatively substituted residues in orange, and nonconserved residues in grey. Q50 is highlighted in yellow for emphasis. DNA is represented as phosphoribose backbone only for clarity. Note that interior surfaces of the Q50-Paired dimer are virtually identical in PITX2. No changes have been made to the published structure, and the sidechains shown are those of Paired rather than PITX2 (where different).

Lower stereoimage: Ribbon diagram illustrating the N-terminal arm, and helices I, II, and III of each paired HD in the dimer. The view is identical to the stereoimage at top. Positions of PITX2 patient mutations discussed in this chapter are shown as space-filling models to illustrate spatial clustering: T68 (red), V83 (orange), R84 (blue), K88 (yellow), and R91 (green).

Bottom panel: Alignment of Q50-Paired and PITX2 HDs illustrating conservation of protein-protein and protein-DNA interaction surfaces. Residues involved in direct or water-mediated inter-HD and HD-DNA contacts are those indicated in (83). Both conserved sidechains and positions of patient mutations studied are highlighted according to the same colour scheme used in the top panel.

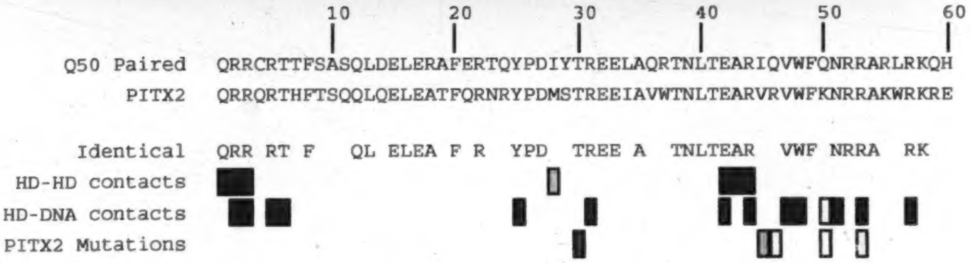
10
20
30
40
50
60
Q50 Paired QRRCRTTFSASQLDELERAFERTQYPDIYTREELAQRTNLTEARIQVWFQNRRARLRKQH
PITX2 QRRQRTHFTSQQLQELEATFQRNRYPDMSTREEIAVWTNLTEARVRVWFKNRRAKWRKRE
Identical QRR RT F QL ELEA F R YPD TREE A TNLTEAR VWF NRRA RK
HD-HD contacts
HD-DNA contacts
PITX2 Mutations

The OAR domain of PITX2, in particular, appears to be important for homomeric and heteromeric protein interactions, as well as transcriptional synergy with other factors. Importantly, truncation of the C-terminal 39 residues of PITX2a ("PITX2 C39", containing the OAR) yields a protein which homodimerises and binds DNA more readily than does full-length PITX2a (101). Furthermore, the C-terminus of PITX2 physically interacts with the pituitary homeoprotein PIT-1 and mediates synergistic activation of reporter constructs based on the prolactin promotor, which is an *in vivo* target of both proteins (101). Coexpression of the PITX2 C39 suppresses both transactivation and PIT-1 synergism of full-length PITX2a *in trans* (101). At present, the simplest model of PITX2's allosteric regulation proposes that the C-terminal tail constitutively inhibits dimerisation and DNA binding in an intramolecular fashion, and that this basal inhibition is relieved when the OAR is bound by cofactors such as PIT-1 (101). However, this view is limited by a poor understanding of the mechanism of PITX2's target transactivation. One large gap in our understanding of PITX2's function is that transactivation domains of any of PITX2's isoforms have not been mapped in any detail.

PITX2a self-interaction

Like Paired or Bicoid, PITX2 forms self-specific protein interactions and binds DNA cooperatively, although it is not known whether self-association occurs through the Paired-like homeodomain, through a domain extrinsic to the HD, or both. PITX2 dimerisation was first observed in EMSA assays, in which both monomerically and dimerically bound complexes with the probe DNA were observed (50). All three PITX2 isoforms can self-interact, and every pairwise combination of PITX2 homo- and heterodimers is observed in EMSAs with even single-site TAATCC binding substrates (50). Dimerisation of PITX2a has been confirmed in GST pull-downs of bacterially expressed PITX2a, suggesting that dimerisation is direct and does not require bridging factors (102). Moreover, DNA binding appears to have a limited role in PITX2a dimerisation, as self-interaction in GST pulldowns is unaffected by the addition of P3 oligonucleotides, and only marginally reduced by the addition of ethidium bromide. Because intrinsic self-interaction is common to all three isoforms of PITX2, this activity is presumably encoded by the shared C-terminal 256 residues of all three proteins. PITX2a's dimerisation domain(s) have been recently mapped in the yeast two-hybrid system, in which both the isolated HD and C-terminal flank contribute to self-interaction (102).

As observed for Bicoid, PITX2a dimerisation enables cooperative binding of PITX2 to multi-site DNA substrates bearing direct, spatially separated repeats of a TAATCC bicoid element (102). However, homeodomain mutations present a complex picture of the relationship of DNA binding and PITX2a dimerisation in the two-hybrid system. One AR-associated mutation of HD position 30 (T68P) ablates interaction with a variety of full-length and truncated PITX2a baits (102). However, a second patient mutation, (K88E), which causes a charge reversal at the crucial HD position 50, actually enhances heterodimerisation with the C-terminus of wildtype PITX2a (102, 103). Importantly, both mutations greatly diminish DNA binding and transactivity *in vitro* (104), so DNA-binding and protein-protein interaction functions of the PITX2 HD may be separable. Similar observations have been obtained for Bicoid, which retains self-interaction capacity when K50 is mutated to an alanine or glutamine (91). These data are consistent with the presence of at least one HD-extrinsic self-interaction domain within PITX2a, allowing cooperative binding over greater distances than permitted by HD-HD interactions alone. This view, however, does not preclude the existence of an HD-intrinsic dimerisation activity of the type structurally determined for Paired. Several published findings lend support to this latter hypothesis. Firstly, bait constructs representing the isolated HD of PITX2 interact with full-length PITX2a in yeast two-hybrids (102). Secondly, interaction of PIT-1 and PITX2a is completely abolished by missense mutations of the HD in same experimental system. Thirdly, the T30P and K88E HD mutations both destroy DNA binding, but produce contradictory effects on dimerisation, respectively suppressing and enhancing interaction with the wild-type protein (102, 104).

Recruitment of coactivators by PITX2

In addition to influencing DNA binding specificity and cooperativity, protein interactions also permit target gene activation via the subsequent recruitment of coactivators and/or corepressors. The most comprehensive account of PITX2's coactivator recruitment has come from studies of PITX2 as a Wnt signaling-responsive factor in the development of the cardiac outflow tract (105). One experimental convenience of the Wnt pathway is that induction is easily evoked by lithium chloride, which provokes nuclear accumulation of β-catenin (106). This induction scheme has been used to study a time-course of PITX2a-mediated activation events on a relevant promotor (*cyclin D2*). Crucially, β-catenin binds both the *PITX2* promotor and the

PITX2a protein in LiCl-induced murine C2C12 cardiomyoblasts (105). Induction of the Wnt pathway converts PITX2a from repressor to activator, as β-catenin displaces a histone deacetylase (HDAC1) which is constitutively bound to PITX2a in uninduced cells. LiCl induction causes coordinated binding of PITX2a and β-catenin to the *CycD2* promotor within thirty minutes; this timing coincides with dismissal of HDAC1 from the promotor. Chromatin immunoprecipitation (ChIP) studies have shown that β-catenin and PITX2 together recruit a program of transcriptional coactivators which subsequently leads to transcription of the *CycD2* gene. The coactivator machinery recruited during *cycD2* induction includes the histone acetyltransferases TIP60 and p300/CBP, the TRAP/mediator complex, and a coactivator of LIM proteins (CLIM-1) (105). Several of these coactivators are essential for induction, as single-cell microinjection of antibodies specific for β-catenin, PITX2, CPB/p300, Tip60, CLIM, or PBP (a TRAP subunit) attenuates LiCl responsiveness of a *CycD2* reporter construct. PITX2 appears crucial for assembly of the chromatin remodeling machinery, and coimmunoprecipitates with endogenous p300/CBP, Tip60, and CLIM from C2C12 lysates (105, 107). The precise mechanism of PITX2 promotor induction is likely to involve a complex program of recruited cofactors, and the regulatory circuitry of activation may vary according to promotor context. For instance, p300 can physically interact with β-catenin, and both proteins can synergistically activate reporters based on some, but not all, Wnt-responsive promotors (108).

Some or many of the protein-protein interactions between PITX2 and this large cofactor machinery may be indirect. Only the association with CLIM has been mapped within PITX2, localizing to regions C-terminal of the HD (107). However, regions N-terminal of the HD are essential for the mitogenic effect of PITX2a in C2C12 cells, while the C-terminus is apparently dispensible for this activity (105). PITX2a's N-terminus is therefore also likely to mediate yet-unknown protein interactions essential for recruitment of activating cofactors.

Forkhead b**ox** transcription factor **C1** (FOXC1)

In 1994, transcripts encoding seven human orthologues of the *Drosophila* Forkhead activator were cloned from a craniofacial cDNA library (109). One such gene, Forkhead-related activator 3 (*FREAC-3*, now named *FOXC1*), was mapped to the chromosome 6p25 subtelomeric region (110). *FOXC1* was noted to be a good positional candidate gene within the 6p25 AR locus, and mutations and balanced translocations within this gene were identified in patients diagnosed with AR and IH (111, 112). Moreover, wholesale duplications and deletions of a segment of the 6p subtelomere containing *FOXC1* were noted in patients with IH and AR respectively, demonstrating that both haploinsufficiency and increased gene dosage of *FOXC1* cause malformations of the anterior segment (113-115). Fourteen AR-associated point mutations of *FOXC1* have been characterised in terms of DNA binding and reporter transactivity in cultured cells (116-119). One such patient allele encodes a product with as much as 56% of wild-type reporter transactivity, suggesting a strictly enforced minimum level of *FOXC1* activity in normal ocular development.

FOXC1 mouse model and expression

Much information regarding FOXC1's developmental function has come from the careful observation of mouse phenotypes, and both naturally occuring and gene-targeted *LacZ* knockouts of murine *Foxc1* have been described (80, 120). Heterozygous *Foxc1* gene-targeted mice have an anterior segment phenotype similar to that of AR patients, including corectopia, iridocorneal synechiae, iris tears, iris hypoplasia, posterior embryotoxon, and a high incidence of sclerocornea and cataract (120, 121). The anterior segment angle defects of *Foxc1*$^{+/-}$ mice have been studied in detail, and noted features included occlusion of the TM by iris or corneal endothelial cells or by excessive basement membrane material, hypoplasia or absence of the TM and/or Schlemm's canal, and direct peripheral adhesion of the iris and cornea. In some sections of *Foxc1*$^{+/-}$ eyes where absence of the TM was noted, this tissue was replaced by what appeared to be a loose, undifferentiated cell mass, suggesting a possible block in mesenchymal condensation. Interestingly, ocular features of *Foxc1*$^{+/-}$ mice manifest with varying severity dependent on genetic background, so one or more modifier loci may be evident. In contrast to the AR-like ocular defects of *Foxc1*$^{+/-}$ mice, homozygous mutants have an embryonic lethal phenotype first observed in the spontaneous mouse mutant *congenital hydrocephalus* (*Ch*), which is in fact allelic with *Foxc1* (80, 120). *Foxc1*$^{-/-}$ mice die perinatally with hemorrhagic hydrocephalus, open eyelids, extensive skeletal abnormalities including absent sternum, and ocular defects similar to those of *Foxc1*$^{+/-}$ mice.

Systemically, the monoexonic *Foxc1* gene is expressed as a 3.9kb transcript which is nearly ubiquitous and is particularly abundant in the heart, liver, skeletal muscle, and kidney (109). An additional transcript of 3.4kb is present in the fetal kidney. In the developing murine eye, Foxc1's expression pattern is remarkably like that of Pitx2, initiating in the periocular mesenchyme prior to the onset of immigration at E11.5 (figure 1-5) (29, 80). Foxc1 is detectable shortly thereafter in the precorneal mesenchyme, in the hyaloid plexus at E12.5, and the TM and conjunctiva by E16.5. Expression in the TM and conjunctiva is seen to persist at least until parturition and potentially thereafter.

Domain structure of FOXC1

All members of the Forkhead gene family bear a conserved, 110-residue forkhead domain (FHD) that mediates DNA binding; this domain occupies residues 69 to 178 of FOXC1 (109). The FHD forms a 'winged helix' structure consisting of a three-helix bundle (structurally akin to a homeodomain) packed against two loop regions which are encoded by a stretch of primary sequence C-terminal of helix III (122). Helix III, the 'recognition helix', traverses and makes sequence-specific contacts with the DNA major groove, while the second wing region inserts lengthwise into the minor groove at the 5' end of the occupied site. The FHD binds to a core consensus RTAAAYA element as a monomer, and DNA binding assays produce observations consistent with a bending of the double helix by about ninety degrees when bound by the isolated FHD of FOXC1 (109). DNA binding of FOXC1 is crucial for activation of developmentally important target genes, and several patient mutations primarily affect this aspect of the FHD's function (116). In addition to DNA binding, however, the FHD may have a functionally separable importance in transactivation, as two patient missense mutations within this domain (F112S and I126M) reduce transactivation but not DNA binding *in vitro*.

In addition to the FHD, FOXC1 has several additional domains defined by molecular dissection of recombinant proteins (123). Full nuclear localisation of FOXC1 requires two distinct stretches of primary sequence: a basic nuclear localisation signal spanning positions 168 to 176 and an additional region from residues 78 to 93. Of these two regions, only the former is sufficient for exclusively nuclear expression of green fluorescent protein (GFP) fusion constructs. It is also worth noting that both signals are resident within the FHD, suggesting an additional role for this domain.

FOXC1 transactivity, like nuclear localisation, is mediated by two discontinuous domains with distinct contributions. Deletion analysis reveals that both the N-terminus (AD1; positions 1-50) and C-terminus (AD2; residues 436-553) of FOXC1 are about equally important for full activation of reporter constructs (123). However, in heterologous fusions with the DNA-binding domain of GAL4, AD2 drives reporter expression about five times more efficiently than does AD1, so AD2 may have a greater degree of intrinsic activity. In addition to its transactivation domains, FOXC1 possesses a central domain, spanning residues 215-366, which attenuates transactivation by AD1 and/or AD2. This module can similarly block the activity of heterologous activators such as GAL4 when fused in *cis*, but does not intrinsically repress constitutively active promotors *in trans*. This central transactivity-regulation domain (TRD) also appears to be a target for inhibitory phosphorylation by protein kinases including p44/42 ERK (123, 124), implying that FOXC1 may be susceptible to regulation via one or more mitogen-activated protein kinase (MAP kinase) pathways.

Criteria for a joint model for PITX2 and FOXC1 in AR

As discussed in the preceding sections, both *PITX2* and *FOXC1* are transcription factors important in the development of the human and mouse anterior segment. Importantly, *PITX2* and *FOXC1* are spatially and temporally coexpressed in mesenchymally-derived components of the eye during development of the aqueous outflow pathway. Both *PITX2* and *FOXC1* are also highly sensitive to changes in gene dosage, an aspect discussed in more detail in the following chapter. While the similar expression patterns and phenotypes of *PITX2* and *FOXC1* would lead us to believe that both genes fulfill a common biological role during ocular development, the precise nature of this coordinated mechanism remains obscure.

We may envision several general, nonexclusive models of circuits relating the activities of *PITX2* and *FOXC1*. For instance, both genes may individually be required for the normal regulation of one or more genes governing immigration or differentiation of the periocular mesenchyme between approximately E10.5 and E14.5. Alternatively, either *PITX2* or *FOXC1* may be a direct or indirect transcriptional target of the other, although there is presently no evidence to assess this possibility directly. Thirdly, PITX2 and FOXC1 might function primarily within a common macromolecular complex within the cell nucleus. This latter hypothesis, which would require that both AR gene products are capable of physical interaction and at least overlapping in localisation, is explored in chapter three.

Chapter two:

Characterisation and prevalence of *PITX2* microdeletions in the aetiology of AR malformations

This chapter contains work published in:

Lines MA, Kozlowski K, Kulak SC, Allingham RR, Heon E, Ritch R, Levin AV, Shields MB, Damji KF, Newlin A, Walter MA. 2004. Characterization and prevalence of PITX2 microdeletions and mutations in Axenfeld-Rieger malformations. *Invest Ophthalmol Vis Sci* 45(3): 828-833.

Introduction

Genetic aetiology of *PITX2* mutations and deletions in AR

To date, thirty-three point mutations of *PITX2* have been reported, nearly all of which either encode a truncated product or produce point alterations of the homeodomain (HD) (44-46, 103, 125-133). A number of chromosomal aberrations involving the *PITX2* locus have also been described, both in the form of cytologically visible deletions and as a result of translocations involving 4q25 (35, 134-138). 4q25 deletions provide the best evidence that simple haploinsufficiency of *PITX2* can result in AR. Haploinsufficiency therefore appears to be a plausible model for the pathogenicity of mutations such as *PITX2*(T68P), which is presumed to be a simple hypomorph due to defective DNA binding and transactivation (84, 104). Grossly increased *PITX2* activity number may also be pathologic, as duplication of a distal region of 4q2 (including 4q25) has been noted in one patient with hypoplasic left heart, atrial septal defects, and outflow tract abnormalities similar to those seen in *PITX2c* gene-targeted mice (139, 140). *PITX2* hyperactivity has also been noted for one AR-causing point mutation, (V83L), which transactivates reporter constructs significantly above wild-type levels (127). Both genomic rearrangements and point mutations therefore illustrate that an optimal level of *PITX2* function, defined between upper and lower thresholds of activity, is required for normal development of the anterior chamber. A similarly strict picture of dosage sensitivity has been described for *FOXC1*, duplications of which variously cause IH, IGD, and AR, and deletions or mutations of which primarily cause AR (111-115). A single case of AR in conjunction with deletion of the PAX6 homeobox gene, which typically causes aniridia, Peters' anomaly, or autosomal dominant keratitis, has been reported (141-144).

Rates of PITX2 and FOXC1 involvement in AR

In large samples of seventy or more patients with congenital anterior segment dysgenesis, the prevalence of *PITX2a* mutations appears to lie within the range of zero to ten percent (114, 126). *FOXC1* mutations are also found a comparable frequency (13%, n=70) in this broad clinical category (114). In our laboratory, only about 40% of AR cases are attributable to identifiable mutations of *PITX2* or *FOXC1*, and *FOXC1* mutations and duplications receive the lion's share with approximately 14% and 16% respectively (Dr. Michael Walter, personal communication). Numerous reports of

FOXC1 duplications have been published, but the commonly employed microsatellite PCR method is difficult to interpret decisively in single-patient pedigrees (113-115). The incidence of gene dosage changes at either locus has therefore not been comprehensively assessed in AR patients. By the best existing estimates, a majority of Axenfeld-Rieger malformation cases cannot be attributed to detectable mutations of either gene. A full appreciation of the aetiology of AR malformations would, in theory, necessarily require study of noncoding mutations or gene dosage alterations of *PITX2* and *FOXC1*, aberrations of yet-unidentified genes, and determination of the rate of stochastic and/or environmental causes. Of these causes, altered gene dosage is the most expedient avenue for investigation within our large collection of patient samples, in which only a few *PITX2* or *FOXC1* mutations are likely to be identified.

This chapter presents a gene dosage screen of *PITX2* in a panel of 81 patients with anterior ocular abnormalities and/or glaucoma, 64 of which have phenotypes previously associated with *PITX2* mutations (AR, IGD, IH, or an unspecified anterior segment dysgenesis). Concurrent with my own analysis, coding regions and splice junctions present in the *PITX2a* transcript were concurrently examined via sequencing; this work was partly performed in our laboratory by Kathy Kozlowski and Steven Kulak, and partially in the laboratory of Dr. Elise Héon at the University of Toronto. Comprehensive screening of the 81 individuals on our panel identified three novel mutations which were predicted to severely disrupt the primary structure of all four PITX2 isoforms (133). A detailed discussion of the mutations identified has been published, but the AR phenotypes of these patients are briefly revisited below to highlight the similar clinical effects of *PITX2* mutations and the microdeletions discussed within this chapter.

The first mutation encountered during analysis of our patient cohort was a heterozygous deletion of nucleotide G114 in exon III of *PITX2*. This change shifts the reading frame of *PITX2* from the first residue of the HD onwards, replacing the majority of the coding region with a lengthy nonsense peptide of 114 amino acids followed by a premature stop codon. The individual in which this mutation was found (patient 1) presented clinically with iris hypoplasia, posterior embryotoxon, corectopia, and glaucoma. No systemic findings were evident in this patient. A second individual (patient 2) was found to harbor a mutation of the *PITX2* exon III splice acceptor site. Patient 2 has bilateral polycoria, displaced 'pinpoint' left pupil, and irregular left iris contour, in conjunction with underdeveloped maxilla and redundant umbilical skin. A third *PITX2* mutation was identified in patient 3, who is a member of a four-generation AR kindred. Ocular findings in this family included iridocorneal adhesions, corectopia, polycoria, IH, iris atrophy, prominent Schwalbe's line, corneal guttata, and glaucoma. Sequencing identified a heterozygous deletion of nucleotide C416 within exon IV of PITX2. This mutation shifts the reading frame from residue T139 onwards, sparing the HD, and encodes a nonsense peptide of 15 residues followed by a premature stop codon. Of 64 cases of AR, IGD, or IH in our primary patient cohort, only three cases could be ascribed to detectable mutations of *PITX2a*. As I will discuss in the following chapter, real-time quantitative PCR analysis reveals a similar rate of gross *PITX2* deletion among the same group of patients, suggesting that wholesale loss of the 4q25 *PITX2* locus may be responsible for a small but significant proportion of cases of AR.

Methods

Human subjects

Written, informed consent was obtained from all studied subjects prior to enrolment in this study. The use of human subjects in this study was approved by the University of Alberta Health Research Ethics Board, in accordance with the tenets specified within the declaration of Helsinki. DNA banking at The Hospital for Sick Children (cases 4 and 5) was done in accordance with HSC Research Ethics Board-approved consent policies. Referring physicians completed a brief questionnaire detailing the ocular phenotype of each patient, and provided an EDTA blood sample suitable for DNA extraction. A previously obtained collection of 50 unaffected, unrelated spouses was used as a normal control panel to validate specificity of the qPCR assay.

Real-time quantitative PCR (qPCR)

A TaqMan fluorogenic PCR assay was used to quantitate the relative abundance of a target amplicon residing in the final (most 3') exon of *PITX2a*. All equipment and reagents indicated were obtained from Applied Biosystems (Foster City, USA). Each qPCR reaction contained 10pmol of forward and reverse *PITX2* primers (CAGTTCAATGGGCTCATGCA, CGGCCCAGTTGTTGTAGGAA) and 4pmol of a dual-label TaqMan probe (VIC-CCCTACGACGACATGTACCCAGGC-TAMRA). The *PITX2* sequence amplified by these primers was designed ABI's Primer Express software and verified to be unique via BLAST analysis. The target amplicon chosen is within a coding region of *PITX2*, so the preceding sequence analysis ruled out an underlying probe or primer site mutation in each patient.

Each reaction was internally controlled for template quality and quantity with a commercial TaqMan assay specific to the human *Connexin 40* (*Cx40*) gene on chromosome 1 (bearing 5' FAM and 3' MGB fluorochrome labels). Each sample was amplified in triplicate, 15μL reactions containing 25ng of lymphocyte DNA. Reactions were cycled in an ABI-9700 thermocycler with the 2x TaqMan kit as per instructions. The reaction mixture also included a passive fluorescent reference (ROX) ensuring normalised optical detection efficiency between wells. Each 384-well plate contained triplicate reactions of two unrelated normal samples and a DNA-free control. Reaction progress was recorded and analysed by the thermocycler software (SDS 2.0). *PITX2* gene dosage was determined by a relative quantification method. Briefly, rate of change in fluorescence (ΔF) in each well, during each cycle, at each reporter wavelength was charted. Threshold values (T) of ΔF were selected for the *PITX2* and *Cx40* probes such that a graph of ΔF was linear in all wells as ΔF approached T. The threshold cycle (Ct) at which ΔF reached T was determined for each reporter in each well. A Ct ratio (Ct_{PITX2}/Ct_{Cx40}) was generated for each reaction. A graph of Ct_{PITX2} versus Ct_{Cx40} (figure 2-1) yielded the expected linear correlation on a panel of 50 unrelated normal controls. Deletions formed a distinct line in which the normalized Ct_{PITX2} was one cycle greater than that of normal controls.

PITX2 dosage was inferred from Ct_{PITX2}/Ct_{Cx40} ratios as follows. The Ct ratios of the three runs of each sample were compared with the Ct ratios of both normal and PITX2-deleted controls using a t-test statistic. The relative likelihood that a given sample is PITX2-hemizygous is represented by the ratio of p-values derived from t-tests versus the deleted and normal sample populations. This relies on the reasonable assumption that Ct ratios measured from a given sample vary normally about a mean value. The tabulated qPCR dataset has been published (http://www.iovs.org/cgi/content/full/45/3/828/DC1) to facilitate independent analysis.

Microsatellite markers

Eight microsatellite markers were designed in the immediate genomic vicinity of PITX2. Briefly, each marker was genotyped via PCR amplification under the following conditions: 25µL total reaction volume, 2mM $MgCl_2$, one unit of Taq DNA polymerase, 35 cycles of [30s at 95°C, 30s at annealing temperature (T_A), 30s at 72°C]. Heterozygosity of each marker was estimated by genotyping six unrelated normal samples. The amplimers, T_A used, and estimated heterozygosity for each novel marker are given in table 2-1. I also genotyped affected individuals with the established markers GATA10G07, D4S2361, D4S1647, D4S2623, D4S2301, D4S2945, D4S193, D4S406, D4S1651, D4S2394, D4S1644, and D4S1625. Amplimer sequences of these markers are available from the Ensembl genome browser (http://www.ensembl.org/Homo_sapiens/) (145). PCR products were labeled during amplification by incorporation of α^{35}S-dATP (Amersham) and subsequently size-separated via 6% denaturing polyacrylamide gel electrophoresis. Gels were dried onto Whatman 3MM filter paper and autoradiograped with KODAK BIOMAX-MR X-ray film.

Table 2-1: Novel microsatellite markers near *PITX2*

Name	Amplimers	T_A (°C)	Heterozygosity
320d3-1	CAGAGGTAGGGTCCAGGTTG TGCAGAGCAATTCCTGTACCT	60	30%
320d3-2	TCAGTTGCATGAATGGAGGA ACCCTGGGACTTTGATGGAT	60	40%
320d3-6	TGTTTGGGTTCCCCAAGTAT CGAGATTGCCCCACTAAACC	60	35%
320d3-7	TGGGTGACAGAGCAAGACAA GGCTTATCAGGAGGGTCCA	60	90%
320d3-14	AAACACAAAGCCTCAACAGGA AAACACAAAGCCTCAACAGGA	53	80%
320d3-15	TGAATGGATAGCCTTCTCAG AAAGCACCAAGGACAACCAG	52	40%
320d3-16	GAAATGAATGGGTTCAGTGGA TCTGCAACATAAGTGGAGTCTCA	50	60%
320d3-17	TCCAGAGAGTGGGTTTCTGA GCCTGGGTGACAAGAACAAG	52	80%

Results

To estimate the contribution of PITX2 mutations and deletions in AR, I screened *PITX2a* gene dosage in a group of 81 probands with mixed clinical phenotypes involving abnormalites of the anterior segment and/or glaucoma. These cases were subdivided into two groups according to specific ocular findings. The primary panel contained 64 individuals bearing iris and iridocorneal angle anomalies classified as AR (39 samples), IGD (19 samples), IH (two samples), or an unspecified anterior segment dysgenesis (ASD) (4 samples). These phenotypes represent the range of common ocular phenotypes in patients bearing *PITX2* or *FOXC1* mutations (44-46). The remaining 17 samples comprised patients with nonmesenchymal anterior segment phenotypes, simple glaucoma, or multiple anomalies, as follows: Peters' anomaly (seven cases), sclerocornea (one case), congenital cataract with glaucoma (one case), corneal endothelial dystrophy (one case), or aniridia plus microdontia (one case), juvenile open-angle glaucoma (two samples), congenital glaucoma (two cases), primary open angle glaucoma (one case), and SHORT syndrome (one case), which is characterised by joint hyperextensibility, ocular depression, Rieger anomaly, and teething delay (SHORT syndrome, Mendelian Inheritance in Man [MIM] #269880).

Real-time qPCR and microsatellite studies of PITX2 dosage

Because some loss-of-function *PITX2* mutations are thought to cause AR via simple haploinsufficiency, we reasoned that this phenotype might also occur due to larger-order *PITX2* deletions in a subset of patients. In order to address this possibility, I developed a real-time qPCR-based assay to determine PITX2 gene dosage in a relatively high-throughput manner. qPCR-based screening of our entire panel identified three samples in which the abundance of an exon IV *PITX2* target amplicon was reduced by one-half relative to that of an internal control within the *connexin40* gene on chromosome 1 (figure 2-1). This apparent change in relative *PITX2* dosage could be attributed either to hemizygous deletion of *PITX2*, or to duplication of the *Cx40* internal reference in these patients. Patient 6, discussed below, was a member of a large kindred, and therefore afforded the opportunity to corroborate deletion of *PITX2* via standard linkage analysis. In order to confirm and determine the approximate extent of each deletion, I developed eight novel polymorphic microsatellite markers spanning a 1Mb interval containing the *PITX2* locus. Genotyping of these markers, and of twelve

Figure 2-1: Real-time qPCR analysis of *PITX2* dosage

Top panel: Sample output of a qPCR experiment. Graph illustrates triplicate PCR reactions of two samples, one of which is hemizygous for *PITX2*. X-axis: reaction progress (cycles). Y-axis: change in fluorescence emission (arbitrary logarithmic units). Threshold cycle (Ct) is defined as the X-axis value at which the amplification curve crosses the threshold shown. Each run of a given sample produces two Ct values (*PITX2* and *Cx40*); *Cx40* is used as an internal normalization control for quantity and quality of template DNA. In the case shown, both samples are present at equal concentration (*Cx40* amplification curves overlap). Note *PITX2* amplification is delayed by one cycle in the deleted sample.

Bottom panel: Specificity of *PITX2* qPCR illustrated by Ct_{PITX2} versus Ct_{Cx40} scatterplot for fifty normal (spousal) control samples and *PITX2* deletion patient 6. Reactions were conducted in parallel triplicate. A best-fit line is shown for both normal samples and for patient 6; points in the upper right represent more dilute (or lower quality) samples. Note that patient 6 is displaced from the normal controls by one cycle, corresponding to a twofold relative decrease in concentration of the *PITX2* target amplicon.

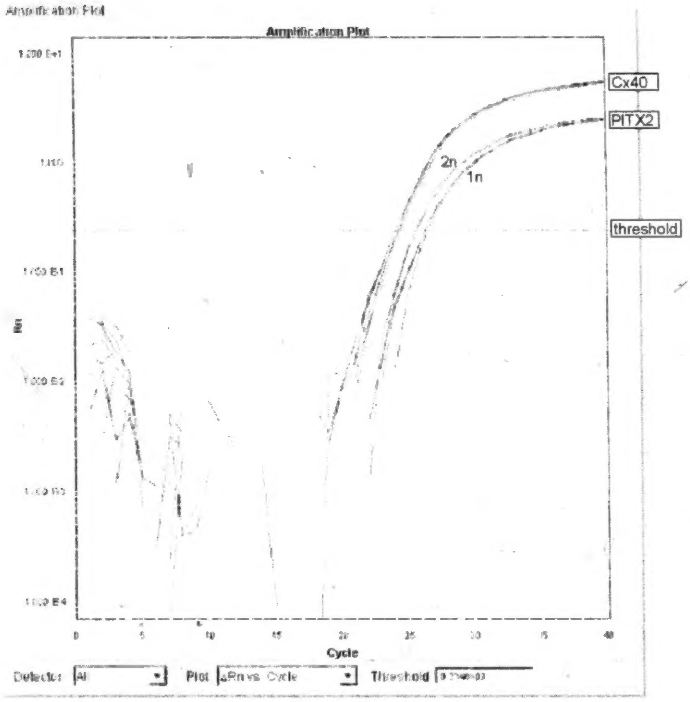

Amplification Plot
Amplification Plot
1.000 E+1
1.000
1.000 E-1
Rn
1.000 E-2
1.000 E-3
1.000 E-4
0
5
10
15
20
25
30
35
40
Cycle
Cx40
PITX2
2n
1n
threshold

Detector All

Plot ΔRn vs. Cycle

Threshold [illegible]

Specificity of real-time *qPCR PITX2* dosage assay

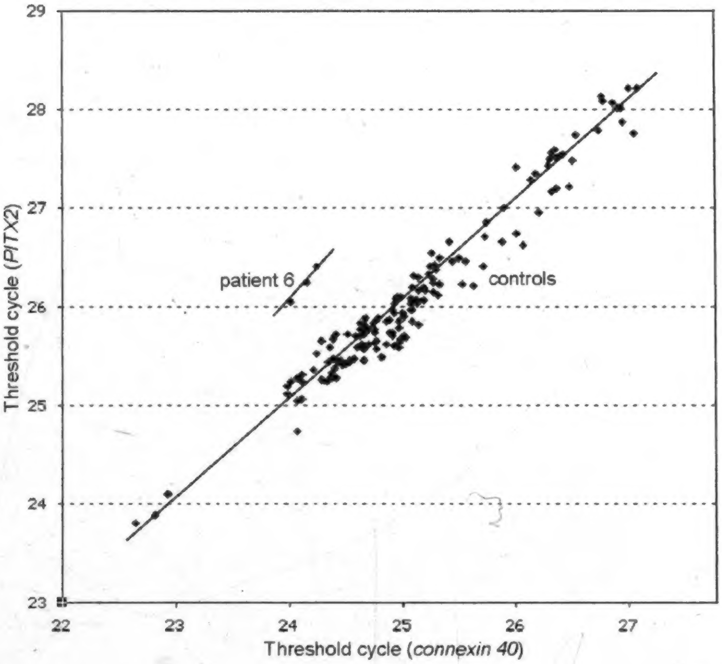

established chromosome 4q markers (detailed in Methods) produced a contig-level map of each deletion (figure 2-2). The clinical and molecular details of each deletion are discussed briefly below.

Patient 4 has an atypical AR phenotype in which corectopia, prominent line of Schwalbe, and iridocorneal adhesions are accompanied by the additional feature of bilateral, anterior polar cataracts. The maximal deleted interval in this patient is bounded by the heterozygous markers 320d3-2 and D4S2394, which flank a region extending 19.3Mb telomeric of PITX2. The centromeric breakpoint of this patient's deletion presumably liesin the 5kb interval between 320d3-2 and the *PITX2* target amplicon in exon IV. It is formally possible that this deletion therefore spares the extreme 3' aspect of *PITX2*.

Patient 5 has pronounced AR malformations including bilateral iris atrophy, posterior embryotoxon, iridocorneal adhesions, miosis, corectopia, and left polycoria. Other features include pointed and maloccluded teeth, as well as redundant periumbilical skin. Interestingly, this patient has markedly short stature, being, at age six, only three inches taller than a two year-old sibling. Patient 5 has deep-set eyes and a prominent mandible, which are also features of SHORT syndrome (MIM#269880). His hearing and speech are normal. This patient's deletion spans a region containing PITX2, with both breakpoints located in the 1.24Mb interval between D4S2623 and D4S1651. This interval contains PITX2, human epidermal growth factor (EGF), long-chain fatty-acyl elongase (LCE), Glutamyl aminopeptidase (ENPEP), and two predicted EST transcripts, denoted ENSG00000164092 and ENSG00000168999 in the Ensembl database (35). The one *bona fide* SHORT syndrome sample on our panel displayed normal PITX2 dosage, so this disorder may, like AR, be genetically heterogeneous if it is indeed part of the same phenotypic continuum. Both pituitary anomalies and short stature due to pituitary growth hormone insufficiency have previously been described in patients with ocular and dental findings of AR, and short stature does occur at reduced penetrance in some AR pedigrees (20, 21, 54).

Patient 6 is an affected member of a large pedigree in which AR cosegregates with a hemizygous deletion of PITX2. Familial haplotyping (Figure 2-3) delineated a maximal deletion of (at most) 417kb, bounded telomerically by 320d3-6 and centromerically by D4S2945. This places the deleted segment well beneath the range visible by cytological staining. The maximal 417kb interval includes PITX2, ENPEP, and ENSG00000164092, and does not include EGF or LCE. Null alleles of the PITX2-

Figure 2-2: Microsatellite hemizygosity mapping of *PITX2*-containing deletions

Each qPCR-detected deletion was physically mapped by identifying the nearest heterozygous markers 5' and 3' of *PITX2* respectively. The maximum possible extent of a contiguous deletion including the *PITX2* locus is shown for each proband (boxed region). Haplotyping of the extended family of patient 6 (Figure 2-3) was used to further define the deleted interval in this family. Nucleotide positions given were derived from the ensembl chromosome 4 supercontig assembly as of March 2003 (145). Heterozygosity of novel markers generated for this study was estimated prior to use by typing five to ten normal control samples. Diamonds indicate microsatellite markers, while the position of the PITX2 quantitative PCR probe is indicated by a star.

Individual marker genotypes are color-coded as follows:
Open symbols: heterozygous markers
Grey symbols: homo-or hemizygous markers
Black symbols: deletion evidenced by qPCR or null allele revealed by haplotype analysis
N: haplotype analysis demonstrates normal copy number at this homozygous position

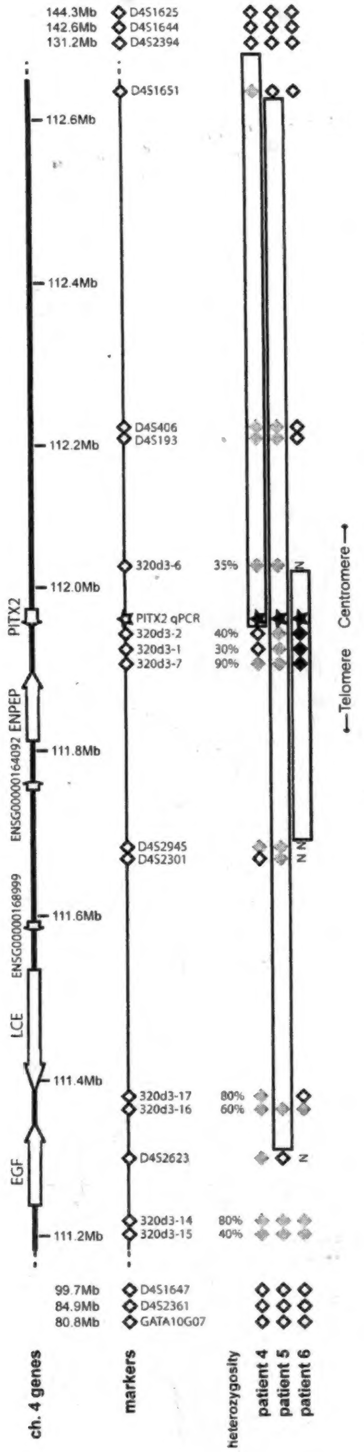

ch. 4 genes
markers
heterozygosity
patient 4
patient 5
patient 6
144.3Mb
142.6Mb
131.2Mb
112.6Mb
112.4Mb
112.2Mb
112.0Mb
111.8Mb
111.6Mb
111.4Mb
111.2Mb
99.7Mb
84.9Mb
80.8Mb
D4S1625
D4S1644
D4S2394
D4S1651
D4S406
D4S193
320d3-6
PITX2 qPCR
320d3-2
320d3-1
320d3-7
D4S2945
D4S2301
320d3-17
320d3-16
D4S2623
320d3-14
320d3-15
D4S1647
D4S2361
GATA10G07
35%
40%
30%
90%
80%
60%
80%
40%
PITX2
ENPEP
ENSG00000164092
ENSG00000168999
LCE
EGF
N
N
N
N
Telomere
Centromere

Figure 2-3: Haplotype analysis illustrating cosegregation of del(PITX2) and AR in the kindred of patient 6

Top panel: Maximally parsimonious haplotypes were inferred from microsatellite genotypes where possible. Because the region haplotyped spans only ~750kb of genomic sequence, recombination was not considered. Each presumed chromosome is depicted as a boxed grouping of alleles; haplotypes of III-9 and III-13 could not be established because of missing parental genotypes. Null alleles (symbol Δ) were identified at several markers in affected individuals, and were transmitted in phase with the *PITX2* qPCR deletion. Asterisk indicates patient 6.
N: ophthalmically examined normal individuals
Question marks: at-risk individuals not clinically ascertained

Bottom panel: Sequencing gel autoradiographs illustrating the raw data used in the above analysis. The two lanes marked 'unrelated' are affected members of an unrelated AR kindred.

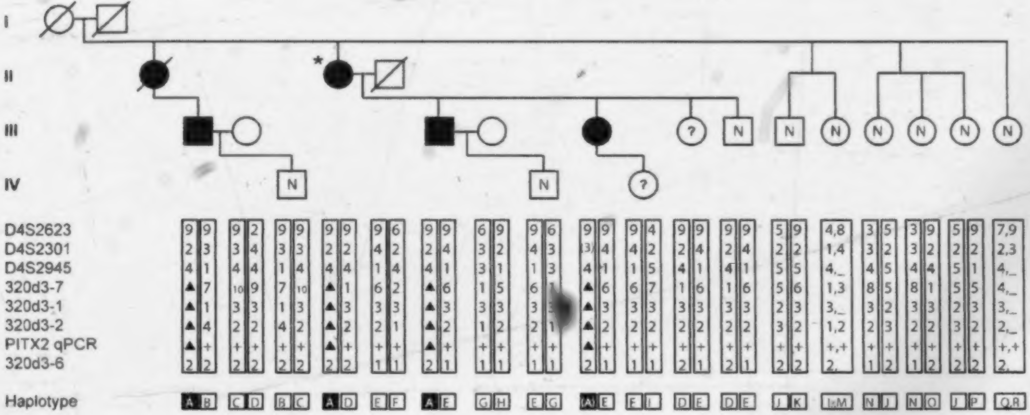
I
II
III
IV
N
?
D4S2623
D4S2301
D4S2945
320d3-7
320d3-1
320d3-2
PITX2 qPCR
320d3-6
Haplotype

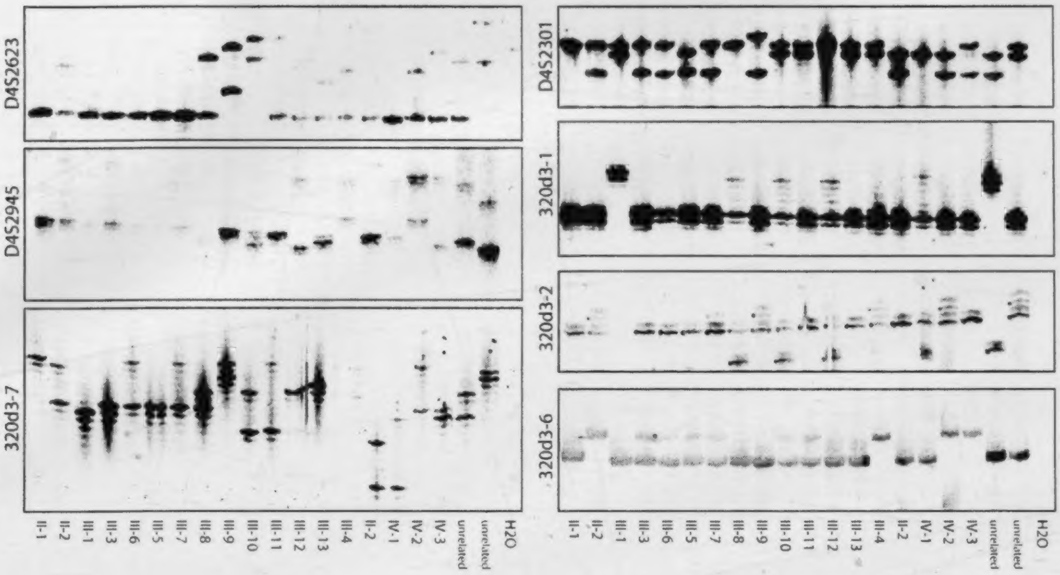
D4S2623
D4S2945
320d3-7
D4S2301
320d3-1
320d3-2
320d3-6
II-1
II-2
III-1
III-3
III-6
III-5
III-7
III-8
III-9
III-10
III-11
III-12
III-13
III-4
II-2
IV-1
IV-2
IV-3
unrelated
unrelated
H2O

adjacent microsatellites 320d3-7, 320d3-1, and 320d3-2 were shown to cosegregate with affected status in this family, providing independent confirmation of a genomic deletion of at least 24kb between 320d3-7 and the *PITX2* target amplicon.

Discussion

Phenotype of *PITX2* mutations versus deletions

Sequencing and qPCR analyses of the *PITX2* gene on 4q25 in 81 patients with anterior segment and/or glaucoma phenotypes identified three mutations and three gross deletions of *PITX2* (133). Perhaps unsurprisingly, *PITX2* deletions and mutations were found only in AR patients, rather than in patients with diagnoses of Peters' anomaly or simple glaucoma. Patients with *PITX2* microdeletions manifested with AR rather than lesser phenotypes such as IGD or IH, in keeping with the relatively severe phenotype of published interstitial 4q25 deletions and translocations (35, 134, 138, 146). Mutations and deletions of *PITX2* caused similar ocular phenotypes with a range of systemic (dental and umbilical) findings, consistent with the suggestion that many *PITX2* point alleles are functionally null. It is interesting to note, however, that patients bearing wholesale deletions of *PITX2* had a handful of additional clinical features not typically noted in AR. For instance, the bilateral cataract of *PITX2* deletion patient 4 may suggest involvement of surface ectoderm-derived structures in this patient, although AR malformations are presently thought to be exclusive to the mesenchymal lineage (20, 147). Mutations of *PITX2* are reported (rarely) in conjunction with ectodermal eye malformations characterized as Peters' anomaly (125, 126). A single instance of *PAX6* deletion in AR suggests that this factor, which typically causes aniridia or iridolenticular defects such as Peters' anomaly, can also affect the genesis of mesenchymal anterior segment structures (142, 143). Although these clinical entities are generally distinct, cataract and/or Peters' anomaly in AR may reflect reciprocal signaling between the lens and immigrating mesenchyme during development.

The possible hypopituitarism of patient 5 is a second unanticipated finding in a *PITX2* deletion patient, and may suggest that SHORT syndrome is a rare phenotypic variant within the AR spectrum of disorders. The most obvious role for PITX2a in growth control is its involvement in pituitary development and growth hormone (GH) expression. PITX2a and the pituitary homeodomain PIT-1 can synergistically activate reporter constructs derived from the GH promotor, while five PITX2a mutants are deficient in this respect (59). Furthermore, in gene-targeted mice, *PITX2* promotes commitment and expansion of both the pituitary gland as a whole, and of the GH-expressing somatotrope lineage in particular (52, 57). Small body size is one of many phenotypic features noted in heterozygous *PITX2* gene-targeted mice (52). Two patients within our cohort had clinical features consistent with SHORT syndrome (short stature, characteristic facial appearance, and AR), yet only one demonstrated an identifiable *PITX2* deletion or *PITX2 / FOXC1* mutation. This disorder, like AR, may therefore be genetically heterogenous, if indeed these two syndromes are nonallelic.

Estimates of prevalence

Among AR, IGD, IH, and ASD patient samples on our panel, six of sixty-four (9.4%) individuals carried an identifiable *PITX2* deletion or mutation. Importantly, the number of *PITX2* microdeletions was comparable to that of point mutations in our sample. Two previous screens of *PITX2* in large anterior segment dysgenesis cohorts have previously estimated the prevalence of mutations in the neighbourhood of zero to ten percent (114, 126). Our findings similarly support a limited prevalence of *PITX2* mutations and deletions in AR. Moreover, it appears that mutation screening alone may be failing to recognise a significant proportion of PITX2-associated anterior segment malformation cases due to *PITX2* dosage alterations. Real-time qPCR may therefore offer a second, straightforward approach to patient diagnostics at the *PITX2* locus.

Chapter three:

Physical interaction, colocalisation, and subnuclear distribution of PITX2 and FOXC1

Introduction

Possible importance of the PITX2 HD in protein interactions

Protein-protein interactions of PITX2 are likely to impinge heavily on both its target specificity and mechanism of transactivation within the cell nucleus. Self-interaction, in particular, is a crucial aspect of PITX2's cooperative DNA binding activity (originally discussed on page 27). Unfortunately, the lack of a solved structure for PITX2 necessitates the use of models based on paralogous homeobox proteins.

PITX2 is often discussed in terms of the classical *Drosophila* morphogen Bicoid, which, like PITX2, is a K50 homeodomain that effectively binds TAATCC elements *in vitro* (84, 89). Both Bicoid and PITX2 can bind DNA cooperatively, and both proteins self-interact in biochemical assays (90, 91, 102). Self-interaction of Bicoid is required for cooperative DNA binding, and is mediated by sequences lying outside of the HD (91). This type of model represents one possible explanation for the cooperativity of PITX2. In terms of phylogeny, however, the HD of Bicoid may not be the best available model for that of PITX2, which more closely resembles the HD of the *Drosophila* morphogen Paired (see figure 1-6, page 21). Paired belongs to a homeoprotein subfamily whose members have the seemingly unique ability to dimerise via a symmetrical protein-protein interaction intrinsic to the HD (82). Paired-like HD dimerisation allows cooperative binding to palindromic TAATNNNATTA or TAATNNATTA (P3 and P2) elements *in vitro*, and the structure of the resulting homeobox dimer-DNA ternary compex has been determined at high resolution (82, 83). Sequences of the *Drosophila* Paired HD that form the inter-HD and HD-DNA interfaces are extremely well conserved in PITX2 (figure 1-7, page 25). On the basis of homology and structural data alone, we might therefore suspect the PITX2 HD to possess an intrinsic potential for self-interaction.

Sufficiency of the PITX2 HD for dimerisation has not been tested to date, but two-hybrid analysis reveals that the HD and C-terminal majority of the protein make distinct contributions to self-interaction with full-length PITX2a baits (102). Moreover, two patient mutations of the homeodomain (T68P and K88E) respectively decrease and increase the affinity of PITX2 dimerisation in the same system (102). In EMSA experiments, PITX2's isolated HD can bind dimerically to substrates bearing even single TAATCC elements, although monomeric binding predominates (101).

The following chapter is concerned with the protein-protein interactions and subnuclear localisation of PITX2a and its mutant alleles. In order to study the importance of the HD and DNA binding in PITX2 dimerisation, I have examined heterodimerisation of differentially tagged PITX2a constructs via immunoprecipitation (IP) in a recombinant expression system. Several AR-causing mutations were tested and appeared not to grossly affect the strength of mutant-wild-type heterodimerisation, suggesting that DNA binding is of limited importance in PITX2a-PITX2a interactions. My biochemical studies have also produced evidence of a physical interaction between PITX2a and FOXC1, implying a common molecular pathway is likely responsible for the AR malformations caused by mutations of either gene. The final part of this chapter is concerned with the localisation patterns of FOXC1 and PITX2a within the cell nucleus, which provide a context for PITX2a-PITX2a and PITX2a-FOXC1 interactions.

Studied patient alleles of PITX2

Both wild-type PITX2a and five previously characterized AR-associated variants were biochemically examined in experiments presented below. A general overview of the clinical and molecular features of each allele is provided below and in table 3-1. In general, the studied patient alleles are grouped into three distinct categories (hypomorph, hypermorph, and dominant negative) on the basis of discrete functional deficits in DNA binding, transactivation, and/or nuclear localization:

The AR-causing T68P mutation of PITX2 introduces a proline at the third residue of helix II of the homeodomain (44). While this position is not highly conserved among homeoproteins, a proline at this position is likely to prevent formation of α-helix II and exert a global effect on homeodomain structure. PITX2 (T30P) binds DNA poorly and with reduced specificity, and drives reporter expression weakly or not at all (84, 103, 104). This mutation does not affect DNA binding of wildtype PITX2a *in trans* and therefore results in a hypomorphic rather than dominant negative allele (103).

A second AR-causing allele, R91P, also introduces a proline residue into a critical alpha-helix of the homeodomain, this time at position 12 of helix III (44). Unsurprisingly, this mutant protein also demonstrates defective DNA binding and transactivation (104), although by one account DNA binding is reduced rather than ablated (59). PITX2a (R91P) has been described as a dominant negative mutant based on its suppression of wildtype PITX2a transactivation of the human PRL, GH and PIT1 reporters in both reporter assays and cell culture (59). Whether this protein represents a *bona fide* dominant negative or a simple hypomorph remains undetermined.

Table 3-1: Patient alleles of PITX2a studied

Phenotype	Allele	DNA binding	Activity*	Locale**	Type
AR	T68P	virtually nil	nil	80% nuclear	severe hypomorph
AR	R91P	virtually nil	nil	40% nuclear	severe hypomorph? dominant negative?
AR	V83L	reduced slightly	230%	nuclear	hypermorph
AR	K88E	virtually nil	nil	not published	dominant negative
IH	R84W	reduced	40%	80% nuclear	hypomorph

* Activity defined as a proportion of the reporter transactivity exhibited by wild-type PITX2a constructs. Where stated as 'nil', the estimated transactivity is not significantly different from that of reporter alone.

** Percentage given is the proportion of cells in which exclusively nuclear staining is seen as per (104). This has been only qualitatively studied for V83L (127).

A third substitution, V83L, produces AR malformations despite only subtly modifying the primary structure of PITX2a. This mutation results in the loss of a single methyl group from the sidechain of valine 83, which is predicted to lie on the hydrophilic face of helix III(127). The DNA-binding affinity of this mutant is marginally decreased (in some experiments by as little as one-half). Interestingly, PITX2a (V83L) displays more than twofold the transactivity of wild-type PITX2a in reporter assays (127). Phenotypically, the V83L mutation causes the full ocular, dental, and umbilical findings of AR, illustrating that hypermorphic PITX2 mutations may also perturb normal development of the anterior chamber.

A fourth homeodomain missense mutation, K88E, is considered a dominant negative allele of PITX2 (102, 103). This mutation causes a charge reversal at position 50 of the homeodomain (residue nine of helix III), which mediates interactions with the latter two bases of the *bicoid* binding consensus (TAATCC) and is crucial for HD binding specificity (81, 89). The K88E allele is functionally null in terms of DNA binding and transactivation (103). However, PITX2a(K88E) dominantly suppresses wild-type PITX2a activity on reporter constructs containing tandem *bicoid* binding sites (102). In two hybrid experiments, PITX2a(K88E) forms mutant-wild-type heterodimers with enhanced affinity but reduced DNA-binding cooperativity (102). These data are consistent with a view of PITX2(K88E) as an inactive protein that antagonizes the wild-type via nonproductive protein-protein interactions.

The fifth and final PITX2 mutation tested, R84W was originally identified in a family with iris hypoplasia (45). This allele retains both DNA binding and approximately 40% of wild-type transactivity in reporter assays, suggesting that it is both functionally and phenotypically the least severe hypomorphic allele examined (104). PITX2 (R84W) was examined by immunofluorescence only, while the remaining four alleles listed were studied by both immunofluorescence and biochemical methods in the following experiments.

Methods

Where not explicitly stated, the compositions of all reagents employed in the following procedures may be found in appendix A.

Expression constructs

N-terminally epitope-tagged, 6xHisXpress fusion proteins were expressed in pcDNA4 His-Max A (Invitrogen). pcDNA-PITX2a and mutant constructs T68P, R91P, V83L, K88E, and R84W were obtained from Kathy Kozlowski; all have been previously published with the exception of K88E (104, 127). Apart from the point mutations indicated, all six constructs are identically built into the BamHI site of pcDNA4A. This resulting construct encodes a 317aa, 35.5kDa fusion protein with 34 vector-derived amino acids and a further twelve residues produced by read-through of the PITX2 5' untranslated region, followed by the peptide sequence of PITX2a proper.

N-terminally flagged hemagglutinin epitope (HA)-PITX2 fusion proteins were expressed in pCI-HA, which which was provided courtesy of Dr. Dallan Young. pCI-HA is a pCI contruct containing a Kozak translation initiation consensus and HA epitope between the NheI and EcoRI sites of pCI (Promega). pCI-HA-PITX2a was produced by Kathy Kozlowski, who subcloned the insert from pcDNA-PITX2 into the EcoRI site of pCI-HA with a short intervening EcoRI to BamHI linker. I subsequently derived the T68P, R91P, V83L, and K88E alleles of this construct by subcloning the homeodomains of the corresponding pcDNA constructs into pCI-HA-PITX2. The HA-PITX2a fusion is 306aa and 34.1kDa, and encodes 23 vector-encoded residues and twelve residues produced by read-through of the PITX2 5' untranslated region, followed by the peptide sequence of PITX2a. The precise peptide sequence encoded by this construct is given in appendix B.

N-terminally tagged 6xHisXpress::FOXC1 fusion proteins were expressed in pcDNA4 His-Max B. The construct used was assembled by Ramsey Saleem and has been previously described in detail (116). The panel of 6xHisXpress-fused FOXC1 deletion constructs used in figures 3-2 and 3-3 were assembled by Fred Berry and have similarly been published (123).

Enhanced green fluorescent protein (eGFP) FOXC1 fusion protein was expressed by subcloning FOXC1 into pEGFP-N1 (Clontech). This construct

(FOXC1GFP) was assembled by Ramsey Saleem and has been previously described (123).

Cell culture and transfection

Cos-7 cells were maintained in Dulbecco's modified Eagle's medium (DMEM) containing 10% (v/v) fetal bovine serum and 1% (v/v) antimycotic (Sigma) in a 37°C, humidified incubator under an atmosphere containing a constant 5% CO_2. The day prior to transfections, plates were seeded (10^6 cells in 10mL media per 100mm dish or 6x25mm multi-well plate) so as to reach approximately 30-50% confluence the following day. Transfections were performed using FuGene 6 reagent (Roche); 3μL of reagent and 500ng of DNA were used per 25mm tissue culture well, as per manufacturer's protocol. Transfections of larger cultures were scaled-up according to surface area, such that transfections of 100mm dishes were performed with 24μL FuGene reagent and 4μg DNA. Exact amounts of each expression construct transfected varied by experiment and are indicated in the corresponding caption for each figure in the Results section. All constructs transfected during a given experiment were quantitated via spectrophotometry immediately prior to transfection; where possible, plasmid maxipreps were performed in parallel in order to minimize variations in DNA quality.

Lysate preparation

Transfected cells were harvested three days post-transfection in order to allow optimal expression of recombinant proteins. Briefly, plates were rinsed three times in phosphate-buffered saline (PBS) at 25°C and harvested in a total of 1mL PBS containing protease inhibitors (PBS-PI) on ice. All subsequent steps were performed at 4°C. A cell pellet was obtained via microcentrifugation at 3000 RPM for 10minutes. The pellet supernatant was removed, and a whole-cell lysate obtained by suspending the pellet in 200μL radioimmunoprotection assay buffer containing protease inhibitors (RIPA-PI). Samples were vortexed briefly and incubated on ice for 45 minutes to allow maximal nuclear lysis. Lysates were cleared of cell debris by microcentrifugation at 13000 RPM for 10 minutes, and assayed for total protein concentration via Bradford dye-binding assay [Bio-Rad] as per standard protocol (148). Lysate concentrations were equalized in a fixed volume of RIPA-PI prior to immunoblot analysis of immunoprecipitation inputs.

Immunoprecipitation (IP)

IPs were performed using epitope tag-specific antibodies; immune complexes were subsequently recovered on protein G-agarose (pG) resin (Sigma). Each putative interaction was confirmed in reciprocal IP experiments performed on the same lysates in parallel. Equalised lysates were first analysed for comparable construct expression via immunoblot of 1-8% of the total input protein. Exact concentrations of sample protein and antibody used in IPs are indicated for each experiment in the corresponding figure caption within the Results section.

IP reactions were kept at 4°C through the entire protocol until elution from the pG resin. Prior to use, pG beads were blocked in PBS containing 1% (w/v) BSA for one hour, and washed three times briefly in RIPA. Lysates were diluted to a total volume of 1.5mL in RIPA-PI. Abundant and nonspecifically interacting proteins were pre-depleted from the lysate by adding 100μL of a 50% suspension of blocked pG beads, incubating for two hours, and removing the beads via microcentrifugation at 13000 RPM for 10 minutes. The resulting pre-cleared lysates were split into two equal (~700μL) portions for reciprocal IPs. IPs were conducted overnight in a total of 1-1.5mL RIPA-PI containing approximately 2μg of primary antibody. Immune complexes were recovered by adding 60μL of a 1/3 (v/v) suspension of blocked pG beads in RIPA to each reaction and incubating for one hour with gentle mixing. Reactions were microfuged gently at 3000 RPM for 7 minutes in order to pellet the pG resin. The first supernatant (containing unbound components of the lysate) was removed with a sterile $26_{5/8}$-gauge syringe and set aside at -80°C. The pG resin was then batch-washed five or more times with 1mL of RIPA-PI. After each ~10 minute wash, samples were microfuged at 3000 RPM for 7 minutes, and supernatants carefully removed with a dedicated syringe. Final elution of bound immune complexes from the beads was accomplished by completely removing RIPA-PI wash buffer, adding 25μL of 2x SDS loading buffer, vortexing briefly, and heating to 95°C for five minutes. Samples were briefly mixed and immediately analysed via immunoblot.

Immunoblot analysis

Samples were separated via reducing 10% polyacrylamide Laemmli gel electrophoresis on a Protean 3 minigel system [Bio-Rad] as per standard protocols (149). Samples were run at a constant 100V for 90 minutes. A prestained protein size marker [New England Biosciences] was used to follow both electrophoresis and transfer.

Gels were blotted onto nitrocellulose membrane [Bio-Rad] using a protean 3 semidry transfer apparatus [Bio-Rad] for 60 minutes at a constant 350mA (approximately 100V) at 4°C in transfer buffer.

Following transfer, all of the following steps were performed at room temperature. Efficient transfer was confirmed by Ponceau S stain (Sigma), and by noting complete transfer of the prestained protein marker lane to the membrane. Blots were blocked in TBST containing 5% (w/v) skim milk powder for one hour. Primary and secondary (HRP-conjugated) antibodies were hybridized to blots in TBST, 5% milk; exact antibody concentration and incubation conditions are specified for each experiment in the corresponding Results section. Following primary hybridization, blots were briefly rinsed three times in TBST and washed six times for five minutes in TBST with agitation. Following secondary hybridization, blots were briefly rinsed three times in TBST and washed four times for five minutes in TBST with agitation. Finally, blots were rinsed once in TBS in order to remove Tween.

HRP-conjugated secondary antibody signal was visualized using SuperSignal West Pico chemiluminescent substrate (Pierce) according to manufacturer's instructions. Blots were exposed to medical X-ray film (Fuji) for various intervals and developed using an M35A X-OMAT automatic film processor (Kodak).

Immunofluorescence

Immunofluorescence was performed three days following transfection of cells plated onto sterile coverslips (1.67x10^5 cells per 25mm well). Specific details of the transfection and antibody hybridization conditions used in each experiment are specified in the corresponding figure caption in the Results section. Plates were kept in the dark at all possible times during the protocol so as to prevent photobleaching of eGFP and fluorochrome-conjugated secondary antibodies.

Cells were rinsed three times in 1xPBS at room temperature to remove media and fixed for 10 minutes in PBS containing 4% w/v paraformaldehyde. Coverslips were rinsed three times in PBS to remove fixative. Three 5-minute washes in PBS containing 0.1% (v/v) Triton X-100 were performed to permeablise cell and organellar membranes. Nonspecific protein interactions were quenched by incubating the coverslips in PBS containing 5% (w/v) bovine serum albumin (BSA; Sigma) for one hour. Coverslips were rinsed twice briefly in PBS containing 1% BSA (PBSA).

For each coverslip, 80μL of PBSA containing primary antibodies at the appropriate concentrations was spotted onto sterile paraffin film. Each coverslip was then carefully removed from its tissue culture well, and placed, inverted, on the bead of primary antibody solution. Primary antibody incubations were conducted for one hour at room temperature, after which coverslips were returned to their corresponding culture wells. Unbound antibody was removed via six five-minute washes in PBSA. Secondary antibody incubations were subsequently conducted in similar fashion, for one hour at room temperature. Bisbenzimide 33342 (Hoechst; Sigma) staining, if performed, was accomplished by adding 50μg/mL Hoechst to the secondary antibody dilution. Coverslips were again rinsed twice for five minutes in PBSA and twice in PBS to remove unbound antibody and/or Hoechst.

Coverslips were mounted onto precleaned glass slides in freshly prepared mounting medium (9:1 glycerol:PBS, 5mM p-phenylenediamine added as antifadant). Nail polish was used to seal mounted slides.

Microscopy and cell imaging

Mounted coverslips were examined by indirect epifluorescence using a Leica DMRE microscope with PL-FLUOTAR 100x oil objective (Leica) adjusted to a numerical aperture of 0.60. Only rounded, intact interphase nuclei with representative staining patterns were imaged. Signals were imaged separately using the following band-pass filtersets (Chroma Technology): 31000 (Hoechst or AMCA signals), 31002 (Cy3), or 41001 (Cy2 or GFP). Captures were performed with a QICAM 10-bit mono CCD camera (QImaging) directed by the Northern Elite imaging suite (Empix imaging). Camera gain was set at a fixed 30% and exposure time was adjusted to produce optimal contrast without oversaturating the image. Channel input and output levels were carefully adjusted for optimal signal detail and background. False-colour merges were produced, and all three colour planes were carefully aligned during post-processing where required. No deconvolution or other digital manipulation of the images was performed.

The linescan analyses shown in figures 3-7 through 3-9 were conducted in NIH image (National Institutes of Health, USA). A diagonal line passing through each nucleus was selected, and RGB densities of each channel (values from 0 to 255) plotted for each point along this line. The data from each channel were normalized to the maximum density of that channel, and the resultant density plots were superimposed to produce the graph shown.

Results

Dimerisation properties of wild-type and mutant PITX2a

It has recently been determined that PITX2 can bind DNA as a dimer, and that, like Bicoid, PITX2a cooperatively binds substrates bearing tandemly repeated TAATCC elements (50, 102). Involvement of the homeodomain in PITX2a dimerisation is suggested by at least one homeobox mutation (K88E), which increases the affinity of mutant-wild-type protein interactions (102). Moreover, mapping of the PITX2a homeodomain onto a cooperative homeodomain dimer (Q50 Paired) revealed that sequences of the homeobox which form protein-protein and protein-DNA contacts in Paired are virtually identical in PITX2 (figure 1-7). We therefore elected to further investigate the role of the HD in PITX2a dimerisation, using a well-characterised panel of patient alleles (T68P, R91P, V83L, and K88E) associated with anterior segment malformations. These four mutant alleles vary in both severity and type of functional deficit(s) in transactivation and DNA-binding assays. PITX2a (T30P), for instance, neither binds DNA nor transactivates in reporter assays (104). The R91P and K88E proteins have similar deficits but have been described as dominant negative alleles in single reports (59, 102, 104). The V83L allele is seemingly unique in that it represents the only hyperactive allele of PITX2 yet described (127). We predicted that any or all of these mutations may alter homeodomain-specific protein-protein interactions of PITX2a, if such an activity indeed exists.

I biochemically confirmed the published PITX2a-PITX2a interaction as follows: 6xHisXpress-tagged constructs of all five of the above PITX2a constructs were each coexpressed with HA-tagged wild-type PITX2a in cos-7 cells. Reciprocal IPs conducted with either α-HA or α-Xpress were used to determine the degree of HA-PITX2a - Xpress-PITX2a heterodimerisation exhibited by each mutant construct (Figure 3-1). Dimerisation of the wild-type protein was demonstrated in this system, as HA-PITX2a was recovered by α-Xpress IP in an Xpress-PITX2a-dependant fashion. The reciprocal IP experiment verified this interaction, as Xpress-PITX2a was precipitated by α-HA only when coexpressed with HA-PITX2a. Mutations of the homeodomain did not greatly affect the heterodimerisation properties of wildtype, T68P, R91P, V83L, and K88E forms of Xpress-PITX2a, as each construct tested was at least qualitatively able to interact with wildtype HA-PITX2a. It should be noted that relatively subtle differences in heterodimerisation affinity may be beneath the discriminating power of this (admittedly

Figure 3-1: Reciprocal immunoprecipitation (IP) of wild-type and mutant PITX2a

Cos cell cultures (1×10^6) were cotransfected with 2μg of [pCI-HA-PITX2a wild-type or empty PCDNA4], and 2μg of [pcDNA4-PITX2a wild-type, mutant, or empty vector] as indicated. Lysates were assayed for relative expression levels (top panel) prior to IP. IP reactions contained 100μg of whole-cell lysate in a total buffer volume of 1.5mL. Reactions were incubated for 16h at 4°C, in the presence of either mouse α-Xpress (2.2μg) or rabbit α-HA (2μg). Please note that the sample load order is different for the top and middle panels; refer to sample numbers above each lane.

Wild-type and mutant Xpress-PITX2a proteins were precipitated by α-HA, in an HA-PITX2a-dependent fashion (middle panel), confirming an interaction. Similarly, Xpress-PITX2a mediated recovery of HA-PITX2a by α-Xpress (lower panel). Additional Ig bands in the α-Xpress IP output were due to inadvertent cross-reaction of the goat α-rabbit-HRP, used for immunoblot analysis, with the mouse α-Xpress used for IP. All five (wild-type, T68P, R91P, V83L, and K88E) PITX2a constructs were seen to interact with wild-type PITX2a in this assay. Both 32.5kDa and 65kDa forms of PITX2a were observed post-IP, as well as in the unpurified inputs. The latter band was not expected and may represent incompletely dissociated PITX2a dimer. This likelihood is addressed in appendix D.

Immunoblot probing conditions:
8% input:
    rabbit α-HA 1:500 16h 4°C; HRP goat α-rabbit IgG 1:3000 1h 25°C
    mouse α-Xpress 1:5000 16h 4°C; HRP goat α-mouse IgG 1:3000 1h 25°C
IP α-HA:
    mouse α-Xpress 1:5000 3h 25°C; HRP goat α-mouse IgG 1:3000 1h 25°C
IP α-Xpress:
    rabbit α-HA 1:500 3h 25°C; HRP goat α-rabbit IgG 1:3000 1h 25°C

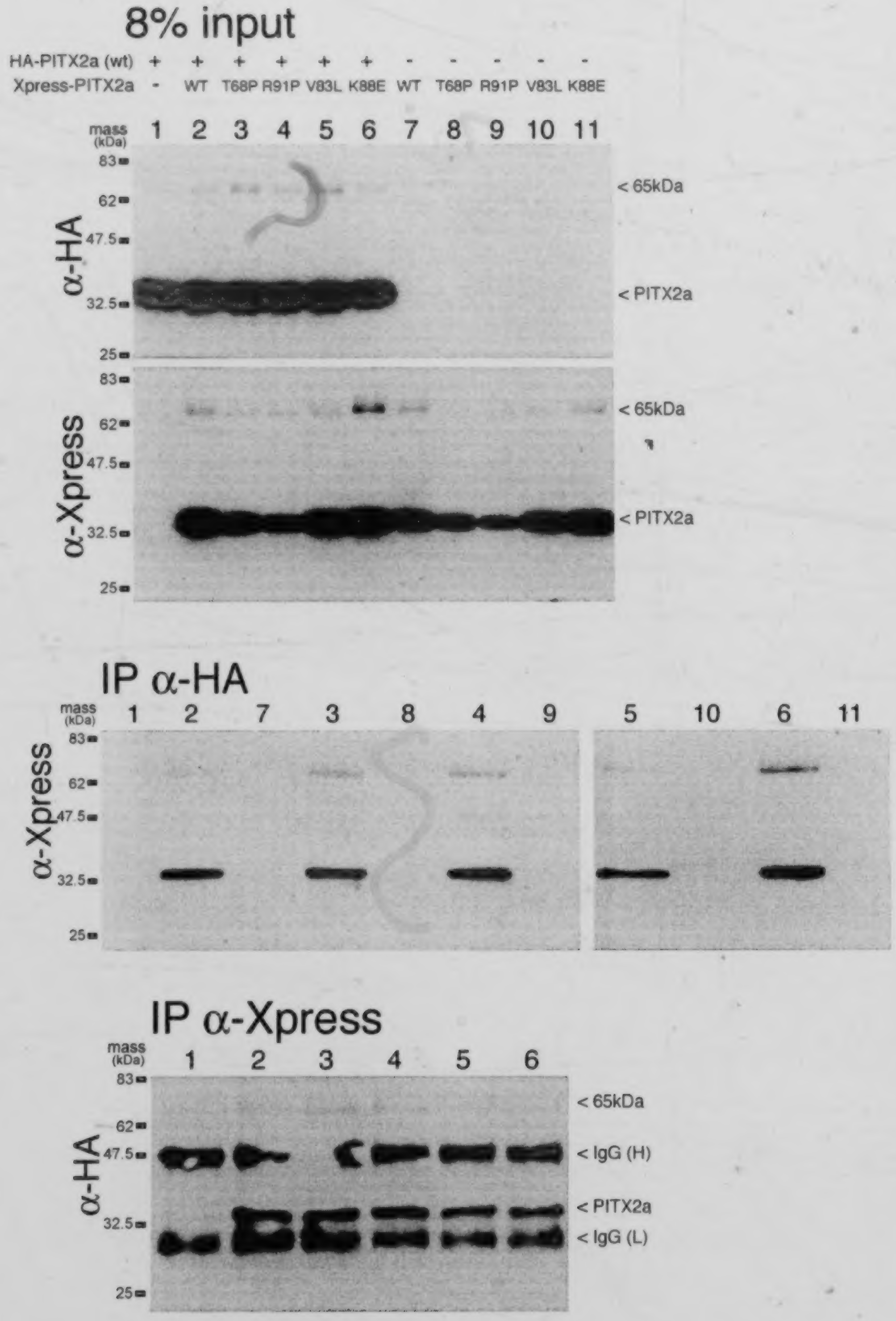
8% input
HA-PITX2a (wt) + + + + + + - - - - -
Xpress-PITX2a - WT T68P R91P V83L K88E WT T68P R91P V83L K88E
mass (kDa) 1 2 3 4 5 6 7 8 9 10 11
83
62
47.5
32.5
25
α-HA
< 65kDa
< PITX2a
α-Xpress
< 65kDa
< PITX2a
IP α-HA
mass (kDa) 1 2 7 3 8 4 9 5 10 6 11
α-Xpress
83
62
47.5
32.5
25
IP α-Xpress
mass (kDa) 1 2 3 4 5 6
α-HA
83
62
47.5
32.5
25
< 65kDa
< IgG (H)
< PITX2a
< IgG (L)

nonquantitative) method.

PITX2a physically interacts with FOXC1

PITX2 and FOXC1 accomplish similar functions during ocular ontogeny, as evidenced by their similar ocular phenotypes and pattern of expression (29, 44, 63, 111, 112). Nonetheless, essentially all functional studies of PITX2 and FOXC1 have focused on either protein individually, and a model relating the two AR-associated factors has therefore remained wholly undefined. One possible element of a putative link between PITX2 and FOXC1 activities might be the coordination of both proteins in a shared physical complex. In order to investigate whether PITX2a and FOXC1 can physically interact, I performed reciprocal IPs of coexpressed HA-PITX2a and 6xHisXpress-FOXC1 in cos-7 cells (Figure 3-2). Crucially, 6xHisXpress-FOXC1 was recovered in α-HA IP isolates in an HA-PITX2a-dependant fashion. Similar results were observed in the reciprocal experiment, in which HA-PITX2a was recovered by α-Xpress in an Xpress-FOXC1-dependant manner. PITX2a and FOXC1 can therefore specifically associate in a physical complex, at least at the relatively high levels of expression obtained in this system.

Having established that PITX2a and FOXC1 can interact, I further undertook mapping of the region(s) of FOXC1 responsible for PITX2a binding. This was achieved by reciprocal IPs of HA-PITX2a versus a panel of FOXC1 deletion constructs originally used to map several discrete activation and regulatory domains within FOXC1 (123). These experiments, shown in figures 3-2 and 3-3, demonstrated the FOXC1 C-terminus to be essential for interaction with PITX2a, as C-terminal truncations of FOXC1 at residues 366, 435, or 475 caused a complete loss of coprec ipitation. Conversely, removal of FOXC1's the N-terminal activation domain (AD1; residues 1-50) had no effect on PITX2a binding. A FOXC1 construct lacking the central regulatory domain (TRD; residues 215-366) produced contrasting results in reciprocal IP experiments (figure 3-2, lanes marked '2'). This construct was not able to coprecipitate PITX2a in α-Xpress IPs, but was effectively copurified along with PITX2a in α-HA IPs. Apart from this single inconsistency, all other constructs tested yielded identical results in reciprocal IP experiments. These data are consistent with a PITX2-binding domain (PITX2BD) situated within the C-terminal third (residues 377 to 553) of FOXC1. Moreover, the lack of interaction between PITX2a and constructs encoding FOXC1(1-435) and FOXC1(1-475) indicates that the PITX2BD overlaps with FOXC1's C-terminal activation domain

(AD2; residues 436-553). The study of further FOXC1 deletion constructs may be necessary to determine if AD2 and the PITX2BD are strictly identical. Nonetheless, these results imply that PITX2 binding may be functionally involved in target gene activation by FOXC1.

Figure 3-2: Physical interaction of PITX2 and FOXC1

Cos-7 cultures ($2x10^6$) were cotransfected with 7μg of [pCI-HA-PITX2a or empty PCDNA4], and 1μg of [pcDNA4-FOXC1, pcDNA4-FOXC1Δ(216-366), pcDNA4-FOXC1Δ(367-553), or empty pcDNA] as indicated. Whole-cell lysates were assayed for relative expression levels (top left panel) prior to IP. IP reactions contained 160μg of whole-cell lysate in a total buffer volume of 1.5mL. Reactions were incubated for 16h at 4°C, in the presence of either mouse α-Xpress (2.1μg) or rabbit α-HA (2μg).

Xpress-FOXC1 was precipitated by α-HA in an HA-PITX2a-dependent fashion (lower panel). Deletion of the central regulatory domain of FOXC1 (residues 216-366) did not ablate this interaction; however, deletion of FOXC1's C-terminal third (residues 367-553) abrogated recovery by HA-PITX2a.

Reciprocal IPs (top right panel) confirmed the PITX2-FOXC1 interaction. Xpress-FOXC1, but not FOXC1Δ(216-366) or FOXC1Δ(367-553) mediated specific recovery of HA-PITX2a by α-Xpress. Additional Ig bands in the α-Xpress IP output were due to inadvertent cross-reaction of the goat α-rabbit-HRP, used for immunoblot analysis, with the mouse α-Xpress used for IP. Both 32.5kDa and 65kDa forms of PITX2a were observed post-IP, as well as in the unpurified inputs.

Immunoblot probing conditions:

α-HA probings:

rabbit α-HA 1:500 16h 4°C; HRP goat α-rabbit IgG 1:3000 1h 25°C

α-Xpress probings:

mouse α-Xpress 1:5000 16h 4°C; HRP goat α-mouse IgG 1:3000 1h 25°C

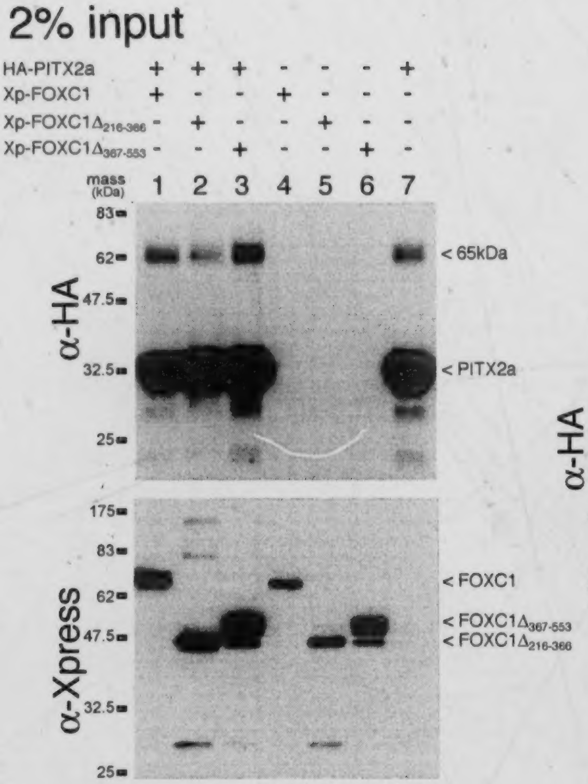
2% input
HA-PITX2a + + + - - - +
Xp-FOXC1 + - - + - - -
Xp-FOXC1Δ216-366 - + - - + - -
Xp-FOXC1Δ367-553 - - + - - + -
mass (kDa)
1 2 3 4 5 6 7
α-HA
83
62
47.5
32.5
25
< 65kDa
< PITX2a
α-Xpress
175
83
62
47.5
32.5
25
< FOXC1
< FOXC1Δ367-553
< FOXC1Δ216-366

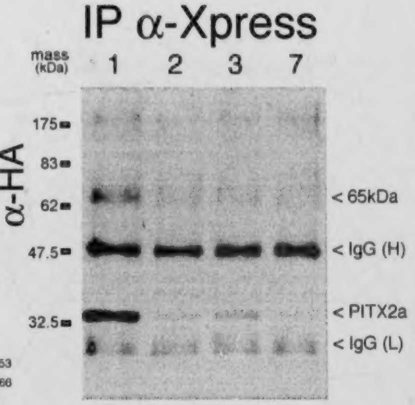
IP α-Xpress
mass (kDa)
1 2 3 7
α-HA
175
83
62
47.5
32.5
< 65kDa
< IgG (H)
< PITX2a
< IgG (L)

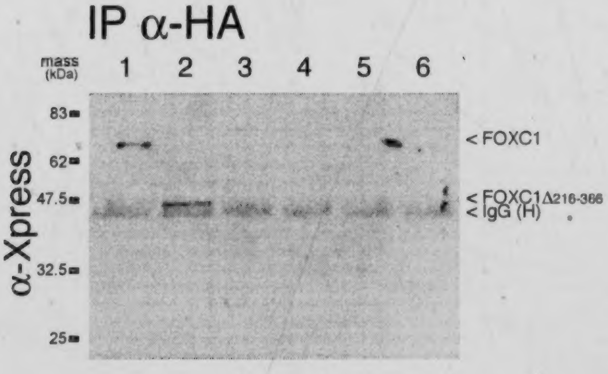
IP α-HA
mass (kDa)
1 2 3 4 5 6
α-Xpress
83
62
47.5
32.5
25
< FOXC1
< FOXC1Δ216-366
< IgG (H)

Figure 3-3: Transactivation and PITX2-binding domains of FOXC1 overlap

Cos-7 cells (2×10^6) were cotransfected with 7μg of [pCI-HA-PITX2a or empty PCDNA4], and 1μg of [pcDNA4-FOXC1, pcDNA4-FOXC1Δ(1-28), pcDNA4-FOXC1Δ(476-553), pcDNA4-FOXC1Δ(436-553) or empty pcDNA] as indicated. Lysates were assayed for expression (top panel) prior to IP. IP reactions contained 115μg of protein in a total volume of 1.5mL. Reactions, containing either mouse α-Xpress (2.1μg) or rabbit α-HA (2μg), were incubated for 16h at 4°C.

Xpress-FOXC1 was coprecipitated by HA-PITX2a as before (center left panel). Disabling the N-terminal activation domain (AD) of FOXC1 by deleting residues 1-28 had no effect; however, deletions C-terminal of residues 436 or 476 caused loss of Xpress-FOXC1 recovery by HA-PITX2a. Both phosphorylated and nonphosphorylated forms of FOXC1 described in (123) were observed to interact with PITX2a (leftmost lane, center left panel).

Reciprocal IPs (center right panel) confirmed this pattern of structural requirements for PITX2-FOXC1 interaction. Additional Ig bands in the α-Xpress IP output were due to inadvertent cross-reaction of the goat α-rabbit-HRP, used for immunoblot analysis, with the mouse α-Xpress used for IP. Both 32.5kDa and 65kDa forms of PITX2a were observed post-IP, as well as in the unpurified inputs.

Bottom panel: Mapping of FOXC1's PITX2-binding domain (PITX2BD). Diagram represents collected IP data presented in this figure and in figure 3-2. The closest mapping supported by these data places the entire PITX2BD between residues 366 and 553 of FOXC1. Part of the PITX2BD extends C-terminally of residue 476, and therefore overlaps substantially with the C-terminal activation domain of FOXC1.

Immunoblot probing conditions:

αHA probings:

rabbit α-HA 1:500 16h 4°C; HRP goat α-rabbit IgG 1:3000 1h 25°C

α-Xpress probings:

mouse α-Xpress 1:5000 16h 4°C; HRP goat α-mouse IgG 1:3000 1h 25°C

2.5% input

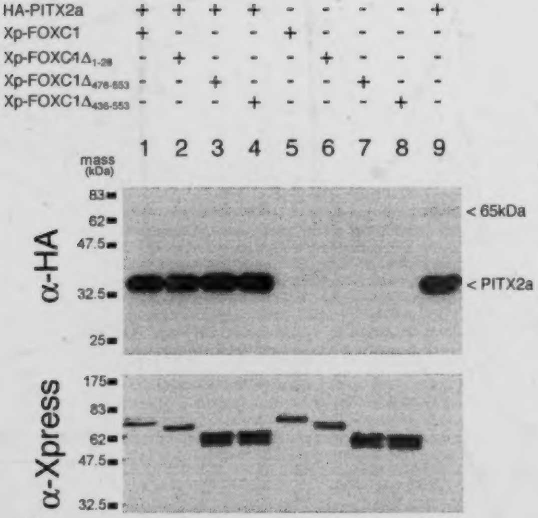
HA-PITX2a + + + + - - - - +
Xp-FOXC1 + - - - + - - - -
Xp-FOXC1Δ1-28 - + - - - + - - -
Xp-FOXC1Δ476-553 - - + - - - + - -
Xp-FOXC1Δ436-553 - - - + - - - + -
1 2 3 4 5 6 7 8 9
mass (kDa)
83
62
47.5
32.5
25
α-HA
< 65kDa
< PITX2a
175
83
62
47.5
32.5
α-Xpress

IP α-HA

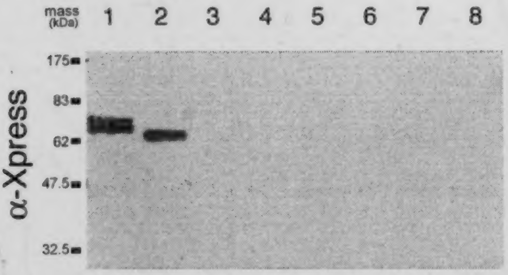
mass (kDa)
1 2 3 4 5 6 7 8
175
83
62
47.5
32.5
α-Xpress

IP α-Xpress

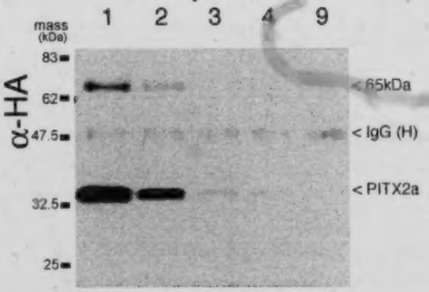
mass (kDa)
1 2 3 4 9
83
62
47.5
32.5
25
α-HA
< 65kDa
< IgG (H)
< PITX2a

Summary - FOXC1 deletion analysis

adapted from Berry FB, Saleem RA, Walter MA. 2002. *JBC* 277:10292-7.

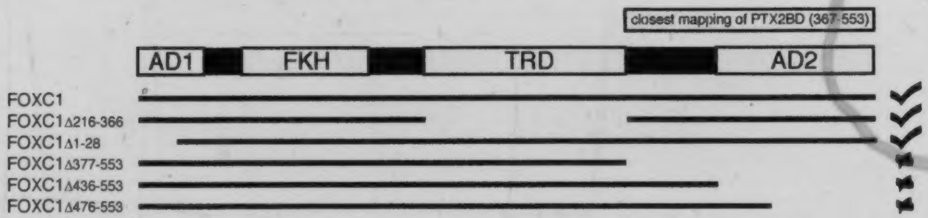
closest mapping of PTX2BD (367-553)
AD1
FKH
TRD
AD2
FOXC1
FOXC1Δ216-366
FOXC1Δ1-28
FOXC1Δ377-553
FOXC1Δ436-553
FOXC1Δ476-553

One logical question stemming from the preceding work was whether AR patient alleles of PITX2 might display altered FOXC1-binding properties. Figure 3-4 displays the results of IP experiments in which 6xHisXpress-FOXC1 was coexpressed with wildtype, T68P, R91P, V83L, and K88E alleles of HA-PITX2a. As observed for the PITX2a-PITX2a IP experiments presented in Figure 3-1, no pronounced differences in FOXC1 interaction were noted between wildtype PITX2a and the various patient mutants. At present, grossly altered PITX2a-PITX2a or PITX2a-FOXC1 interactions are not an apparent feature of the patient PITX2a alleles tested. However, subtle quantitative differences in protein-protein interactions may be beneath the resolution of this (admittedly nonquantitative) technique.

Subnuclear localization of PITX2 and FOXC1

As discussed in the preceding section, biochemical analysis of FOXC1 and PITX2a demonstrated that both proteins physically interacted in whole-cell lysates, and that this interaction was not drastically perturbed by AR-causing PITX2 mutations. However, we reasoned that interaction of PITX2a and FOXC1 may be influenced by the *in vivo* structural organisation of the cell nucleus, and that relevant structures would likely be disrupted during cell lysis. I therefore undertook a microscopic study of PITX2a and FOXC1 distribution in the nucleus to provide a live-cell context for our biochemical findings. Both wild-type and mutant PITX2a proteins were imaged to determine whether any of the mutants might compromise PITX2a-FOXC1 interaction via altered protein targeting *in vivo*. Briefly, I compared the localization patterns of Xpress-PITX2a, a FOXC1::GFP fusion, and general chromatin (stained with Hoechst 33342) via indirect epifluorescence microscopy of cos-7 cells. This analysis (figure 3-5) demonstrated that FOXC1GFP and wildtype PITX2a are indeed highly colocalised within the cell nucleus. Both proteins are confined to a subset of Hoechst-stained bulk chromatin, and are excluded from the largest, densest Hoechst foci. The high degree of colocalisation observed for PITX2 and FOXC1 confirmed that both proteins are indeed available for interaction in the context of a shared intranuclear compartment, while their exclusion from certain heterochromatic sites may indicate that chromatin state is an important determinant of their subnuclear trafficking.

Immunofluorescence also revealed that patient mutations of the PITX2 HD may interfere with the normal targeting of PITX2a to FOXC1-containing chromatin. With the exception of the hyperactive V83L allele, each of the AR-associated PITX2a mutations

Figure 3-4: Immunoprecipitation of wildtype and mutant PITX2a by FOXC1

Cos-7 cultures ($2x10^6$) were cotransfected with 7μg of [pCI-HA-PITX2a (indicated wild-type or mutant construct), or empty PCDNA4], and 1μg of pcDNA4-FOXC1. Whole-cell lysates were assayed for relative expression levels (top and middle panels) prior to IP. IP reactions contained 225μg of protein in a total buffer volume of 1.5mL. Reactions containing 2.1μg mouse α-Xpress were incubated for 16h at 4°C. Reciprocal IPs were not considered necessary as the specificity of this assay is well-established (Figures 3-2 and 3-3).

Wildtype PITX2a, and each of the mutant constructs examined, were each coprecipitated by XpressFOXC1 to an appreciable extent. Additional Ig bands in the IP eluate were due to inadvertent cross-reaction of the goat α-rabbit-HRP, used for immunoblot analysis, with the mouse α-Xpress used for IP. Both 32.5kDa and 65kDa PITX2a species were observed in the IP eluate and unpurified inputs.

Immunoblot probing conditions:
α-HA probings:
    rabbit α-HA 1:500 16h 4°C; HRP goat α-rabbit IgG 1:3000 1h 25°C
α-Xpress probings:
    mouse α-Xpress 1:5000 16h 4°C; HRP goat α-mouse IgG 1:3000 1h 25°C

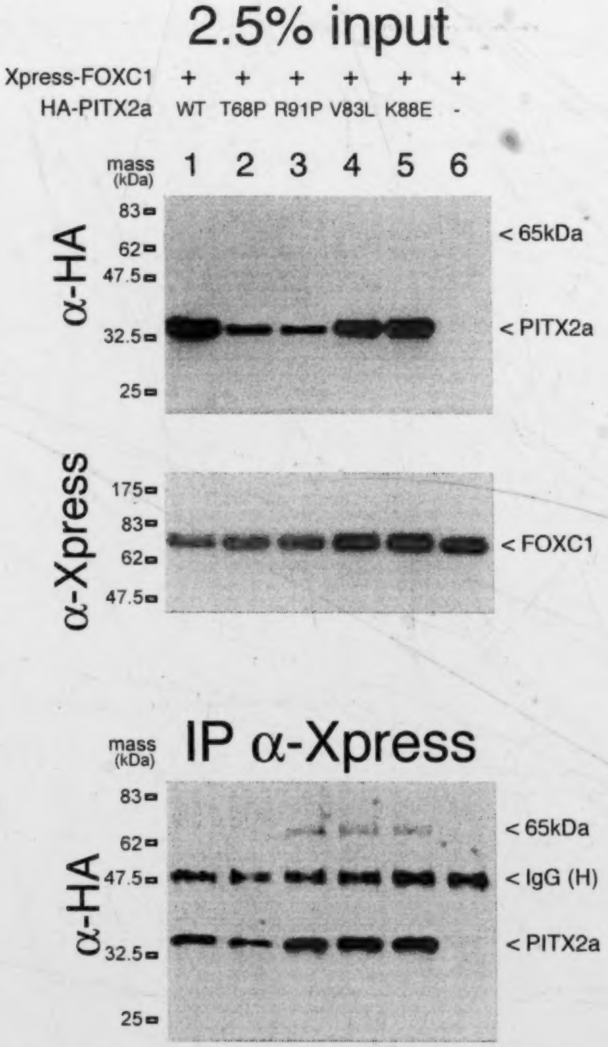
2.5% input
Xpress-FOXC1 + + + + + +
HA-PITX2a WT T68P R91P V83L K88E -
mass (kDa)
1 2 3 4 5 6
α-HA
83
62
47.5
32.5
25
< 65kDa
< PITX2a
α-Xpress
175
83
62
47.5
< FOXC1
IP α-Xpress
mass (kDa)
α-HA
83
62
47.5
32.5
25
< 65kDa
< IgG (H)
< PITX2a

Figure 3-5: Colocalisation of FOXC1 and PITX2 within a subdomain of the cell nucleus

Cos-7 cells (1x10^6 per 6-well tissue culture plate) were seeded onto glass coverslips and transfected with 80ng pEGFP-N1 (FOXC1 or empty vector), 260ng pcDNA4-PITX2a (wild-type or indicated mutant construct), and 260ng empty pCI-HA. Immunofluorescence was performed following a three-day expression period. Antibody control (no α-Xpress) was entirely negative and is not depicted. A control for the eGFP moiety of FOXC1GFP is shown ('eGFP ctrl'). Only representative, intact nuclei with moderate transgene expression levels were imaged to minimise artifacts intrinsic to overexpresssion. These experiments were done in parallel with the triple-imaging experiment depicted in figure 3-6. Scale bar shown indicates 5µm; all images are shown at the same scale.

Wild-type Xpress-PITX2a colocalises closely with FOXC1GFP on a subset of bulk chromatin (bottom row, columns I to IV). PITX2a and FOXC1 signals overlap extensively with the Hoechst 33342 stain, representing AT-rich DNA (bottom row, columns V and VI). Both proteins are excluded from nucleoli and from the densest Hoechst foci, representing pericentromeric constitutive heterochromatin.

Two non-binding mutations (T68P and R91P) produced a coarsening of the PITX2 localisation pattern, loss of PITX2-FOXC1 colocalisation, and formation of Hoechst-excludingfoci in some cells. In contrast, the hyperactive V83L allele was indistinguishable from wild-type PITX2a. Each of these three constructs presented a fairly uniform picture among the asynchronous population of transfected cells. However, the R84W and K88E constructs, in particular, displayed a highly variable appearance, and some nuclei demonstrated no change whatsoever from the wild-type localization pattern. Two nuclei are shown in order to illustrate the continuum of cell phenotypes found in the R84W and K88E cultures.

Primary: mouse α-Xpress (1:400); rabbit α-HA (1:100)

Secondary: goat-α-mouse(IgG)-Cy3 (1:400); donkey-α-rabbit-Cy2 (1:100); Hoechst 33342 (50µg/mL)

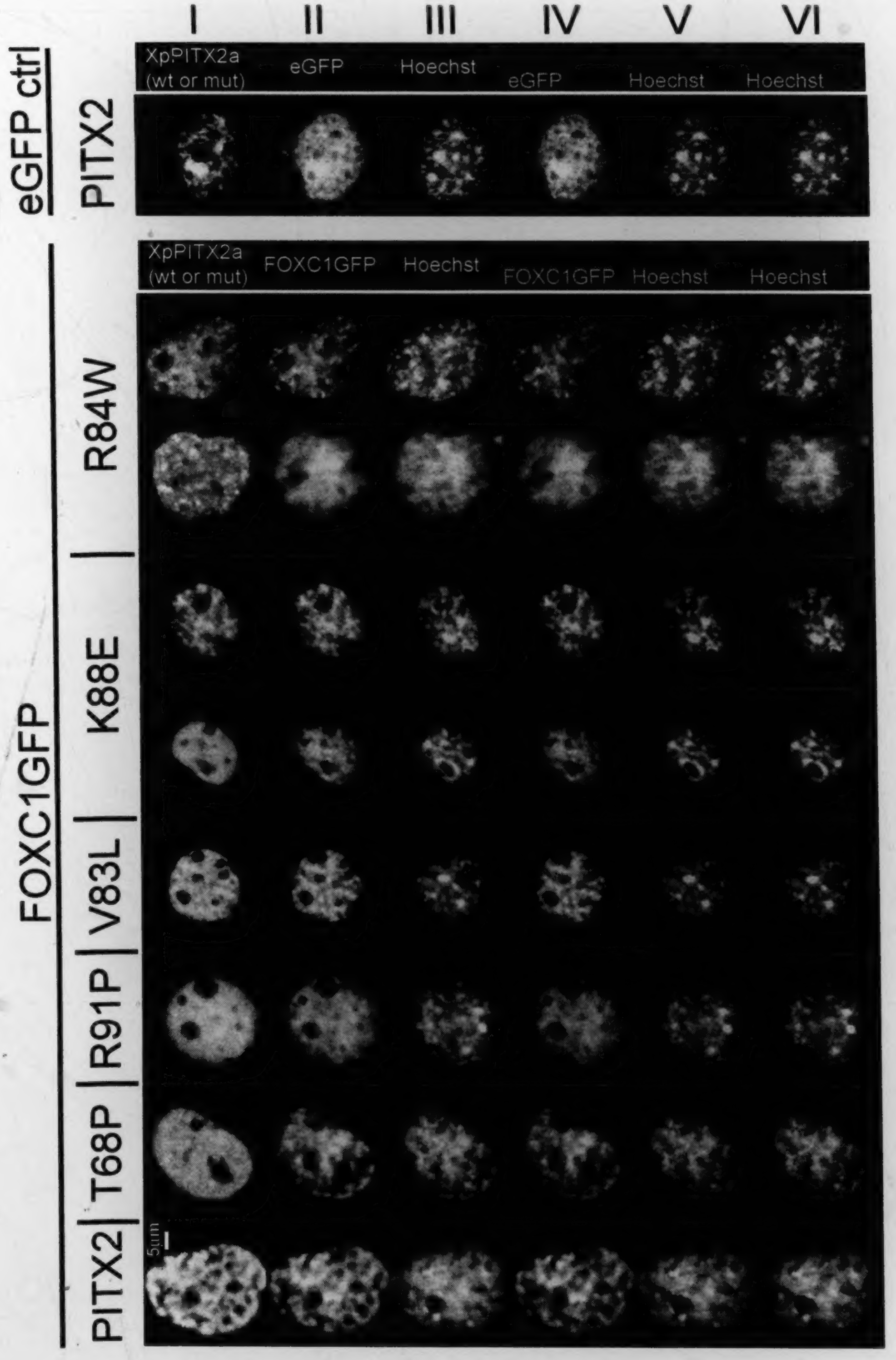
I
II
III
IV
V
VI
eGFP ctrl
PITX2
XpPITX2a (wt or mut)
eGFP
Hoechst
eGFP
Hoechst
Hoechst
FOXC1GFP
R84W
K88E
V83L
R91P
T68P
PITX2
XpPITX2a (wt or mut)
FOXC1GFP
Hoechst
FOXC1GFP
Hoechst
Hoechst
5μm

reduced colocalisation with both FOXC1GFP and bulk chromatin, albeit to varying extent (Figure 3-5). In particular, the non-binding T68P and R91P mutants displayed clearly reduced colocalisation with FOXC1GFP, and tended to occupy cavities in the Hoechst stain. The same was observed, albeit less uniformly, for the dominant negative K88E and mild hypomorph R84W alleles. These latter two constructs varied somewhat in appearance between nuclei, and formed Hoechst-excluding foci in only a subset of cells. In other nuclei, K88E and R84W proteins remained perfectly colocalised with FOXC1GFP. The two K88E and R84W nuclei shown in figure 3-5 therefore represent the extremes of the continuum of distributions observed for these two mutants in healthy cells. It is likely that the observed mislocalisation of mutant PITX2a proteins may indicate a propensity to aggregate at the exaggerated level of expression used in this system, although this phenomenon was not observed for wild-type PITX2a.

As PITX2 mutations are genetically dominant, AR patients retain one wild-type allele of the gene, and heterodimeric interactions between mutant and wild-type PITX2a are possible. The *in vivo* localization defect of mutant PITX2a may therefore be mitigated *in trans* by interaction with the wildtype protein. Similarly, mutant PITX2a might interfere with the activity of the wild-type protein by altering its normal subnuclear targeting. In order to test these two hypotheses, I simultaneously imaged wild-type HAPITX2a, FOXC1::GFP, and either wild-type or mutant XpressPITX2a in transfected cos-7 cells (Figure 3-6). In general, this experiment produced observations similar to the simple PITX2a versus FOXC1GFP immunofluorescence experiment discussed above. The T68P and R91P loss-of-function mutant proteins colocalised poorly with either the wildtype HAPITX2a or FOXC1GFP, while the hypermorphic V83L allele was indistinguishable from wild-type. The K88E and R84W mutants, when coexpressed with wild-type PITX2a, were more uniformly colocalised with FOXC1, suggesting that some degree of rescue may have occured. In no case was mutant PITX2a observed to reduce the colocalisation of wild-type HAPITX2a with FOXC1GFP, suggesting the absence of a dominant negative effect. Linescan analyses of the images in figure 3-6 produced a more detailed accounting of the relative distribution of all three proteins (Figure 3-7), in which the centers of mass of T68P and R91P but not wildtype, V83L, K88E, or R84W are displaced from both HAPITX2a and FOXC1GFP.

Figure 3-6: Mutant PITX2a does not affect the subnuclear localisation of wild-type PITX2a or FOXC1

Cos-7 cultures (1x10^6 per 6-well tissue culture plate) were seeded onto glass coverslips and transfected with 80ng pEGFP-N1 (FOXC1 or empty vector), 260ng pcDNA4-PITX2a (wild-type or indicated mutant construct), and 260ng pCI-HA-PITX2. Immunofluorescence was performed following a three-day expression period. Antibody controls (no α-Xpress and no α-HA) were entirely negative and are not depicted. A control for the eGFP moiety of FOXC1GFP is shown (rightmost image). These experiments were done in parallel with the immunofluorescence experiment depicted in figure 3-5. All images are shown at the same scale; scale bar indicates 5µm.

Identical subnuclear distributions were observed for HA-PITX2a and Xpress-PITX2a (wild-type), demonstrating that the N-terminal epitope tags did not affect localisation (bottom row, columns I and II). Wild-type, V83L, K88E, and R84W Xpress-PITX2a constructs were each colocalised with both wild-type HA-PITX2a and FOXC1GFP (columns IV and V). The T68P and R91P constructs remained aberrantly localised relative to both FOXC1GFP and wild-type HA-PITX2a.

The addition of wild-type PITX2a appeared to rescue the subtle, variable localisation defect of PITX2a (K88E or R84W) noted in figure 3-5. However, wild-type PITX2a was unable to prevent mislocalisation and aggregation of the T68P and R91P null alleles. In no case was the addition of a mutant allele observed to reduce the colocalisation of wild-type HA-PITX2a and FOXC1GFP (column VI).

Primary: mouse α-Xpress (1:400); rabbit α-HA (1:100)
Secondary: goat-α-mouse(IgG)-Cy3 (1:400); donkey-α-rabbit-AMCA (1:100)

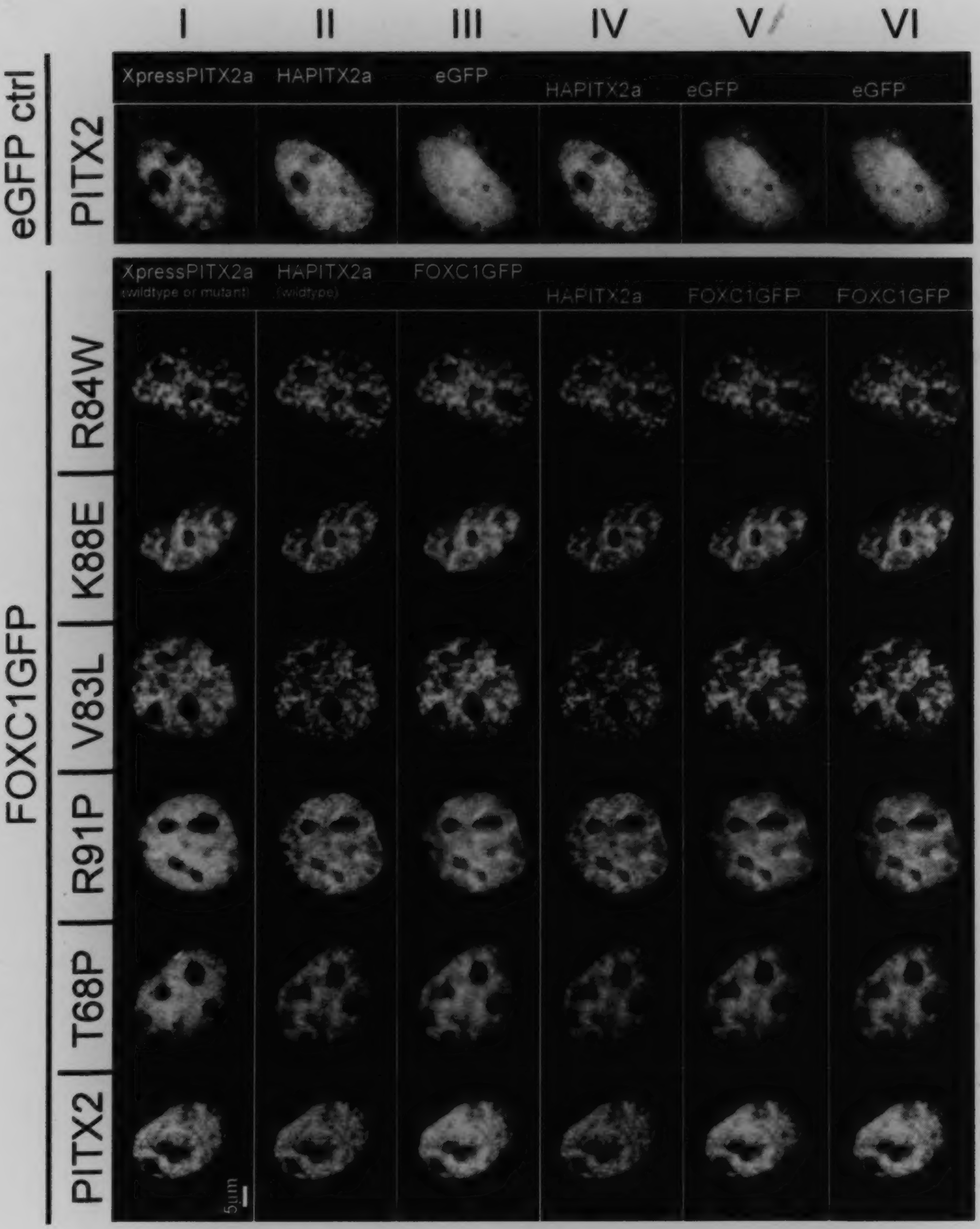
I
II
III
IV
V
VI
eGFP ctrl
PITX2
XpressPITX2a
HAPITX2a
eGFP
HAPITX2a
eGFP
eGFP
FOXC1GFP
R84W
K88E
V83L
R91P
T68P
PITX2
XpressPITX2a
(wildtype or mutant)
HAPITX2a
(wildtype)
FOXC1GFP
HAPITX2a
FOXC1GFP
FOXC1GFP
5μm

Figure 3-7: Detailed analysis of PITX2a-PITX2a-FOXC1 triple localisation

At left: Three-colour merges of images from figure 3-6. Image at top is a control for the eGFP moiety of FOXC1GFP.

At right: Linescan plots showing density of each channel at each point along the diagonal line illustrated at top (top left to bottom right). Colour scheme for both panels is as follows: Xpress-PITX2a (wildtype or mutant) - red; FOXC1GFP or eGFP control - green; HA-PITX2a - blue. The precise method used in this analysis is described in the Methods section of this chapter.

Note that centers of mass (peaks) of all three channels overlap for the wild-type, V83L, K88E, and R84W images. Red (Xpress-PITX2a) channel peaks are displaced in T68P and R91P images. Green (GFP) channel peaks are displaced in the GFP-only control as expected.

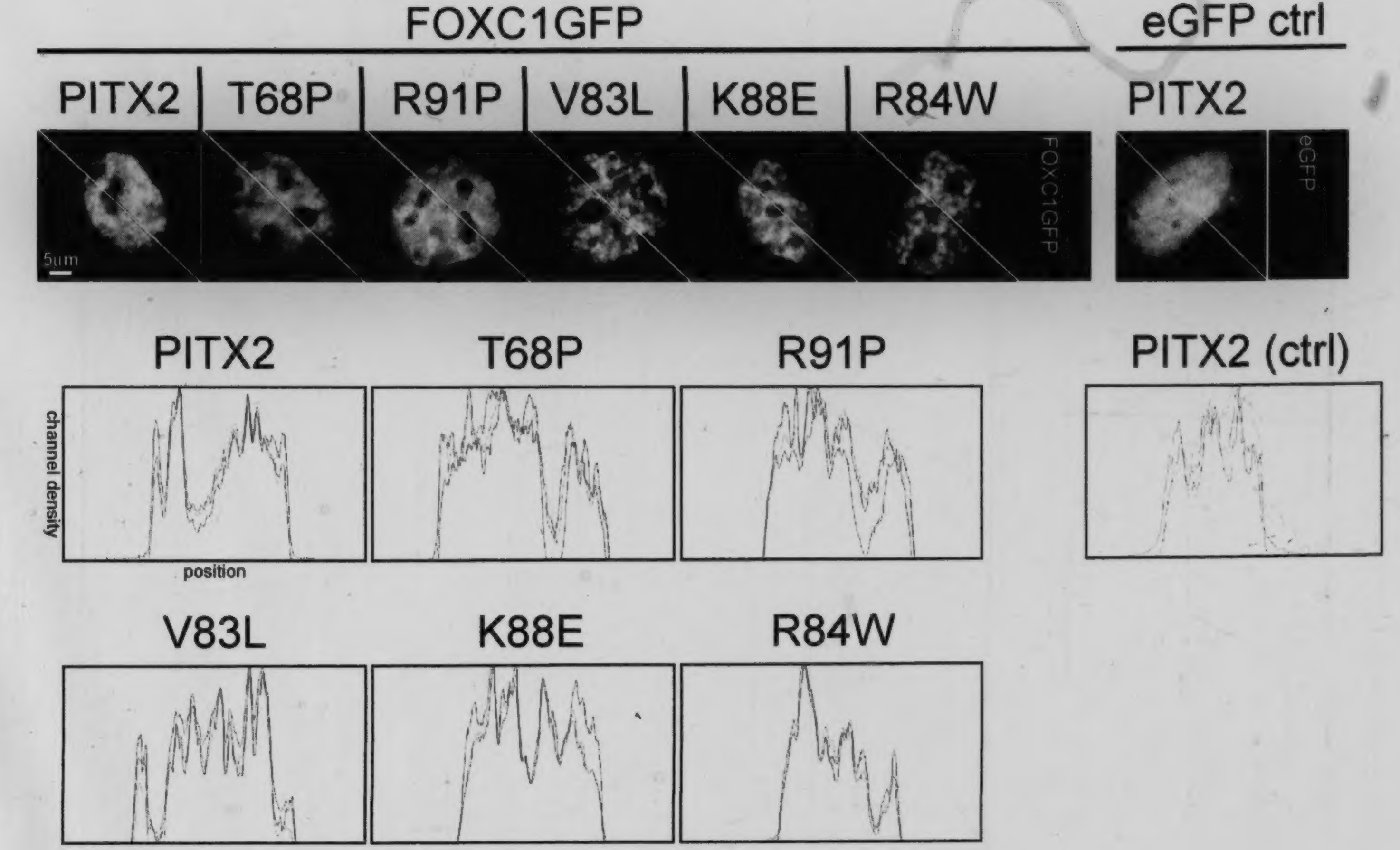
FOXC1GFP
eGFP ctrl
PITX2
T68P
R91P
V83L
K88E
R84W
PITX2
FOXC1GFP
eGFP
5μm
PITX2
T68P
R91P
PITX2 (ctrl)
channel density
position
V83L
K88E
R84W

Immunofluorescence of PITX2a versus nuclear landmarks

The preceding immunofluorescence experiments demonstrated that PITX2a and FOXC1 share a specific chromatin compartment, and that several hypomorphic PITX2a mutants were incompletely targeted to this domain. These experiments also provided a handful of clues regarding the chromatin compartment occupied by wild-type PITX2a and FOXC1, namely exclusion from nucleoli and from large heterochromatic condensates visible as large Hoechst foci. In the interests of describing this compartment in more detail, I examined the relative subnuclear distributions of PITX2 and several other nuclear landmarks via immunofluorescence.

In figure 3-5, it was shown that PITX2 and FOXC1 are both excluded from certain large Hoechst domains. These foci, which are particularly pronounced in cos nuclei, represent constitutively silent, AT-rich pericentromeric heterochromatin occupied by the heterochromatin proteins HP1α and HP1β (150). In order to directly demonstrate exclusion of PITX2 from these sites, I performed colocalisation experiments on recombinant, HA-tagged PITX2a and endogenous HP1α in cos cells. Figure 3-8 illustrates that HP1α foci clearly demarcate Hoechst-positive 'holes' in PITX2a's subnuclear distribution. HP1α and PITX2a therefore occupy mutually exclusive subsets of the overall Hoechst stain. Moreover, it appears that HP1α- and PITX2a-demarcated chromatin compartments together recapitulate most (or all) of the Hoechst-stained DNA in the cell. This duality may allow us to use HP1α as a landmark for the inverse of PITX2a's typical distribution within the nucleus.

A second colocalisation experiment indicated that PITX2a is similarly excluded from chromatic foci containing lysine twenty-trimethylated histone H4 (Figure 2-8). This particular histone modification has only recently been described in mammals, and is associated with silent chromatin (151, 152). These data indicate that PITX2a, and by extension, FOXC1, may associate only poorly, if at all, with repressive heterochromatin under the culture and expression conditions tested.

Nuclear speckles are extrachromatic structures which serve as processing and trafficking centres for nascent pre-mRNAs, and are found closely adjacent to transcriptionally active euchromatin within the nucleus (153-155). Speckles are defined by punctate staining of the mRNA splicing factor SC35, which is involved in assembly of the spliceosome (156). Microscopically, nascent transcripts tend to be associated with the speckle periphery, consistent with cotranscriptional processing of mRNAs (157). In order to examine whether PITX2a might be enriched within or adjacent to this

Figure 3-8: Subnuclear localisation of PITX2a versus HP1 α and trimethyllysyl-20 histone H4 [$(Me)_3$K20H4]

Cos-7 cells ($1x10^6$ per 6-well tissue culture plate) were seeded onto glass coverslips and transfected with 500ng pCI-HA-PITX2 (top panel) or pCDNA4A-PITX2a (bottom panel) 24h later. Immunofluorescence was performed after a two-day expression period as described in Methods. Antibody specificity controls (no α-HP1α, and no α-$(Me)_3$K20H4) were entirely negative and are not depicted. HA-PITX2-nonexpressing cells demonstrated the α-HA and anti-rabbit antibodies to be sufficiently specific.

All pairwise merges of the three channels are depicted. A three-colour merge is also shown along with a density profile plot for each of the three channels along the diagonal line illustrated (bottom left to top right). Scale bar indicates 5μm.

Top panel: HA-PITX2a is excluded from large heterochromatin foci marked by HP1α staining. This finding is consistent with the previously noted exclusion of PITX2 from the largest visible Hoechst foci (figures 3-5 through 3-7).
Primary: rabbit α-HA (1:50); mouse α-HP1α (1:100).
Secondary: goat-α-mouse(IgG)-Cy3 (1:400); donkey-α-rabbit-Cy2 (1:200); Hoechst 33342 (50ng/mL).

Bottom panel: Xpress-PITX2a does not localise to lysine-20 trimethylated histone H4 silent chromatin foci.
Primary: mouse α-Xpress (1:400); rabbit α-$(Me)_3$K20H4 (1:1000)
Secondary: goat-α-mouse(IgG)-Cy3 (1:400); donkey-α-rabbit-Cy2 (1:100); Hoechst 33342 (50ng/mL)

HP1α

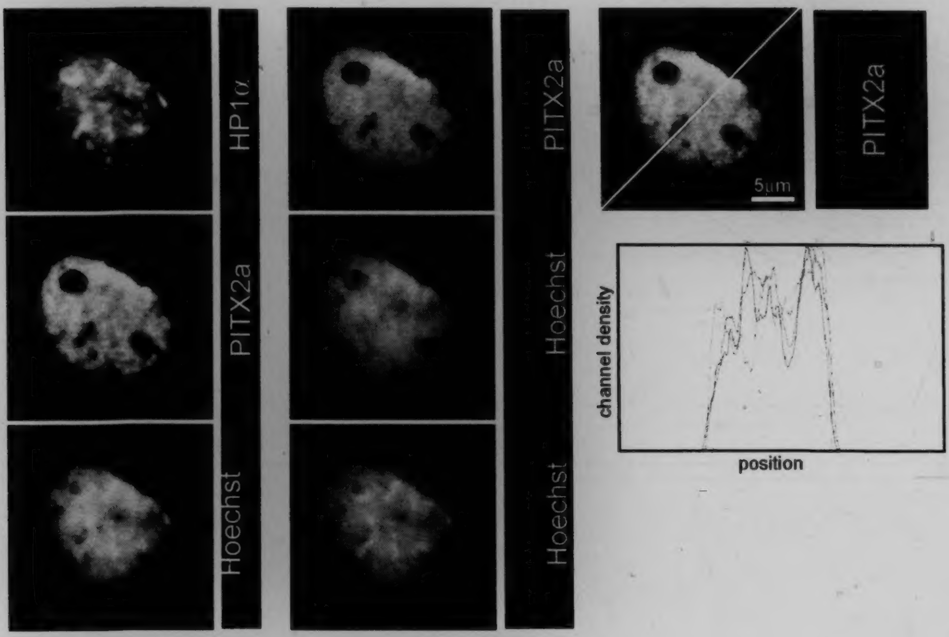
HP1α
PITX2a
Hoechst
PITX2a
Hoechst
Hoechst
5μm
PITX2a
channel density
position

(Me)$_3$K20H4

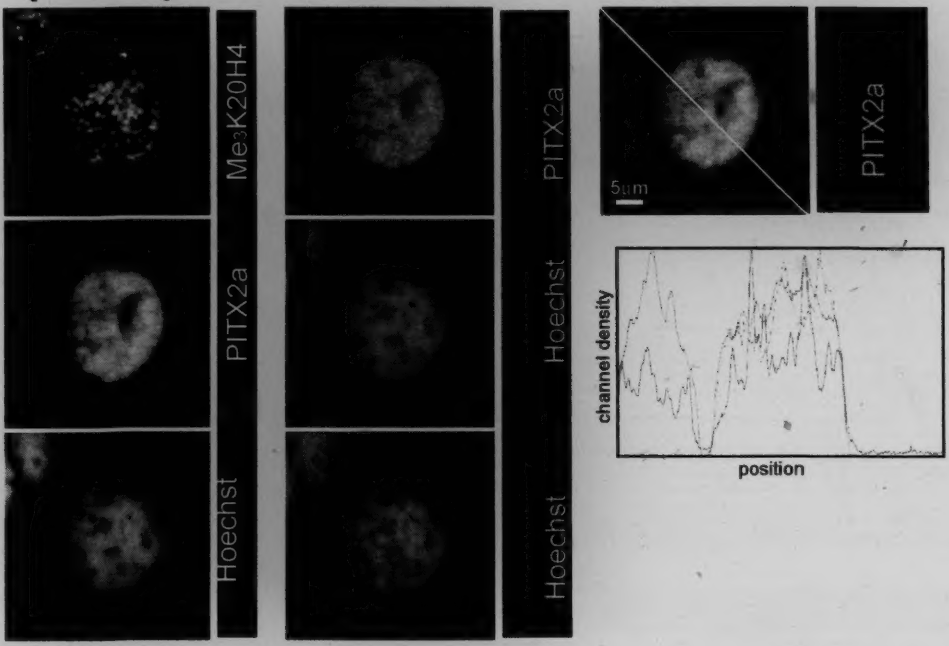
Me$_3$K20H4
PITX2a
Hoechst
PITX2a
Hoechst
Hoechst
5μm
PITX2a
channel density
position

compartment, I colocalised HA-PITX2a versus SC35 in cos nucliei (Figure 3-9). Wild-type HA-PITX2a, which is chromatic in distribution, is excluded from SC35 domains, and is not enriched to any great extent at the speckle periphery.

I considered one additional landmark in my efforts to further define the subnuclear distribution of PITX2a. Like PITX2a, the transcriptional adaptor protein and histone acetyltransferase CBP/p300 occupies a chromatin domain which is exclusive of pericentromeres in transiently transfected cells (158). Moreover, PITX2a coimmunoprecipitates with both p300 and CBP in C2C12 cells (105). To test whether p300 might colocalise with HA-PITX2a, I performed dual immunofluorescence experiments in cos cells (figure 3-9). While both PITX2a and p300 occupy a specular distribution in cos nuclei, and both are excluded from the largest Hoechst foci, only limited overlap between localisation patterns is observed, and numerous foci containing either PITX2a or p300 alone are visible. PITX2a and p300 are neither highly colocalised nor mutually exclusive, suggesting that both proteins' distributions are independent of each other. This result suggests that the previously noted PITX2a-p300 interaction (105) takes place on only a limited subset of chromatic sites within the nucleus. PITX2-p300 interaction has never been shown to be direct, and may therefore be mediated by other cofactors and/or DNA in a promotor-specific fashion.

Figure 3-9: Subnuclear localisation of PITX2 versus SC35 and p300

This experiment was conducted similarly to those described in the caption of figure 3-8. Antibody specificity controls (no α-SC35, and no α-p300) were entirely negative and are not depicted. HA-PITX2-nonexpressing cells demonstrated demonstrated the α-HA and anti-rabbit antibodies to be sufficiently specific. Scale bar indicates 5μm.

Top panel: HA-PITX2a does not localise to SC35-positive splicing speckles (interchromatin granule clusters). A specular localisation on Hoechst-stained chromatin is observed, and PITX2 is excluded from dense Hoechst foci (pericentromeres) as previously noted (figures 3-5 through 3-7).
Primary: rabbit α-HA (1:400) in undiluted mouse α-SC35-containing hybridoma supernatant. Note that hybridoma supernatant rather than PBSA was used as diluent in this case.
Secondary: goat-α-mouse(IgG)-Cy3 (1:400); donkey-α-rabbit-Cy2 (1:100); Hoechst 33342 (50ng/mL)

Bottom panel: HA-PITX2a and p300 localisation patterns are overlapping but nonidentical. Both proteins are found in a specular pattern on chromatin. Like PITX2a, p300 is excluded from the largest heterochromatin condensates.
Primary: rabbit α-HA (1:50); mouse α-p300 (1:100)
Secondary: goat-α-mouse(IgG)-Cy3 (1:400); donkey-α-rabbit-Cy2 (1:200); Hoechst 33342 (50ng/mL)

SC35

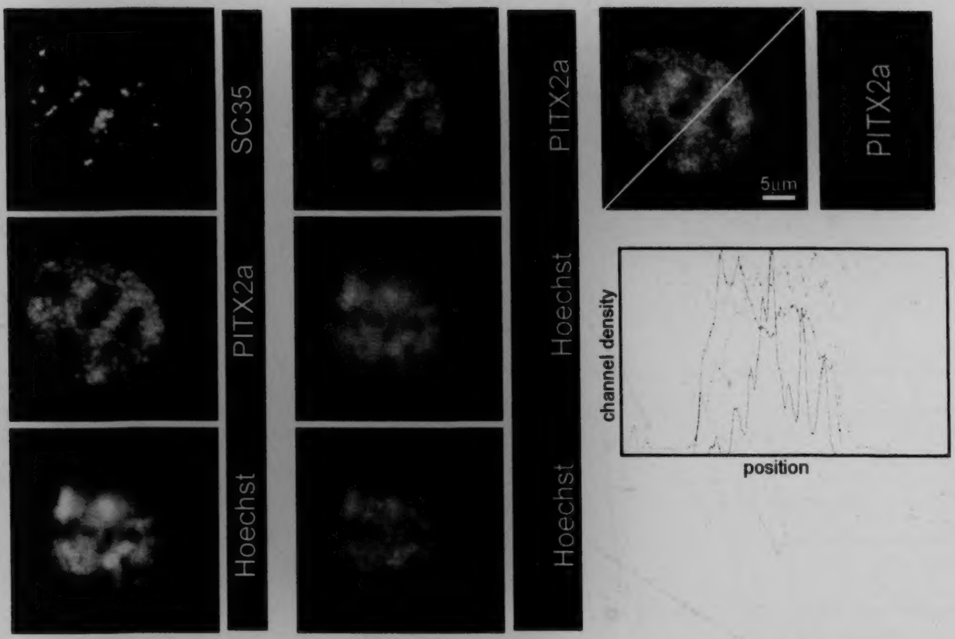
SC35
PITX2a
Hoechst
PITX2a
Hoechst
Hoechst
PITX2a
5µm
channel density
position

p300

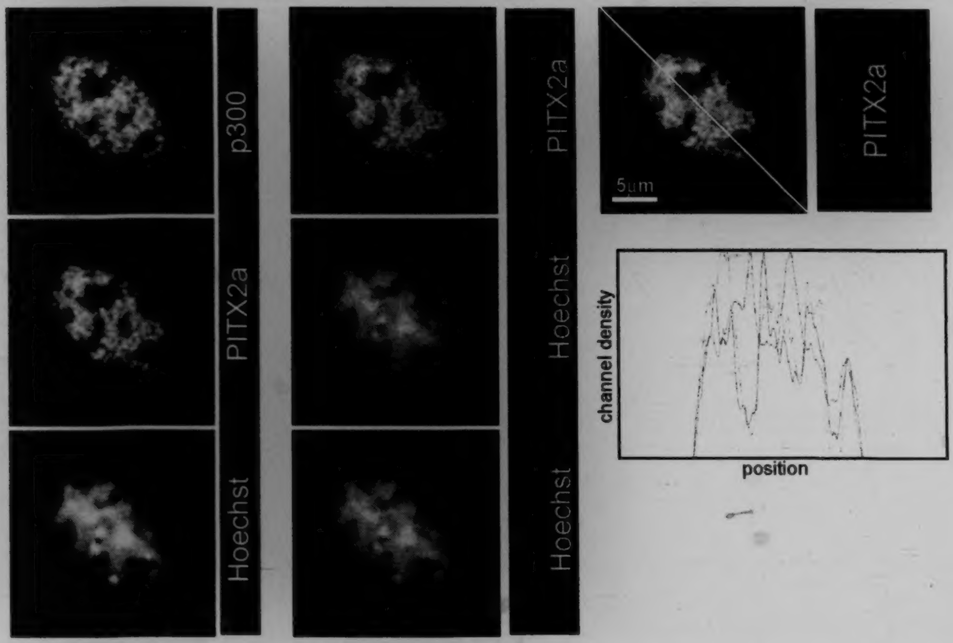
p300
PITX2a
Hoechst
PITX2a
Hoechst
Hoechst
PITX2a
5µm
channel density
position

Discussion

Protein-protein interactions of PITX2a are likely to impinge heavily on its regulation of transcriptional targets in the developing and mature eye. In this chapter, I have presented biochemical and microscopic observations concerning PITX2a-PITX2a and PITX2a-FOXC1 protein interactions, as well as the context within which these interactions occur in the cell nucleus. My findings demonstrate that recombinant PITX2a and FOXC1 can interact, and that this association requires regions of FOXC1 including a previously defined transactivation domain. A number of AR-associated homeodomain mutations of PITX2a were tested for their effect on PITX2-PITX2 and PITX2-FOXC1 binding, and did not exert a discernible effect on either interaction. I have also confirmed that PITX2a and FOXC1 are colocalised within the cell nucleus, and that multiple patient mutations of *PITX2* reduce colocalisation with FOXC1. In experiments in which I colocalised wild-type PITX2a, mutant PITX2a, and FOXC1, none of the mutants tested were able to disturb the normal subnuclear trafficking of wild-type PITX2a *in trans*. Recombinant PITX2a occupies a subset of the bulk chromatin in the cell, and is excluded from heterochromatin marked by HP1α or by lysine 20 trimethylation of histone H4. The following discussion outlines what statements can now be made regarding the protein-protein interactions of PITX2, as well as what questions remain to be answered.

PITX2-PITX2 interactions

While the structural basis of PITX2a-PITX2a interaction is not yet understood, both the HD and C-terminal regions may have distinct contributions to dimerisation (102). Studies of PITX2-related morphogens such as Paired and Bicoid illustrate that self-interaction is a crucial determinant of target specificity and a prerequisite for cooperativity. While both of the latter two proteins dimerise and bind multisite DNA substrates cooperatively, they do so via different mechanisms. Paired-like homeoproteins dimerise via HD-HD interactions on palindromic elements, and therefore require a very precise binding substrate for cooperativity (82). Conversely, bicoid self-interacts via regions extrinsic to the HD, and can cooperatively bind spatially separated elements in various positions and orientations (90, 91). It is not clear which of these models may best describe the intermolecular cooperativity of PITX2. While there is a preponderance of published data demonstrating that PITX2 can bind to the spatially separated TAATCC elements preferred by Bicoid, conservation of exposed surface residues (figure 1-7) suggests that the Paired-like HD of PITX2 might also self-interact via the homeobox itself. I investigated the role of the PITX2 HD in homodimerisation by examining coprecipitation of differentially tagged recombinant PITX2a proteins. Wild-type PITX2a was observed to dimerise with wild-type PITX2a and with each of a panel of homeodomain mutants (T68P, R91P, V83L, or K88E) associated with AR malformations. While it is not feasible to determine the relative affinities of each heterodimer interaction precisely in this system, a conservative estimate would place the equilibrium constants involved within a range of one (or, at most, two) orders of magnitude. It may be noted that several missense mutations causing a profound loss of HD-DNA recognition did not have an obvious effect on mutant-wild-type heterodimerisation in IPs. This negative finding is consistent with similar observations that both PITX2a and Bicoid dimerise normally (or with increased affinity) even when DNA-binding is ablated by mutation of the crucial lysine at HD position 50 (91, 102). Taken together, the above data suggest that PITX2a's HD may exert only a subtle influence on dimerisation. These findings contrast with those of Saadi *et al (102)*, who have found that the T68P and K88E alleles suppress and enhance dimerisation respectively in the two-hybrid system. Mapping of PITX2a's self-interaction activity by coimmunoprecipitation analysis of deletion constructs may allow us to test in a more direct sense whether PITX2's HD is responsible for dimerisation. If the HD is indeed sufficient for PITX2 dimerisation, this finding would lend further support to the conception of K88E as a dominant negative allele.

FOXC1-PITX2a interactions

The most significant single result of my work to date is that recombinant FOXC1 and PITX2a may be functionally coupled by the formation of a physical complex. While the FOXC1-interaction domain of PITX2 remains to be mapped, deletion analysis revealed that the C-terminus of FOXC1 is necessary for PITX2 binding. Two truncations of the extreme C-terminus of FOXC1 also demonstrated that its PITX2-binding domain includes regions previously implicated in transactivation (123). One limitation of this approach is that only the necessity (rather than sufficiency) of the FOXC1 C-terminus was established. It would be interesting to test whether amino acids 367-553 of FOXC1 fully recapitulate the interaction with PITX2a, or if other regions may also be required. Additionally, I have not examined the role of the forkhead DNA-binding domain of FOXC1 in PITX2a binding. As residues in the forkhead box are essential for nuclear localization, removal of this region would cause the resulting constructs to localise to the cytoplasm, where they would be unavailable for interaction with PITX2 (123). A logical extension of my work would be to express various C-terminal fragments of FOXC1 fused to an exogenous nuclear localization signal. IPs of these FOXC1 constructs versus PITX2 should more clearly define a minimal (sufficient) PITX2BD. Mapping of the FOXC1-binding domain within PITX2a should also be a high priority in subsequent experiments. Still unexamined at present is the importance, if any, of additional protein-protein or protein-DNA interactions in FOXC1-PITX2 heteromerisation, and an indirect interaction mediated by accessory factors cannot be ruled out. These questions could best be addressed by examining the interactions of bacterially-expressed or *in vitro* translated purified proteins in a cell-free system.

Immunofluorescence experiments confirm that the structural context of the nucleus is appropriate to permit interaction of wild-type PITX2 and FOXC1, at least in cos-7 cells. Both PITX2 and FOXC1 are found in a common chromatin compartment which remains to be identified. The PITX2-containing nuclear subdomain is distinct from SC35-positive splicing speckles, from silenced chromatin marked by K20 trimethylation of histone H4, and from HP1α-containing heterochromatic sites such as pericentromeres. PITX2 is neither colocalised with nor exclusive of another nuclear protein, p300, although both proteins are similarly excluded from the largest heterochromatic foci in the cell. While I have not yet identified a nuclear landmark representing the PITX2-FOXC1 chromatin domain, there are a handful of other transcription factors which interact with PITX2 and/or occupy a grossly similar localization. Such landmarks may be useful in defining the functional role of the putative PITX2a-FOXC1 complex. β-catenin, for instance, interacts with PITX2 in C2C12 cells and has a subnuclear distribution possibly resembling PITX2's, including perinucleolar staining and large zones of exclusion (105, 159). Pit-1, which interacts with PITX2a *in vitro*, also has a potentially PITX2-like subnuclear distribution in pituitary GHFT1-5 cells, and can recruit the coactivator C-EBPα to this same locale (84, 160). Interestingly, C-EBPα normally occupies a reciprocal localisation in from that of PITX2a, associating exclusively with pericentromeric heterochromatin (161). A detailed examination of the colocalisation of PITX2a and each of the above factors may indicate which cofactors are targeted to FOXC1-containing chromatin. Knowledge of the chromatin composition of this subnuclear domain may, in turn, provide clues with respect to the mechanism of target activation of both PITX2 and FOXC1.

The subnuclear targeting of PITX2a may also be relevant to the molecular pathology of AR malformations, as some patient mutations appear to sequester PITX2a from FOXC1. Previous reports of the intracellular distribution of wildtype and mutant PITX2a have been limited to distinctions between the nuclear and cytoplasmic compartments (104, 127). In these studies, both wild-type PITX2a and V83L proteins are properly directed to the nuclei of cos-7 cells. In contrast, T68P, R84W, or R91P PITX2a constructs are aberrantly localized to the cytoplasm in 18%, 23%, and 64% of cells respectively. A correlation between nuclear localization, transactivity, and phenotypic severity of the mutations implicated has been suggested (104). My own analysis made use of these same mutants, but included only those cells with both normal nuclear morphology and completely nuclear PITX2a staining; this approach revealed a more subtle deficit in trafficking of PITX2a within the nucleus. In the absence of recombinant wild-type PITX2a, the T68P, R91P, R84W, and K88E alleles each show reduced colocalisation with FOXC1. Tellingly, these same alleles have published defects in nuclear import, suggesting that both the nuclear and subnuclear targeting defects of all four mutants may be less or more subtle manifestations of the same phenomenon.

I also posed an additional question not addressed in previous studies of PITX2a's localisation, namely the role of wild-type-mutant heterodimerisation on the distribution of both proteins. Coexpression of wild-type and mutant PITX2a constructs did not reveal any evidence of a *trans* effect on subnuclear targeting of the wild-type protein, ruling out sequestration as a mechanism of dominance. Similarly, cotransfected wild-type PITX2a did not repair the marked localization defect of the T68P and R91P mutants. However, wild-type PITX2a did rescue the (relatively subtle) localization defect of K88E and R84W constructs. Direct interaction of mutant and wild-type PITX2a explains this substantial rescue of localization only if one presumes the large majority of K88E or R84W protein to be complexed with wild-type PITX2a, an assumption lacking experimental support at present. Alternatively, the observed localisation rescue may be an indication that wild-type *PITX2* directs the expression of cofactors necessary for its own subnuclear targeting. A third explanation is that expression of wild-type PITX2 relieves a cytotoxic effect of expressing the mutants in culture. It will be difficult to distinguish whether altered nuclear and subnuclear distribution of mutant PITX2 proteins represents a biologically relevant datum, or if aggregate formation and cytoplasmic expression are both attributable to the high level of expression characteristic of this system. It is interesting, in either case, that substantially different localization patterns are elicited by point substitutions within the PITX2a HD. It would appear that some point substitutions of the HD produce gross changes in the solubility and/or trafficking of PITX2a as a whole, confirming the prime importance of the HD in the normal function of this factor.

Chapter four:

General Discussion and Conclusions

In the preceding chapters, I have presented my own, incremental, contributions to an evolving understanding of the molecular basis of Axenfeld-Reiger malformations. In terms of the genetic basis of AR, microdeletions of the *PITX2* locus represent a previously unrecognised aetiology which may be as (un)common as *PITX2* point mutations. The fortunate observation of cosegregation with AR in one extended kindred provides verification of this technique as well as strong support for simple *PITX2* haploinsufficiency as one cause of AR.

Biochemical studies have also revealed an appealingly straightforward link between *PITX2* and *FOXC1*, which may hint at a common transcriptional role for both genes. In a recombinant expression system, PITX2a and FOXC1 physically interact and share a distinctive subnuclear localisation on chromatin. Moreover, several AR patient alleles of PITX2a transactivity were aberrantly localised within the nucleus and potentially less available for interaction with *FOXC1*. These findings place PITX2 and FOXC1 in a common molecular and sub-organellar setting which is consistent with a common role for both proteins in the activation of target genes essential for normal development of the anterior chamber. The following discussion is intended to place the putative PITX2-FOXC1 interaction in a physiological context within the cell, as well as to suggest a tentative model revisiting gene dosage sensitivity in light of these new findings.

Extracellular signals involved in mesenchymal immigration

The existence of a putative PITX2-FOXC1 functional complex is likely to have important implications for the molecular biology of AR malformations in patients. Most obvious of these is that coordinated function in a common complex may be a root cause of the clinically indistinguishable phenotypes of human *PITX2* and *FOXC1* mutations. Because PITX2 and FOXC1 are coexpressed in the periocular mesenchyme prior to immigration and formation of the anterior segment, and because mutations of either gene produce equivalent AR-spectrum phenotypes, it is reasonable to presume that both genes govern the response of the presumptive anterior chamber angle to morphogenetic signals (29, 44, 63, 111, 112). In particular, *PITX2* and *FOXC1* may potentiate mesenchymal responses to signals required for normal migration and condensation into endothelia such as those of the cornea and trabecular meshwork. Elaboration of the anterior chamber angle is likely to involve the action of both soluble chemotactic agents and mechanical messages transduced by the cytoskeleton and extracellular matrix during migration. As PITX2 and FOXC1 have been shown to respond to distinct types of extracellular signals, interaction of these two proteins may allow the cell to coordinate distinct suites of developmentally important stimuli.

One such stimulus may be soluble signals of the β-type transforming growth factor (TGFβ) family. In animal models of the developing eye, these proteins promote proliferation and migration of the periocular mesenchyme while concurrently suppressing differentiation. Immunohistochemistry reveals that TGFβ1, and, to a lesser extent, TGFβ2 and TGFβ3, are expressed in fibers of the developing lens between 14.5dpc and 17.5dpc in mouse (162). TGFβ1 overexpression in the lens of transgenic mice is catastrophic to anterior segment development, and leads to a hypercellular, undifferentiated, and vascularised mesenchyme where the anterior chamber, corneal endothelium, and iris stroma normally form (163). Altered matrix composition and cell adhesion properties may be responsible for this dramatically increased mesenchymal influx, as the adhesive glycoproteins Fibronectin and Thrombospondin-1 are greatly induced by TGFβ1 in the mesenchyme during migration. Fibronectin and Thrombospondin-1 are among an assortment of extracellular matrix proteins which promote early neural crest cell adhesion and migration (164-166). Interestingly, FOXC1 is upregulated by TGFβ1 and mediates TGFβ1-mediated growth arrest at the G0/G1 checkpoint in HeLa cells and other human cancer lines (167) Furthermore, TGFβ1 causes chondrogenic differentiation of mesenchymal cell cultures of the primodial sternum in mouse, while similar cells derived from FOXC1$^{-/-}$ knockout mice are unresponsive (80). The above data suggest that TGFβ factors may be one soluble signal communicated from lens to invading mesenchyme by FOXC1 during elaboration of the anterior segment. In avian embryos, experimental removal of the lens vesicle causes failure of corneal endothelial differentiation and lack of an anterior chamber, so at least one such ectodermal-mesenchymal signal appears essential for anterior segment development (28).

In addition to β-type transforming growth factors, epidermal growth factor (EGF)-like peptide growth hormones may play a similar role in lens-mesenchyme communication during anterior chamber formation, although through a distinct intracellular signaling pathway. Ectopic expression of TGFα or EGF in the lens causes anterior segment dysgenesis in transgenic mice, and the resultant morphological defects are reminiscent of ectopic TGFβ1 expression (168, 169). In particular, differentiation of the presumptive corneal endothelium is arrested, and the anterior chamber remains filled with undifferentiated mesenchyme in contact with the lens vesicle (30). In similarly constructed mice expressing a yet higher level of ectopic TGFα in the lens, invading mesenchyme fills both the anterior and vitreous chambers of the eye and completely surrounds the lens (169). *In-situ* hybridisation shows the EGF receptor (EGFR), which can bind either TGFα or EGF, to be highly expressed in the periocular mesenchyme and corneal epithelium during the crucial period from E13 through E15 (30, 169). As could be expected, EGFR is required for TGFα-responsive mesenchymal chemotaxis in the eye, and excess TGFα in the lens of EGFR$^{-/-}$ *waved-2* mice does not cause mesenchymal overrun of the anterior and posterior chambers (169). Loss of this pathway also causes anterior segment dysgenesis, which is among the ocular phenotypes seen in TGF$\alpha^{-/-}$ (*waved-1*) mice (170, 171). Receptor tyrosine kinases such as EGFR signal their activities via mitogen activated protein kinase (MAP kinase) cascades in the cell. One such MAP kinase, p44/42 ERK, phosphorylates and inhibits FOXC1 in HeLa cells, so EGF-like soluble messages may inform the development of the anterior chamber via a mechanism involving FOXC1 (123, 124).

While FOXC1 responds to several soluble growth factors, PITX2 appears to be involved in a feedback loop involving the actin cytoskeleton, the small GTPases RhoA and Rac, and β-catenin. As discussed previously in the context of *PITX2* coactivator recruitment, Wnt pathway stimulation causes nuclear import of β-catenin, which stimulates *PITX2* by inducing its transcription while concurrently forming a synergistic protein interaction with PITX2a (105). β-catenin is a point at which numerous signaling pathways converge at the cytoskeleton, and acts both as a transcriptional coactivator in the nucleus and as an adaptor between actin stress fibers and cadherin-containing complexes such as adherens junctions (172). As an anchor for cell-cell contacts and the cytoskeleton, adherens junctions are de- and reconstructed during repolarisation of stress fibers following the application of shear forces (173). β-catenin may therefore transduce stress and shear forces to *PITX2* via mechanisms including regulated liberation from intercellular junctions. *PITX2* can also reciprocally remodel the actin cytoskeleton, as expression of PITX2a in HeLa cells stimulates assembly of actin and myosin filaments, causes cell spreading, decreases motility, and increases N-cadherin and β-catenin localisation at cell-cell contacts (174). The mechanism of PITX2-directed cytoskeletal rearrangement proceeds via upregulation of the small GTPases RhoA and

Rac1. Small GTPases such as Rho, when activated, promote actin polymerisation and myosin light chain phosphorylation via downstream effectors including the ROCK protein kinase (175). This latter pathway may be prominent in the regulation of intraocular pressure by the mature trabecular meshwork. RhoA, for instance, increases outflow facility of perfused eyes and decreases contractility of cultured TM cells (176, 177). Furthermore, a glaucoma-causing corticosteroid, dexamethasone, produces rearrangements of β-catenin and actin cytoskeleton in epithelial cells via a mechanism involving downregulation of RhoA (178). Between cDNA libraries and Northen analysis, we can demonstrate that at least the transcripts of *PITX2* and *FOXC1* are coexpressed in cell lines derived from the mature human TM, so the involvement of this pathway in the regulation of IOP may be an interesting area for future investigation (appendix E) (65).

For the sake of clarity, I have outlined the above signal transduction pathways as though they were discrete cascades focused on activation of either *FOXC1* or *PITX2*. However, EGF-like, TGFβ, and catenin/cadherin signaling are interconnected with a significant degree of crosstalk. Several points of signal integration are discussed below, and a purely schematic diagram of the scheme discussed is shown in figure 4-1. Firstly, mechanical signals transduced by the actin cytoskeleton can feed into the MAP kinase pathway, as RhoA and Rac1 cause nuclear translocation of ERK in response to mechanical stretch (179). Reciprocally, receptor tyrosine kinases can direct morphological changes mediated by the actin cytoskeleton, as receptor tyrosine kinases including EGFR and the vascular endothelial growth factor receptor (VEGFR) can phosphorylate β-catenin at adherens junctions (180, 181). EGFR-mediated phosphorylation of β-catenin precedes a physical interaction of these two proteins, which occurs in response to relief of cell-cell contacts by trypsinisation (180). TGFβ signaling also appears important for remodeling of the actin cytoskeleton in the trabecular meshwork. In cultured bovine trabecular meshwork cells, TGFβ1 promotes cell spreading, increases the size and number of actin stress fibers, and stimulates contractile behaviour (177). These changes mirror those induced by PITX2 in HeLa cells and have a similar mechanistic requirement for Rho and Rac1 activity (174, 177). A complete accounting of these complex pathways is far beyond the scope of this discussion. Rather, the intention is merely to illustrate that PITX2 and FOXC1 respond to canonical signaling pathways implicated in the development and function of the anterior chamber, and that these cascades are interconnected through a complex and

Figure 4-1: Possible circuit for integration of soluble and mechanical signals by a PITX2-FOXC1 complex

This figure is a schematic illustration of the soluble and mechanical signals outlined in the accompanying discussion. Lines with triangular arrowheads represent activating circuits, while inhibitory relationships are represented as lines with blunt arrowheads. For the sake of clarity, not all pathways discussed are illustrated. Dashed arrows represent target gene transactivation. Literature references are provided (numbered circles). Many circuits shown proceed via complex or incompletely defined multistep pathways, such as the induction of FOXC1 by TGFβ1. The pathways shown are drawn from a wide variety of cell types and experimental systems, and may not be preserved in a given cell of interest.

Dex: Dexamethasone

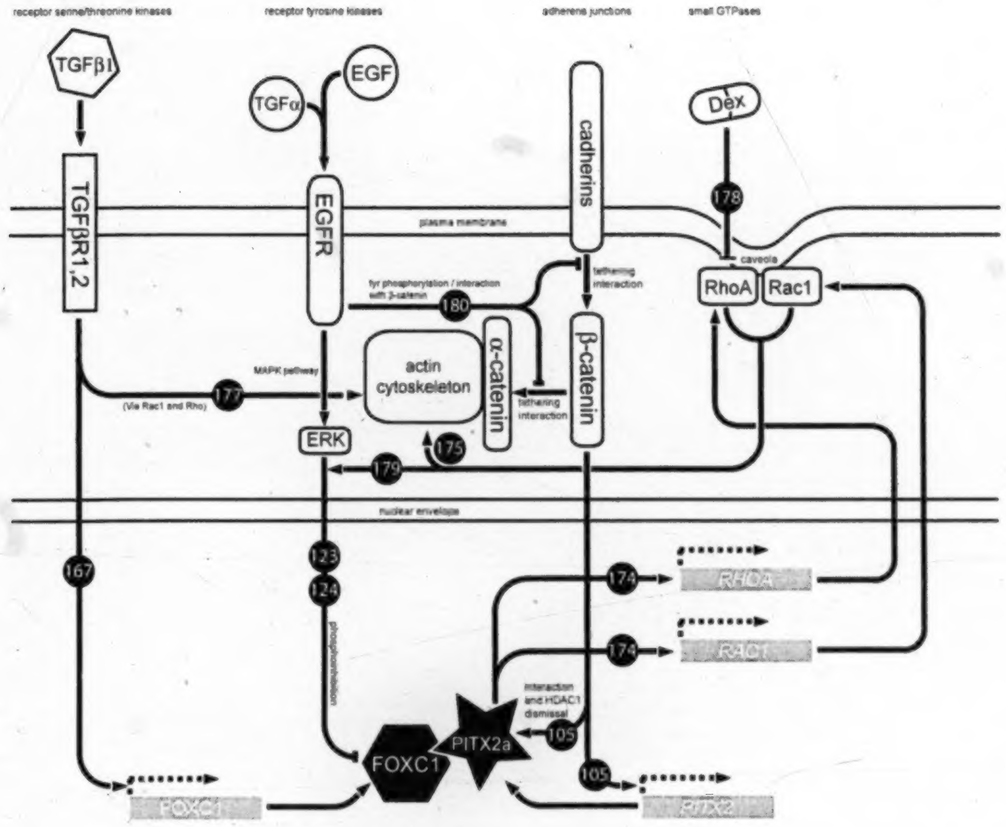
receptor serine/threonine kinases
receptor tyrosine kinases
adherens junctions
small GTPases
TGFβ1
TGFα
EGF
Dex
TGFβR1,2
EGFR
cadherins
plasma membrane
178
caveola
tyr phosphorylation / interaction with β-catenin
180
tethering interaction
RhoA
Rac1
MAPK pathway
177
(Via Rac1 and Rho)
actin cytoskeleton
α-catenin
tethering interaction
β-catenin
ERK
175
179
nuclear envelope
167
123
124
phosphorylation
174
RHOA
174
RAC1
interaction and HDAC1 dismissal
105
FOXC1
PITX2a
105
FOXC1
PITX2

redundant circuitry. A putative PITX2a- and FOXC1-containing complex on chromatin could represent an additional link allowing coordinated transcriptional responses to soluble and mechanical signals. At present, the importance of *PITX2* and *FOXC1* in cytoskeletal remodeling of the trabecular meshwork has not been examined directly. It may also be interesting to determine what effect, if any, disrupting PITX2-FOXC1 interactions will have on cell cytoskeletal remodeling. Experiments addressing the latter question will be greatly facilitated by defining the region of PITX2a responsible for FOXC1 binding, as well as elucidating the effect of interaction on the transactivity of both partners. Biochemically determining what other proteins interact with PITX2a and FOXC1 may also provide clues as to the physiological role of this complex.

Outstanding questions regarding dosage sensitivity and protein interactions

Hypo- and hypermorphic mutations, deletions, and duplications of both *PITX2* and *FOXC1* demonstrate that both genes are required at a strictly enforced optimum of activity during normal development of the anterior segment (44, 111, 112, 115, 133). Simple haploinsufficiency is a thoroughly defensible explanation for the pathogenicity of PITX2 microdeletions and loss-of-function mutations such as T68P and R91P. However, this term is of limited value in the construction of a model for dosage sensitivity, and offers no insight into the essentially identical phenotype caused by duplications or hyperactive mutations of *FOXC1* and *PITX2* respectively. Our understanding of the molecular basis of AR malformations will necessarily involve a model which explains the phenotypes of both increased and decreased *PITX2* and *FOXC1* activity in terms of a common molecular pathology.

Protein interactions may offer one explanation for the strict dosage sensitivity of *PITX2* and *FOXC1*, given that PITX2-PITX2 and PITX2-FOXC1 complexes may form in a concentration- and/or cofactor-dependent fashion. Variations in the expression of either gene may alter the relative abundance of both types of complex. If PITX2-PITX2 and PITX2-FOXC1 complexes are mutually exclusive, they may interact with distinct cofactors and/or activate differing suites of target genes. Alternatively, PITX2-PITX2 and PITX2-FOXC1 complexes may compete for a common pool of transcriptional cofactors and/or binding sites. Before the validity of this model can be tested, a number of basic biochemical and functional analyses of the PITX2-FOXC1 interaction will be necessary. For instance, it will be instructive to determine whether PITX2-PITX2 and PITX2-FOXC1 complexes are mutually exclusive. If the 65kDa PITX2 species seen in figures 3-2 and

3-3 does indeed constitute incompletely denatured PITX2a dimer, then a ternary PITX2-PITX2-FOXC1 interaction can be inferred. This possibility could be further tested by studying the effect of coexpressed FOXC1 on PITX2-PITX2 interactions via IP. Additionally, it remains to be seen whether the PITX2-FOXC1 interaction is activating or repressive, and what effect, if any, this association has on the activation of specific promotors by *PITX2* and *FOXC1*. These and other questions are outlined in the following, final, section of this discussion.

Future Prospects

As appears to be a common experience in biology, my investigation of the molecular basis of Axenfeld-Rieger malformations has yielded only a handful of answers but a relative wealth of possible questions. My observations support the existence of a PITX2a- and FOXC1- containing chromatin complex, the nature of which otherwise remains completely undefined.

Characterisation of the putative PITX2/FOXC1 complex can proceed along several parallel streams. Biochemically, gel filtration and other chromatographic methods (such as immunoaffinity purification) may be the best available methods to identify other proteins present in this complex. Putative interactions identified in this system can be validated by immunoprecipitation, and IP or pull-down assays of bacterially expressed proteins may be used to determine which of the validated interactions are direct, as well as which interactions are mutually exclusive. HA-tagged PITX2 deletion constructs are presently being constructed and will, together with the FOXC1 panel already in use, allow domain mapping of interactions between both proteins and any of the dozens of chromatin proteins likely to be present in the same complex. Ethidium bromide or DNAse/RNAse treatments can be used to determine which of these interactions are DNA- (or RNA-) dependent and which can occur in the absence of nucleic acid binding. A number of chromatin proteins identified as PITX2a cofactors by Kioussi *et al.* in the Wnt pathway, such as p300/CBP, β-catenin, and CLIM, should provide a good launchpad for this analysis (105). Immunofluorescence experiments may provide a second avenue to characterise the presumed PITX2/FOXC1 complex, and work is underway in our laboratory to determine whether a number of general chromatin proteins with grossly similar subnuclear distributions might colocalise well with PITX2 and FOXC1.

Functional characterisation of the complex will be a more complex task, and experimental limitations are somewhat more restrictive. In the absence of common transcriptional targets for both PITX2 and FOXC1, reporter assays will be indispensible as a transactivity read-out given different cofactors and/or extracellular stimuli. This approach, unfortunately, lacks a proper chromatin context for activation or repression, and requires (often problematic) assumptions regarding the sequence antecedents of PITX2/FOXC1 binding. Sequential chromatin immunoprecipitation (ChIP) of both PITX2 and FOXC1 would be perhaps the most powerful way of flagging promotors regulated by both factors, and should be more specific than ChIP against either protein alone. CpG island microarray-based ChIP has recently become a practicable method for identifying ChIP-enriched genomic elements in a high-throughput fashion (182). A commercial CpG island microarray is now available from the Canadian University Health Network Microarray Centre (www.microarrays.ca). It would be preferable to perform such experiments in a human cell line derived from the trabecular meshwork, using endogenous PITX2 and FOXC1. Unfortunately, this line of inquiry has been forestalled by a lack of both high-quality PITX2 antisera and robust, appropriate cell lines. Putative targets identified by ChIP will, in any case, require validation by one or more additional methods, such as reporter assays or Northern and immunoblot analyses. Compromises on the cell line and expression system used may therefore be justifiable in order to advance the understanding of the transcriptional role of PITX2 and FOXC1, both individually and in concert.

Because variable developmental angle defects are seen in AR patients, physical occlusion of the angle is one potential mechanism for glaucoma pathogenesis. However, dysfunction, rather than blockage, of the TM may also be a contributing factor. In terms of my personal hopes for the future of this work, it would be very gratifying to see PITX2 and FOXC1 eventually tied into a common pathway involved in extracellular matrix secretion and/or contraction of the TM. As outlined in the above discussion, both PITX2 and FOXC1 affect cell motility, adhesion, and cytoskeletal remodeling in cultured cells, and both may be responsive to a variety of signals transduced at the plasma membrane. At some point in the future, pharmacologic modulation of PITX2 and FOXC1 activities may become a viable option employed in the therapy of AR, or in the treatment of glaucoma in general.

Bibliography

1. Quigley, H.A. (1996) Number of people with glaucoma worldwide. *Br J Ophthalmol,* **80,** 389-93.
2. Weinreb, R.N. and Khaw, P.T. (2004) Primary open-angle glaucoma. *Lancet,* **363,** 1711-20.
3. Bonomi, L., Marchini, G., Marraffa, M., Bernardi, P., De Franco, I., Perfetti, S., Varotto, A. and Tenna, V. (1998) Prevalence of glaucoma and intraocular pressure distribution in a defined population. The Egna-Neumarkt Study. *Ophthalmology,* **105,** 209-15.
4. Bartels, S.P. (1989) Aqueous Humor Formation. In Ritch, R., Shields, M.B. and Krupin, T. (eds.), *The Glaucomas.* Mosby, St. Louis, Vol. 1, pp. 199-218.
5. Kaufman, P.L. (1989) Pressure-dependent Outflow. In Ritch, R., Shields, M.B. and Krupin, T. (eds.), *The Glaucomas.* Mosby, St. Louis, Vol. 1, pp. 219-240.
6. Lowe, R.F. and Ritch, R. (1989) Angle-closure glaucoma: mechanisms and epidemiology. In Ritch, R., Shields, M.B. and Krupin, T. (eds.), *The Glaucomas.* Mosby, St. Louis, Vol. 2, pp. 825-38.
7. Normal Eye Anatomy. National Eye Institute, National Institutes of Health USA, Vol. 2004.
8. Tripathi, B.J. and Tripathi, R.C. (1989) Embryology of the anterior segment of the human eye. In Ritch, R., Shields, M.B. and Krupin, T. (eds.), *The Glaucomas.* Mosby, St. Louis, Vol. 1, pp. 3-40.
9. Pederson, J.E. (1989) Uveoscleral Outflow. In Ritch, R., Shields, M.B. and Krupin, T. (eds.), *The Glaucomas.* Mosby, St. Louis, Vol. 1, pp. 241-8.
10. Tripathi, B.J. and Tripathi, R.C. (1989) Neural crest origin of human trabecular meshwork and its implications for the pathogenesis of glaucoma. *Am J Ophthalmol,* **107,** 583-90.
11. Darwin, C. (1875) Inheritance. In *The Variation of Animals and Plants Under Domestication.* 2 ed. John Murray, London, Vol. 1, pp. 453-454.
12. Vossius, A. (1883) Congenitale abnormalien der iris. *Klin Monatsbl Augenheilkd,* **21,** 233-237.
13. Axenfeld, T.H. (1920) Embryotoxon cornea posterius. *Klin. Monastbl. Augenheilkd.,* **65,** 381-382.
14. Lines, M.A., Kozlowski, K. and Walter, M.A. (2002) Molecular genetics of Axenfeld-Rieger malformations. *Hum Mol Genet,* **11,** 1177-84.
15. Amendt, B.A., Semina, E.V. and Alward, W.L. (2000) Rieger syndrome: a clinical, molecular, and biochemical analysis. *Cell Mol Life Sci,* **57,** 1652-66.
16. Rieger, H. (1935) Dysgenesis mesodermalis coreneal et iridis. *Z. Augenheilkd.,* **86,** 333.
17. Alkemade, P. (1969) *Dysgenesis Mesodermalis of the Iris and the Cornea: A Study of Rieger's Syndrome and Peter's Anomaly.* Van Gorcum, Assen, The Netherlands.

18. Reese, A. and Ellsworth, R. (1966) The anterior chamber cleavage syndrome. *Arch Ophthalmol,* **75,** 307-318.
19. Waring, G.O., 3rd, Rodrigues, M.M. and Laibson, P.R. (1975) Anterior chamber cleavage syndrome. A stepladder classification. *Surv Ophthalmol,* **20,** 3-27.
20. Shields, M.B. (1983) Axenfeld-Rieger syndrome: a theory of mechanism and distinctions from the iridocorneal endothelial syndrome. *Trans Am Ophthalmol Soc,* **81,** 736-84.
21. Sadeghi-Nejad, A. and Senior, B. (1974) Autosomal dominant transmission of isolated growth hormone deficiency in iris-dental dysplasia (Rieger's syndrome). *J Pediatr,* **85,** 644-8.
22. Cunningham, E.T., Jr., Eliott, D., Miller, N.R., Maumenee, I.H. and Green, W.R. (1998) Familial Axenfeld-Rieger anomaly, atrial septal defect, and sensorineural hearing loss: a possible new genetic syndrome. *Arch Ophthalmol,* **116,** 78-82.
23. Moog, U., Bleeker-Wagemakers, E.M., Crobach, P., Vles, J.S. and Schrander-Stumpel, C.T. (1998) Sibs with Axenfeld-Rieger anomaly, hydrocephalus, and leptomeningeal calcifications: a new autosomal recessive syndrome? *Am J Med Genet,* **78,** 263-6.
24. Bekir, N.A. and Gungor, K. (2000) Atrial septal defect with interatrial aneurysm and Axenfeld-Rieger syndrome. *Acta Ophthalmol Scand,* **78,** 101-3.
25. Franco, D. and Campione, M. (2003) The role of Pitx2 during cardiac development. Linking left-right signaling and congenital heart diseases. *Trends Cardiovasc Med,* **13,** 157-63.
26. Fitch, N. and Kaback, M. (1978) The Axenfeld syndrome and the Rieger syndrome. *J Med Genet,* **15,** 30-4.
27. Cvekl, A. and Tamm, E.R. (2004) Anterior eye development and ocular mesenchyme: new insights from mouse models and human diseases. *Bioessays,* **26,** 374-86.
28. Beebe, D.C. and Coats, J.M. (2000) The lens organizes the anterior segment: specification of neural crest cell differentiation in the avian eye. *Dev Biol,* **220,** 424-31.
29. Kidson, S.H., Kume, T., Deng, K., Winfrey, V. and Hogan, B.L. (1999) The forkhead/winged-helix gene, Mf1, is necessary for the normal development of the cornea and formation of the anterior chamber in the mouse eye. *Dev Biol,* **211,** 306-22.
30. Reneker, L.W., Silversides, D.W., Xu, L. and Overbeek, P.A. (2000) Formation of corneal endothelium is essential for anterior segment development - a transgenic mouse model of anterior segment dysgenesis. *Development,* **127,** 533-42.
31. Johnston, M.C., Noden, D.M., Hazelton, R.D., Coulombre, J.L. and Coulombre, A.J. (1979) Origins of avian ocular and periocular tissues. *Exp Eye Res,* **29,** 27-43.

32. Kaiser-Kupfer, M.I. (1989) Neural crest origin of trabecular meshwork cells and other structures of the anterior chamber. *Am J Ophthalmol,* **107,** 671-2.

33. Trainor, P.A. and Tam, P.P. (1995) Cranial paraxial mesoderm and neural crest cells of the mouse embryo: co-distribution in the craniofacial mesenchyme but distinct segregation in branchial arches. *Development,* **121,** 2569-82.

34. Steinsapir, K.D., Lehman, E., Ernest, J.T. and Tripathi, R.C. (1990) Systemic neurocristopathy associated with Rieger's syndrome. *Am J Ophthalmol,* **110,** 437-8.

35. Vaux, C., Sheffield, L., Keith, C.G. and Voullaire, L. (1992) Evidence that Rieger syndrome maps to 4q25 or 4q27. *J Med Genet,* **29,** 256-8.

36. Heon, E., Sheth, B.P., Kalenak, J.W., Sunden, S.L., Streb, L.M., Taylor, C.M., Alward, W.L., Sheffield, V.C. and Stone, E.M. (1995) Linkage of autosomal dominant iris hypoplasia to the region of the Rieger syndrome locus (4q25). *Hum Mol Genet,* **4,** 1435-9.

37. Datson, N.A., Semina, E., van Staalduinen, A.A., Dauwerse, H.G., Meershoek, E.J., Heus, J.J., Frants, R.R., den Dunnen, J.T., Murray, J.C. and van Ommen, G.J. (1996) Closing in on the Rieger syndrome gene on 4q25: mapping translocation breakpoints within a 50-kb region. *Am J Hum Genet,* **59,** 1297-305.

38. Semina, E.V., Datson, N.A., Leysens, N.J., Zabel, B.U., Carey, J.C., Bell, G.I., Bitoun, P., Lindgren, C., Stevenson, T., Frants, R.R. *et al.* (1996) Exclusion of epidermal growth factor and high-resolution physical mapping across the Rieger syndrome locus. *Am J Hum Genet,* **59,** 1288-96.

39. Walter, M.A., Mirzayans, F., Mears, A.J., Hickey, K. and Pearce, W.G. (1996) Autosomal-dominant iridogoniodysgenesis and Axenfeld-Rieger syndrome are genetically distinct. *Ophthalmology,* **103,** 1907-15.

40. Gould, D.B., Mears, A.J., Pearce, W.G. and Walter, M.A. (1997) Autosomal dominant Axenfeld-Rieger anomaly maps to 6p25. *Am J Hum Genet,* **61,** 765-8.

41. Mirzayans, F., Mears, A.J., Guo, S.W., Pearce, W.G. and Walter, M.A. (1997) Identification of the human chromosomal region containing the iridogoniodysgenesis anomaly locus by genomic-mismatch scanning. *Am J Hum Genet,* **61,** 111-9.

42. Phillips, J.C., del Bono, E.A., Haines, J.L., Pralea, A.M., Cohen, J.S., Greff, L.J. and Wiggs, J.L. (1996) A second locus for Rieger syndrome maps to chromosome 13q14. *Am J Hum Genet,* **59,** 613-9.

43. Ferguson, J.G., Jr. and Hicks, E.L. (1987) Rieger's anomaly and glaucoma associated with partial trisomy 16q. Case report. *Arch Ophthalmol,* **105,** 323.

44. Semina, E.V., Reiter, R., Leysens, N.J., Alward, W.L., Small, K.W., Datson, N.A., Siegel-Bartelt, J., Bierke-Nelson, D., Bitoun, P., Zabel, B.U. *et al.* (1996) Cloning and characterization of a novel bicoid-related homeobox transcription factor gene, RIEG, involved in Rieger syndrome. *Nat Genet,* **14,** 392-9.

45. Alward, W.L., Semina, E.V., Kalenak, J.W., Heon, E., Sheth, B.P., Stone, E.M. and Murray, J.C. (1998) Autosomal dominant iris hypoplasia is caused by a mutation in the Rieger syndrome (RIEG/PITX2) gene. *Am J Ophthalmol,* **125,** 98-100.
46. Kulak, S.C., Kozlowski, K., Semina, E.V., Pearce, W.G. and Walter, M.A. (1998) Mutation in the RIEG1 gene in patients with iridogoniodysgenesis syndrome. *Hum Mol Genet,* **7,** 1113-7.
47. Gage, P.J. and Camper, S.A. (1997) Pituitary homeobox 2, a novel member of the bicoid-related family of homeobox genes, is a potential regulator of anterior structure formation. *Hum Mol Genet,* **6,** 457-64.
48. Kitamura, K., Miura, H., Yanazawa, M., Miyashita, T. and Kato, K. (1997) Expression patterns of Brx1 (Rieg gene), Sonic hedgehog, Nkx2.2, Dlx1 and Arx during zona limitans intrathalamica and embryonic ventral lateral geniculate nuclear formation. *Mech Dev,* **67,** 83-96.
49. Arakawa, H., Nakamura, T., Zhadanov, A.B., Fidanza, V., Yano, T., Bullrich, F., Shimizu, M., Blechman, J., Mazo, A., Canaani, E. *et al.* (1998) Identification and characterization of the ARP1 gene, a target for the human acute leukemia ALL1 gene. *Proc Natl Acad Sci U S A,* **95,** 4573-8.
50. Cox, C.J., Espinoza, H.M., McWilliams, B., Chappell, K., Morton, L., Hjalt, T.A., Semina, E.V. and Amendt, B.A. (2002) Differential regulation of gene expression by PITX2 isoforms. *J Biol Chem,* **277,** 25001-10.
51. Kozak, M. (1987) At least six nucleotides preceding the AUG initiator codon enhance translation in mammalian cells. *J Mol Biol,* **196,** 947-50.
52. Gage, P.J., Suh, H. and Camper, S.A. (1999) Dosage requirement of Pitx2 for development of multiple organs. *Development,* **126,** 4643-51.
53. Kitamura, K., Miura, H., Miyagawa-Tomita, S., Yanazawa, M., Katoh-Fukui, Y., Suzuki, R., Ohuchi, H., Suehiro, A., Motegi, Y., Nakahara, Y. *et al.* (1999) Mouse Pitx2 deficiency leads to anomalies of the ventral body wall, heart, extra- and periocular mesoderm and right pulmonary isomerism. *Development,* **126,** 5749-58.
54. Feingold, M., Shiere, F., Fogels, H.R. and Donaldson, D. (1969) Rieger's syndrome. *Pediatrics,* **44,** 564-9.
55. Noden, D.M. (1988) Interactions and fates of avian craniofacial mesenchyme. *Development,* **103 Suppl,** 121-40.
56. Noden, D.M., Marcucio, R., Borycki, A.G. and Emerson, C.P., Jr. (1999) Differentiation of avian craniofacial muscles: I. Patterns of early regulatory gene expression and myosin heavy chain synthesis. *Dev Dyn,* **216,** 96-112.
57. Suh, H., Gage, P.J., Drouin, J. and Camper, S.A. (2002) Pitx2 is required at multiple stages of pituitary organogenesis: pituitary primordium formation and cell specification. *Development,* **129,** 329-37.
58. Quentien, M.H., Manfroid, I., Moncet, D., Gunz, G., Muller, M., Grino, M., Enjalbert, A. and Pellegrini, I. (2002) Pitx factors are involved in basal and hormone-regulated activity of the human prolactin promoter. *J Biol Chem,* **277,** 44408-16.

59. Quentien, M.H., Pitoia, F., Gunz, G., Guillet, M.P., Enjalbert, A. and Pellegrini, I. (2002) Regulation of prolactin, GH, and Pit-1 gene expression in anterior pituitary by Pitx2: An approach using Pitx2 mutants. *Endocrinology,* **143,** 2839-51.
60. Suszko, M.I., Lo, D.J., Suh, H., Camper, S.A. and Woodruff, T.K. (2003) Regulation of the rat follicle-stimulating hormone beta-subunit promoter by activin. *Mol Endocrinol,* **17,** 318-32.
61. Muccielli, M.L., Martinez, S., Pattyn, A., Goridis, C. and Brunet, J.F. (1996) Otlx2, an Otx-related homeobox gene expressed in the pituitary gland and in a restricted pattern in the forebrain. *Mol Cell Neurosci,* **8,** 258-71.
62. Mucchielli, M.L., Mitsiadis, T.A., Raffo, S., Brunet, J.F., Proust, J.P. and Goridis, C. (1997) Mouse Otlx2/RIEG expression in the odontogenic epithelium precedes tooth initiation and requires mesenchyme-derived signals for its maintenance. *Dev Biol,* **189,** 275-84.
63. Hjalt, T.A., Semina, E.V., Amendt, B.A. and Murray, J.C. (2000) The Pitx2 protein in mouse development. *Dev Dyn,* **218,** 195-200.
64. Wirtz, M.K., Samples, J.R., Xu, H., Severson, T. and Acott, T.S. (2002) Expression profile and genome location of cDNA clones from an infant human trabecular meshwork cell library. *Invest Ophthalmol Vis Sci,* **43,** 3698-704.
65. Tomarev, S.I., Wistow, G., Raymond, V., Dubois, S. and Malyukova, I. (2003) Gene expression profile of the human trabecular meshwork: NEIBank sequence tag analysis. *Invest Ophthalmol Vis Sci,* **44,** 2588-96.
66. St Amand, T.R., Zhang, Y., Semina, E.V., Zhao, X., Hu, Y., Nguyen, L., Murray, J.C. and Chen, Y. (2000) Antagonistic signals between BMP4 and FGF8 define the expression of Pitx1 and Pitx2 in mouse tooth-forming anlage. *Dev Biol,* **217,** 323-32.
67. Hjalt, T.A., Amendt, B.A. and Murray, J.C. (2001) PITX2 regulates procollagen lysyl hydroxylase (PLOD) gene expression: implications for the pathology of Rieger syndrome. *J Cell Biol,* **152,** 545-52.
68. Espinoza, H.M., Cox, C.J., Semina, E.V. and Amendt, B.A. (2002) A molecular basis for differential developmental anomalies in Axenfeld-Rieger syndrome. *Hum Mol Genet,* **11,** 743-53.
69. Schweickert, A., Campione, M., Steinbeisser, H. and Blum, M. (2000) Pitx2 isoforms: involvement of Pitx2c but not Pitx2a or Pitx2b in vertebrate left-right asymmetry. *Mech Dev,* **90,** 41-51.
70. Yu, X., St Amand, T.R., Wang, S., Li, G., Zhang, Y., Hu, Y.P., Nguyen, L., Qiu, M.S. and Chen, Y.P. (2001) Differential expression and functional analysis of Pitx2 isoforms in regulation of heart looping in the chick. *Development,* **128,** 1005-13.
71. Ryan, A.K., Blumberg, B., Rodriguez-Esteban, C., Yonei-Tamura, S., Tamura, K., Tsukui, T., de la Pena, J., Sabbagh, W., Greenwald, J., Choe, S. *et al.* (1998) Pitx2 determines left-right asymmetry of internal organs in vertebrates. *Nature,* **394,** 545-51.
72. Logan, M., Pagan-Westphal, S.M., Smith, D.M., Paganessi, L. and Tabin, C.J. (1998) The transcription factor Pitx2 mediates situs-specific

morphogenesis in response to left-right asymmetric signals. *Cell,* **94,** 307-17.

73. Campione, M., Ros, M.A., Icardo, J.M., Piedra, E., Christoffels, V.M., Schweickert, A., Blum, M., Franco, D. and Moorman, A.F. (2001) Pitx2 expression defines a left cardiac lineage of cells: evidence for atrial and ventricular molecular isomerism in the iv/iv mice. *Dev Biol,* **231,** 252-64.
74. Linask, K.K., Yu, X., Chen, Y. and Han, M.D. (2002) Directionality of heart looping: effects of Pitx2c misexpression on flectin asymmetry and midline structures. *Dev Biol,* **246,** 407-17.
75. McGinnis, W., Garber, R.L., Wirz, J., Kuroiwa, A. and Gehring, W. (1984) A homologous protein-coding sequence in Drosophila homeotic genes and its conservation in other metazoans. *Cell,* **37,** 403-8.
76. Kissinger, C.R., Liu, B.S., Martin-Blanco, E., Kornberg, T.B. and Pabo, C.O. (1990) Crystal structure of an engrailed homeodomain-DNA complex at 2.8 A resolution: a framework for understanding homeodomain-DNA interactions. *Cell,* **63,** 579-90.
77. Billeter, M., Qian, Y.Q., Otting, G., Muller, M., Gehring, W. and Wuthrich, K. (1993) Determination of the nuclear magnetic resonance solution structure of an Antennapedia homeodomain-DNA complex. *J Mol Biol,* **234,** 1084-93.
78. Desplan, C., Theis, J. and O'Farrell, P.H. (1988) The sequence specificity of homeodomain-DNA interaction. *Cell,* **54,** 1081-90.
79. Hoey, T. and Levine, M. (1988) Divergent homeo box proteins recognize similar DNA sequences in Drosophila. *Nature,* **332,** 858-61.
80. Kume, T., Deng, K.Y., Winfrey, V., Gould, D.B., Walter, M.A. and Hogan, B.L. (1998) The forkhead/winged helix gene Mf1 is disrupted in the pleiotropic mouse mutation congenital hydrocephalus. *Cell,* **93,** 985-96.
81. Treisman, J., Gonczy, P., Vashishtha, M., Harris, E. and Desplan, C. (1989) A single amino acid can determine the DNA binding specificity of homeodomain proteins. *Cell,* **59,** 553-62.
82. Wilson, D., Sheng, G., Lecuit, T., Dostatni, N. and Desplan, C. (1993) Cooperative dimerization of paired class homeo domains on DNA. *Genes Dev,* **7,** 2120-34.
83. Wilson, D.S., Guenther, B., Desplan, C. and Kuriyan, J. (1995) High resolution crystal structure of a paired (Pax) class cooperative homeodomain dimer on DNA. *Cell,* **82,** 709-19.
84. Amendt, B.A., Sutherland, L.B., Semina, E.V. and Russo, A.F. (1998) The molecular basis of Rieger syndrome. Analysis of Pitx2 homeodomain protein activities. *J Biol Chem,* **273,** 20066-72.
85. Banerjee-Basu, S. and Baxevanis, A.D. (2001) Molecular evolution of the homeodomain family of transcription factors. *Nucleic Acids Res,* **29,** 3258-69.
86. Semina, E.V., Reiter, R.S. and Murray, J.C. (1997) Isolation of a new homeobox gene belonging to the Pitx/Rieg family: expression during lens development and mapping to the aphakia region on mouse chromosome 19. *Hum Mol Genet,* **6,** 2109-16.

87. Lamonerie, T., Tremblay, J.J., Lanctot, C., Therrien, M., Gauthier, Y. and Drouin, J. (1996) Ptx1, a bicoid-related homeo box transcription factor involved in transcription of the pro-opiomelanocortin gene. *Genes Dev,* **10,** 1284-95.
88. Szeto, D.P., Ryan, A.K., O'Connell, S.M. and Rosenfeld, M.G. (1996) P-OTX: a PIT-1-interacting homeodomain factor expressed during anterior pituitary gland development. *Proc Natl Acad Sci U S A,* **93,** 7706-10.
89. Hanes, S.D. and Brent, R. (1989) DNA specificity of the bicoid activator protein is determined by homeodomain recognition helix residue 9. *Cell,* **57,** 1275-83.
90. Ma, X., Yuan, D., Diepold, K., Scarborough, T. and Ma, J. (1996) The Drosophila morphogenetic protein Bicoid binds DNA cooperatively. *Development,* **122,** 1195-206.
91. Yuan, D., Ma, X. and Ma, J. (1996) Sequences outside the homeodomain of bicoid are required for protein-protein interaction. *J Biol Chem,* **271,** 21660-5.
92. Gibson, G. (2000) Evolution: hox genes and the cellared wine principle. *Curr Biol,* **10,** R452-5.
93. Stauber, M., Jackle, H. and Schmidt-Ott, U. (1999) The anterior determinant bicoid of Drosophila is a derived Hox class 3 gene. *Proc Natl Acad Sci U S A,* **96,** 3786-9.
94. Brouwer, A., ten Berge, D., Wiegerinck, R. and Meijlink, F. (2003) The OAR/aristaless domain of the homeodomain protein Cart1 has an attenuating role in vivo. *Mech Dev,* **120,** 241-52.
95. Driever, W. and Nusslein-Volhard, C. (1989) The bicoid protein is a positive regulator of hunchback transcription in the early Drosophila embryo. *Nature,* **337,** 138-43.
96. Struhl, G., Struhl, K. and Macdonald, P.M. (1989) The gradient morphogen bicoid is a concentration-dependent transcriptional activator. *Cell,* **57,** 1259-73.
97. Furukawa, T., Kozak, C.A. and Cepko, C.L. (1997) rax, a novel paired-type homeobox gene, shows expression in the anterior neural fold and developing retina. *Proc Natl Acad Sci U S A,* **94,** 3088-93.
98. Galliot, B., de Vargas, C. and Miller, D. (1999) Evolution of homeobox genes: Q50 Paired-like genes founded the Paired class. *Dev Genes Evol,* **209,** 186-97.
99. Beverdam, A. and Meijlink, F. (2001) Expression patterns of group-I aristaless-related genes during craniofacial and limb development. *Mech Dev,* **107,** 163-7.
100. Norris, R.A. and Kern, M.J. (2001) Identification of domains mediating transcription activation, repression, and inhibition in the paired-related homeobox protein, Prx2 (S8). *DNA Cell Biol,* **20,** 89-99.
101. Amendt, B.A., Sutherland, L.B. and Russo, A.F. (1999) Multifunctional role of the Pitx2 homeodomain protein C-terminal tail. *Mol Cell Biol,* **19,** 7001-10.

102. Saadi, I., Kuburas, A., Engle, J.J. and Russo, A.F. (2003) Dominant negative dimerization of a mutant homeodomain protein in Axenfeld-Rieger syndrome. *Mol Cell Biol,* **23,** 1968-82.

103. Saadi, I., Semina, E.V., Amendt, B.A., Harris, D.J., Murphy, K.P., Murray, J.C. and Russo, A.F. (2001) Identification of a dominant negative homeodomain mutation in Rieger syndrome. *J Biol Chem,* **276,** 23034-41.

104. Kozlowski, K. and Walter, M.A. (2000) Variation in residual PITX2 activity underlies the phenotypic spectrum of anterior segment developmental disorders. *Hum Mol Genet,* **9,** 2131-9.

105. Kioussi, C., Briata, P., Baek, S.H., Rose, D.W., Hamblet, N.S., Herman, T., Ohgi, K.A., Lin, C., Gleiberman, A., Wang, J. *et al.* (2002) Identification of a Wnt/Dvl/beta-Catenin --> Pitx2 pathway mediating cell-type-specific proliferation during development. *Cell,* **111,** 673-85.

106. Hedgepeth, C.M., Conrad, L.J., Zhang, J., Huang, H.C., Lee, V.M. and Klein, P.S. (1997) Activation of the Wnt signaling pathway: a molecular mechanism for lithium action. *Dev Biol,* **185,** 82-91.

107. Bach, I., Carriere, C., Ostendorff, H.P., Andersen, B. and Rosenfeld, M.G. (1997) A family of LIM domain-associated cofactors confer transcriptional synergism between LIM and Otx homeodomain proteins. *Genes Dev,* **11,** 1370-80.

108. Hecht, A., Vleminckx, K., Stemmler, M.P., van Roy, F. and Kemler, R. (2000) The p300/CBP acetyltransferases function as transcriptional coactivators of beta-catenin in vertebrates. *Embo J,* **19,** 1839-50.

109. Pierrou, S., Hellqvist, M., Samuelsson, L., Enerback, S. and Carlsson, P. (1994) Cloning and characterization of seven human forkhead proteins: binding site specificity and DNA bending. *Embo J,* **13,** 5002-12.

110. Larsson, C., Hellqvist, M., Pierrou, S., White, I., Enerback, S. and Carlsson, P. (1995) Chromosomal localization of six human forkhead genes, freac-1 (FKHL5), -3 (FKHL7), -4 (FKHL8), -5 (FKHL9), -6 (FKHL10), and -8 (FKHL12). *Genomics,* **30,** 464-9.

111. Nishimura, D.Y., Swiderski, R.E., Alward, W.L., Searby, C.C., Patil, S.R., Bennet, S.R., Kanis, A.B., Gastier, J.M., Stone, E.M. and Sheffield, V.C. (1998) The forkhead transcription factor gene FKHL7 is responsible for glaucoma phenotypes which map to 6p25. *Nat Genet,* **19,** 140-7.

112. Mears, A.J., Jordan, T., Mirzayans, F., Dubois, S., Kume, T., Parlee, M., Ritch, R., Koop, B., Kuo, W.L., Collins, C. *et al.* (1998) Mutations of the forkhead/winged-helix gene, FKHL7, in patients with Axenfeld-Rieger anomaly. *Am J Hum Genet,* **63,** 1316-28.

113. Lehmann, O.J., Ebenezer, N.D., Jordan, T., Fox, M., Ocaka, L., Payne, A., Leroy, B.P., Clark, B.J., Hitchings, R.A., Povey, S. *et al.* (2000) Chromosomal duplication involving the forkhead transcription factor gene FOXC1 causes iris hypoplasia and glaucoma. *Am J Hum Genet,* **67,** 1129-35.

114. Nishimura, D.Y., Searby, C.C., Alward, W.L., Walton, D., Craig, J.E., Mackey, D.A., Kawase, K., Kanis, A.B., Patil, S.R., Stone, E.M. *et al.* (2001) A spectrum of FOXC1 mutations suggests gene dosage as a

mechanism for developmental defects of the anterior chamber of the eye. *Am J Hum Genet,* **68,** 364-72.

115. Lehmann, O.J., Ebenezer, N.D., Ekong, R., Ocaka, L., Mungall, A.J., Fraser, S., McGill, J.I., Hitchings, R.A., Khaw, P.T., Sowden, J.C. *et al.* (2002) Ocular developmental abnormalities and glaucoma associated with interstitial 6p25 duplications and deletions. *Invest Ophthalmol Vis Sci,* **43,** 1843-9.
116. Saleem, R.A., Banerjee-Basu, S., Berry, F.B., Baxevanis, A.D. and Walter, M.A. (2001) Analyses of the effects that disease-causing missense mutations have on the structure and function of the winged-helix protein FOXC1. *Am J Hum Genet,* **68,** 627-41.
117. Saleem, R.A., Murphy, T.C., Liebmann, J.M. and Walter, M.A. (2003) Identification and analysis of a novel mutation in the FOXC1 forkhead domain. *Invest Ophthalmol Vis Sci,* **44,** 4608-12.
118. Saleem, R.A., Banerjee-Basu, S., Berry, F.B., Baxevanis, A.D. and Walter, M.A. (2003) Structural and functional analyses of disease-causing missense mutations in the forkhead domain of FOXC1. *Hum Mol Genet,* **12,** 2993-3005.
119. Murphy, T.C., Saleem, R.A., Footz, T., Ritch, R., McGillivray, B. and Walter, M.A. (2004) The Wing 2 Region of the FOXC1 Forkhead Domain Is Necessary for Normal DNA-Binding and Transactivation Functions (In press). *Invest Ophthalmol Vis Sci,* **45**.
120. Hong, H.K., Lass, J.H. and Chakravarti, A. (1999) Pleiotropic skeletal and ocular phenotypes of the mouse mutation congenital hydrocephalus (ch/Mf1) arise from a winged helix/forkhead transcriptionfactor gene. *Hum Mol Genet,* **8,** 625-37.
121. Smith, R.S., Zabaleta, A., Kume, T., Savinova, O.V., Kidson, S.H., Martin, J.E., Nishimura, D.Y., Alward, W.L., Hogan, B.L. and John, S.W. (2000) Haploinsufficiency of the transcription factors FOXC1 and FOXC2 results in aberrant ocular development. *Hum Mol Genet,* **9,** 1021-32.
122. Clark, K.L., Halay, E.D., Lai, E. and Burley, S.K. (1993) Co-crystal structure of the HNF-3/fork head DNA-recognition motif resembles histone H5. *Nature,* **364,** 412-20.
123. Berry, F.B., Saleem, R.A. and Walter, M.A. (2002) FOXC1 transcriptional regulation is mediated by N- and C-terminal activation domains and contains a phosphorylated transcriptional inhibitory domain. *J Biol Chem,* **277,** 10292-7.
124. Mirzayans, F., Berry, F.B., Saleem, R.A. and Walter, M.A. (2003) Negative regulation of FOXC1 activity by the p44/42 MAP kinase pathway. *American Society for Human Genetics.* Los Angeles, Vol. 73 (Suppl.), p. S988.
125. Doward, W., Perveen, R., Lloyd, I.C., Ridgway, A.E., Wilson, L. and Black, G.C. (1999) A mutation in the RIEG1 gene associated with Peters' anomaly. *J Med Genet,* **36,** 152-5.
126. Perveen, R., Lloyd, I.C., Clayton-Smith, J., Churchill, A., van Heyningen, V., Hanson, I., Taylor, D., McKeown, C., Super, M., Kerr, B. *et al.* (2000)

Phenotypic variability and asymmetry of Rieger syndrome associated with PITX2 mutations. *Invest Ophthalmol Vis Sci,* **41,** 2456-60.

127. Priston, M., Kozlowski, K., Gill, D., Letwin, K., Buys, Y., Levin, A.V., Walter, M.A. and Heon, E. (2001) Functional analyses of two newly identified PITX2 mutants reveal a novel molecular mechanism for Axenfeld-Rieger syndrome. *Hum Mol Genet,* **10,** 1631-8.
128. Phillips, J.C. (2002) Four novel mutations in the PITX2 gene in patients with Axenfeld-Rieger syndrome. *Ophthalmic Res,* **34,** 324-6.
129. Borges, A.S., Susanna, R., Jr., Carani, J.C., Betinjane, A.J., Alward, W.L., Stone, E.M., Sheffield, V.C. and Nishimura, D.Y. (2002) Genetic analysis of PITX2 and FOXC1 in Rieger Syndrome patients from Brazil. *J Glaucoma,* **11,** 51-6.
130. Idrees, F., Fraser, S., Brice, G., Childs, A., Khaw, P.T., Willis, K. and Sowden, J.C. (2002) Identification of PITX2 mutations in Axenfeld-Rieger syndrome patients. *Association for Research in Vision and Ophthalmology*. Fort Lauderdale, USA, p. Poster 3402.
131. Richards, J., Brooks, B., Othman, M., Semina, E. and Moroi, S. (2001) A novel mutation in the PITX2 gene causes Rieger syndrome. *Invest Ophthalmol Vis Sci,* **42,** S566.
132. Wang, Y., Zhao, H., Zhang, X. and Feng, H. (2003) Novel Identification of a Four-base-pair Deletion Mutation in PITX2 in a Rieger Syndrome Family. *J Dent Res,* **82,** 1008-12.
133. Lines, M.A., Kozlowski, K., Kulak, S.C., Allingham, R.R., Heon, E., Ritch, R., Levin, A.V., Shields, M.B., Damji, K.F., Newlin, A. *et al.* (2004) Characterization and prevalence of PITX2 microdeletions and mutations in Axenfeld-Rieger malformations. *Invest Ophthalmol Vis Sci,* **45,** 828-33.
134. Kulharya, A.S., Maberry, M., Kukolich, M.K., Day, D.W., Schneider, N.R., Wilson, G.N. and Tonk, V. (1995) Interstitial deletions 4q21.1q25 and 4q25q27: phenotypic variability and relation to Rieger anomaly. *Am J Med Genet,* **55,** 165-70.
135. Makita, Y., Masuno, M., Imaizumi, K., Yamashita, S., Ohba, S., Ito, D. and Kuroki, Y. (1995) Rieger syndrome with de novo reciprocal translocation t(1;4) (q23.1;q25). *Am J Med Genet,* **57,** 19-21.
136. Flomen, R.H., Gorman, P.A., Vatcheva, R., Groet, J., Barisic, I., Ligutic, I., Sheer, D. and Nizetic, D. (1997) Rieger syndrome locus: a new reciprocal translocation t(4;12)(q25;q15) and a deletion del(4)(q25q27) both break between markers D4S2945 and D4S193. *J Med Genet,* **34,** 191-5.
137. Schinzel, A., Brecevic, L., Dutly, F., Baumer, A., Binkert, F. and Largo, R.H. (1997) Multiple congenital anomalies including the Rieger eye malformation in a boy with interstitial deletion of (4) (q25-->q27) secondary to a balanced insertion in his normal father: evidence for haplotype insufficiency causing the Rieger malformation. *J Med Genet,* **34,** 1012-4.
138. Flomen, R.H., Vatcheva, R., Gorman, P.A., Baptista, P.R., Groet, J., Barisic, I., Ligutic, I. and Nizetic, D. (1998) Construction and analysis of a sequence-ready map in 4q25: Rieger syndrome can be caused by

haploinsufficiency of RIEG, but also by chromosome breaks approximately 90 kb upstream of this gene. *Genomics,* **47,** 409-13.

139. Velinov, M., Gu, H., Yeboa, K., Warburton, D., Tubo, T., Dhuper, S., Lanter, S., Delprino, D., Kupchik, G. and Jenkins, E.C. (2002) Hypoplastic left heart in a female infant with partial trisomy 4q due to de novo 4;21 translocation. *Am J Med Genet,* **107,** 330-3.
140. Liu, C., Liu, W., Palie, J., Lu, M.F., Brown, N.A. and Martin, J.F. (2002) Pitx2c patterns anterior myocardium and aortic arch vessels and is required for local cell movement into atrioventricular cushions. *Development,* **129,** 5081-91.
141. Riise, R., Storhaug, K. and Brondum-Nielsen, K. (2001) Rieger syndrome is associated with PAX6 deletion. *Acta Ophthalmol Scand,* **79,** 201-3.
142. Jordan, T., Hanson, I., Zaletayev, D., Hodgson, S., Prosser, J., Seawright, A., Hastie, N. and van Heyningen, V. (1992) The human PAX6 gene is mutated in two patients with aniridia. *Nat Genet,* **1,** 328-32.
143. Hanson, I.M., Fletcher, J.M., Jordan, T., Brown, A., Taylor, D., Adams, R.J., Punnett, H.H. and van Heyningen, V. (1994) Mutations at the PAX6 locus are found in heterogeneous anterior segment malformations including Peters' anomaly. *Nat Genet,* **6,** 168-73.
144. Mirzayans, F., Pearce, W.G., MacDonald, I.M. and Walter, M.A. (1995) Mutation of the PAX6 gene in patients with autosomal dominant keratitis. *Am J Hum Genet,* **57,** 539-48.
145. Birney, E., Andrews, D., Bevan, P., Caccamo, M., Cameron, G., Chen, Y., Clarke, L., Coates, G., Cox, T., Cuff, J. *et al.* (2004) Ensembl 2004. *Nucleic Acids Res,* **32 Database issue,** D468-70.
146. Ligutic, I., Brecevic, L., Petkovic, I., Kalogjera, T. and Rajic, Z. (1981) Interstitial deletion 4q and Rieger syndrome. *Clin Genet,* **20,** 323-7.
147. Shields, M.B., Buckley, E., Klintworth, G.K. and Thresher, R. (1985) Axenfeld-Rieger syndrome. A spectrum of developmental disorders. *Surv Ophthalmol,* **29,** 387-409.
148. (1996) Using the Bradford Method to Determine Protein Concentration. In Ausubel, F., Brent, R., Kingston, R., Moore, D., Seidman, J., Smith, J. and Struhl, K. (eds.), *Current Protocols in Molecular Biology.* John Wiley and Sons, Vol. 2, p. 10.1.4.
149. (1996) Denaturing (SDS) Discontinuous Gel Electrophoresis: Laemmli Gel Method. In Ausubel, F., Brent, R., Kingston, R., Moore, D., Seidman, J., Smith, J. and Struhl, K. (eds.), *Current Protocols in Molecular Biology.* John Wiley and Sons, Vol. 1, p. 10.2.4.
150. Filesi, I., Cardinale, A., van der Sar, S., Cowell, I.G., Singh, P.B. and Biocca, S. (2002) Loss of heterochromatin protein 1 (HP1) chromodomain function in mammalian cells by intracellular antibodies causes cell death. *J Cell Sci,* **115,** 1803-13.
151. Nishioka, K., Rice, J.C., Sarma, K., Erdjument-Bromage, H., Werner, J., Wang, Y., Chuikov, S., Valenzuela, P., Tempst, P., Steward, R. *et al.* (2002) PR-Set7 is a nucleosome-specific methyltransferase that modifies

lysine 20 of histone H4 and is associated with silent chromatin. *Mol Cell,* **9,** 1201-13.

152. Sarg, B., Koutzamani, E., Helliger, W., Rundquist, I. and Lindner, H.H. (2002) Postsynthetic Trimethylation of Histone H4 at Lysine 20 in Mammalian Tissues Is Associated with Aging. *J. Biol. Chem.,* **277,** 39195-39201.
153. Caceres, J.F., Misteli, T., Screaton, G.R., Spector, D.L. and Krainer, A.R. (1997) Role of the Modular Domains of SR Proteins in Subnuclear Localization and Alternative Splicing Specificity. *J. Cell Biol.,* **138,** 225-238.
154. Johnson, C., Primorac, D., McKinstry, M., McNeil, J., Rowe, D. and Lawrence, J.B. (2000) Tracking COL1A1 RNA in Osteogenesis Imperfecta: Splice-defective Transcripts Initiate Transport from the Gene but Are Retained within the SC35 Domain. *J. Cell Biol.,* **150,** 417-432.
155. Shopland, L.S., Johnson, C.V., Byron, M., McNeil, J. and Lawrence, J.B. (2003) Clustering of multiple specific genes and gene-rich R-bands around SC-35 domains: evidence for local euchromatic neighborhoods. *J. Cell Biol.,* **162,** 981-990.
156. Fu, X.D. and Maniatis, T. (1990) Factor required for mammalian spliceosome assembly is localized to discrete regions in the nucleus. *Nature,* **343,** 437-41.
157. Wei, X., Somanathan, S., Samarabandu, J. and Berezney, R. (1999) Three-dimensional visualization of transcription sites and their association with splicing factor-rich nuclear speckles. *J Cell Biol,* **146,** 543-58.
158. McManus, K.J. and Hendzel, M.J. (2003) Quantitative analysis of CBP- and P300-induced histone acetylations in vivo using native chromatin. *Mol Cell Biol,* **23,** 7611-27.
159. Behrens, J., von Kries, J.P., Kuhl, M., Bruhn, L., Wedlich, D., Grosschedl, R. and Birchmeier, W. (1996) Functional interaction of beta-catenin with the transcription factor LEF-1. *Nature,* **382,** 638-42.
160. Enwright, J.F., III, Kawecki-Crook, M.A., Voss, T.C., Schaufele, F. and Day, R.N. (2003) A PIT-1 Homeodomain Mutant Blocks the Intranuclear Recruitment Of the CCAAT/Enhancer Binding Protein {alpha} Required for Prolactin Gene Transcription. *Mol Endocrinol,* **17,** 209-222.
161. Enwright, J.F., 3rd, Kawecki-Crook, M.A., Voss, T.C., Schaufele, F. and Day, R.N. (2003) A PIT-1 homeodomain mutant blocks the intranuclear recruitment of the CCAAT/enhancer binding protein alpha required for prolactin gene transcription. *Mol Endocrinol,* **17,** 209-22.
162. Pelton, R.W., Saxena, B., Jones, M., Moses, H.L. and Gold, L.I. (1991) Immunohistochemical localization of TGF beta 1, TGF beta 2, and TGF beta 3 in the mouse embryo: expression patterns suggest multiple roles during embryonic development. *J Cell Biol,* **115,** 1091-105.
163. Flugel-Koch, C., Ohlmann, A., Piatigorsky, J. and Tamm, E.R. (2002) Disruption of anterior segment development by TGF-beta1 overexpression in the eyes of transgenic mice. *Dev Dyn,* **225,** 111-25.

164. Testaz, S., Delannet, M. and Duband, J. (1999) Adhesion and migration of avian neural crest cells on fibronectin require the cooperating activities of multiple integrins of the (beta)1 and (beta)3 families. *J Cell Sci,* **112 (Pt 24),** 4715-28.
165. Tucker, R.P., Hagios, C., Chiquet-Ehrismann, R., Lawler, J., Hall, R.J. and Erickson, C.A. (1999) Thrombospondin-1 and neural crest cell migration. *Dev Dyn,* **214,** 312-22.
166. Perris, R. and Perissinotto, D. (2000) Role of the extracellular matrix during neural crest cell migration. *Mech Dev,* **95,** 3-21.
167. Zhou, Y., Kato, H., Asanoma, K., Kondo, H., Arima, T., Kato, K., Matsuda, T. and Wake, N. (2002) Identification of FOXC1 as a TGF-beta1 responsive gene and its involvement in negative regulation of cell growth. *Genomics,* **80,** 465-72.
168. Thaung, C., West, K., Clark, B.J., McKie, L., Morgan, J.E., Arnold, K., Nolan, P.M., Peters, J., Hunter, A.J., Brown, S.D. *et al.* (2002) Novel ENU-induced eye mutations in the mouse: models for human eye disease. *Hum Mol Genet,* **11,** 755-67.
169. Reneker, L.W., Silversides, D.W., Patel, K. and Overbeek, P.A. (1995) TGF alpha can act as a chemoattractant to perioptic mesenchymal cells in developing mouse eyes. *Development,* **121,** 1669-80.
170. Luetteke, N.C., Qiu, T.H., Peiffer, R.L., Oliver, P., Smithies, O. and Lee, D.C. (1993) TGF alpha deficiency results in hair follicle and eye abnormalities in targeted and waved-1 mice. *Cell,* **73,** 263-78.
171. Mann, G.B., Fowler, K.J., Gabriel, A., Nice, E.C., Williams, R.L. and Dunn, A.R. (1993) Mice with a null mutation of the TGF alpha gene have abnormal skin architecture, wavy hair, and curly whiskers and often develop corneal inflammation. *Cell,* **73,** 249-61.
172. Nelson, W.J. and Nusse, R. (2004) Convergence of Wnt, beta-catenin, and cadherin pathways. *Science,* **303,** 1483-7.
173. Noria, S., Cowan, D.B., Gotlieb, A.I. and Langille, B.L. (1999) Transient and steady-state effects of shear stress on endothelial cell adherens junctions. *Circ Res,* **85,** 504-14.
174. Wei, Q. and Adelstein, R.S. (2002) Pitx2a expression alters actin-myosin cytoskeleton and migration of HeLa cells through Rho GTPase signaling. *Mol Biol Cell,* **13,** 683-97.
175. Maekawa, M., Ishizaki, T., Boku, S., Watanabe, N., Fujita, A., Iwamatsu, A., Obinata, T., Ohashi, K., Mizuno, K. and Narumiya, S. (1999) Signaling from Rho to the actin cytoskeleton through protein kinases ROCK and LIM-kinase. *Science,* **285,** 895-8.
176. Vittitow, J.L., Garg, R., Rowlette, L.L., Epstein, D.L., O'Brien, E.T. and Borras, T. (2002) Gene transfer of dominant-negative RhoA increases outflow facility in perfused human anterior segment cultures. *Mol Vis,* **8,** 32-44.
177. Nakamura, Y., Hirano, S., Suzuki, K., Seki, K., Sagara, T. and Nishida, T. (2002) Signaling Mechanism of TGF-{beta}1-Induced Collagen

Contraction Mediated by Bovine Trabecular Meshwork Cells. *Invest. Ophthalmol. Vis. Sci.,* **43,** 3465-3472.

178. Rubenstein, N.M., Guan, Y., Woo, P.L. and Firestone, G.L. (2003) Glucocorticoid down-regulation of RhoA is required for the steroid-induced organization of the junctional complex and tight junction formation in rat mammary epithelial tumor cells. *J Biol Chem,* **278,** 10353-60.
179. Kawamura, S., Miyamoto, S. and Brown, J.H. (2003) Initiation and transduction of stretch-induced RhoA and Rac1 activation through caveolae: cytoskeletal regulation of ERK translocation. *J Biol Chem,* **278,** 31111-7.
180. Takahashi, K., Suzuki, K. and Tsukatani, Y. (1997) Induction of tyrosine phosphorylation and association of beta-catenin with EGF receptor upon tryptic digestion of quiescent cells at confluence. *Oncogene,* **15,** 71-8.
181. Esser, S., Lampugnani, M.G., Corada, M., Dejana, E. and Risau, W. (1998) Vascular endothelial growth factor induces VE-cadherin tyrosine phosphorylation in endothelial cells. *J Cell Sci,* **111 (Pt 13),** 1853-65.
182. Weinmann, A.S., Yan, P.S., Oberley, M.J., Huang, T.H. and Farnham, P.J. (2002) Isolating human transcription factor targets by coupling chromatin immunoprecipitation and CpG island microarray analysis. *Genes Dev,* **16,** 235-44.

Appendix A: Composition of reagents used

Phosphate-buffered saline (PBS)
- 137mM NaCl
- 2.7mM KCl
- 10mM Na_2HPO_4
- 1.7mM KH_2PO_4
- Adjust to pH 6.8 (or otherwise indicated pH)

PBS with protease inhibitors (PBS-PI)
- 1x PBS as per above
- 1% (v/v) 1M phenylmethylsulphonyl fluoride; solution in 2-propanol
- 0.5% (v/v) Mammalian Protease Inhibitor Cocktail [Sigma]

Radioimmunoprotection assay buffer (RIPA)
- 1x PBS, pH 7.4
- 1% (v/v) IGEPAL CA-630
- 0.5% (w/v) sodium deoxycholate
- 0.1% (w/v) sodium dodecyl sulphate

RIPA-PI
- 1x RIPA as per above
- 1% (v/v) 1M phenylmethylsulphonyl fluoride; solution in isopropanol
- 0.5% (v/v) Mammalian Protease Inhibitor Cocktail [Sigma]

2x SDS-PAGE loading buffer
- 17.5% (v/v) glycerol
- 8.7% (v/v) 2-mercaptoethanol
- 5.2% (w/v) sodium dodecyl sulphate
- 220mM Tris pH 6.8
- 0.35g/L bromophenol blue

Immunoblot transfer buffer
- 29% (v/v) methanol
- 275mM glycine
- 36mM Tris base
- 0.07% (w/v) sodium dodecyl sulphate
- no pH adjustment required

Tris-buffered saline (TBS)
- 10mM Tris pH 6.8
- 150mM NaCl

Tris-buffered saline, tween (TBST)
- 1x TBS
- 0.05% (v/v) Tween-20

Appendix B: Peptide sequence expressed by pCI-HA-PITX2a

1 - ***MASSYPYDVP DYASLGGPSE FPGIQQLSPG SRYRG***METNC RKLVSACVQL
EKDKSQQGKN EDVGAEDPSK KKRQRRQRTH FTSQQLQELE ATFQRNRYPD
MSTREEIAVW TNLTEARVRV WFKNRRAKWR KRERNQQAEL CKNGFGPQFN
GLMQPYDDMY PGYSYNNWAA KGLTSASLST KSFPFFNSMN VNPLSSQSMF
SPPNSISSMS MSSSMVPSAV TGVPGSSLNS LNNLNNLSSP SLNSAVPTPA
CPYAPPTPPY VYRDTCNSSL ASLRLKAKQH SSFGYASVQK PASNLSACQY
AVDRPV - 306aa

The sequence of wild-type PITX2a is shown in unstyled type.
Sequences shown in bolded italics are N-terminal additions encoded by the vector.
Underlined sequences represent the influenza A virus haemagglutinin epitope (HA) tag.

Appendix C: Antibody information and suppliers

Primary antibody	Supplier and product number
mouse IgG$_1$ monoclonal α-Xpress	Invitrogen; R910-25
rabbit α-HA	Santa Cruz Biotechnology; sc-805
mouse monoclonal α-HP1α	Upstate Biotechnology; 05-0689
rabbit polyclonal α-Me$_3$K20H4	Abcam; ab6301
mouse monoclonal α-SC35	Developmental Studies Hybridoma Bank
mouse monoclonal α-p300	Abcam; ab3164

Secondary antibody	Supplier and product number
HRP goat α-mouse IgG	Jackson ImmunoResearch, 115-035-003
HRP goat α-rabbit IgG	Jackson ImmunoResearch, 111-035-003
AMCA donkey α-rabbit IgG	Jackson ImmunoResearch, 711-155-152
Cy2 donkey α-rabbit IgG	Jackson ImmunoResearch, 711-225-152
Cy2 donkey α-mouse IgG	Jackson ImmunoResearch, 715-225-150
Cy3 goat α-mouse IgG	

Appendix D: Explanation of 65kDa PITX2a immunoblot species

When size-separated via reducing SDS-PAGE, a small fraction of recombinant 6xHisXpress-PITX2 is detected at an apparent mass of approximately 65kDa, although the majority of signal runs at the expected 32.5kDa (see figure 2-1, for instance). We were initially concerned that the 65kDa species represented either a post-translationally modified form of PITX2a, or an anomalous run-on translation product specific to our pcDNA expression construct. However, this same 65kDa band is reproducibly observed in lysates containing HA-tagged PITX2a in pCI (Figure 2-1), as well as lysates of bacterially expressed, T7-tagged PITX2a (Michael Sharp, personal communication). In one published report, in-vitro transcribed and translated PITX2a is also observed as a 65kDa dimer (figure 2d of reference 1 below). Furthermore, a 65kDa construct consisting of PITX2a fused to an exogenous progesterone receptor ligand binding domain is also expressed in cos as both 65kDa and ~130kDa immunoreactive bands, consistent with dimerisation of this larger protein (Tim Footz, personal communication). These unexpected PITX2a species likely represent a minority of PITX2a protein remaining undissociated after sodium dodecyl sulfate (SDS) denaturation, as a consequence of expressing relatively high amounts of the recombinant proteins in cos cells. Similarly SDS-resistant, noncovalent interactions have been reported for a handful of high-avidity complexes, including serine protease / serpin heterodimers and homodimers of inducible nitric oxide synthase (2-4).

1. Saadi, I., Semina, E.V., Amendt, B.A., Harris, D.J., Murphy, K.P., Murray, J.C. and Russo, A.F. (2001) Identification of a dominant negative homeodomain mutation in Rieger syndrome. *J Biol Chem*, **276**, 23034-41.
2. Dahlen, J.R., Jean, F., Thomas, G., Foster, D.C. and Kisiel, W. (1998) Inhibition of soluble recombinant furin by human proteinase inhibitor 8. *J Biol Chem*, **273**, 1851-4.
3. Quan, L.T., Caputo, A., Bleackley, R.C., Pickup, D.J. and Salvesen, G.S. (1995) Granzyme B is inhibited by the cowpox virus serpin cytokine response modifier A. *J Biol Chem*, **270**, 10377-9.
4. Kolodziejski, P.J., Rashid, M.B. and Eissa, N.T. (2003) Intracellular formation of "undisruptable" dimers of inducible nitric oxide synthase. *Proc Natl Acad Sci U S A*, **100**, 14263-8.

Appendix E: Expression of *FOXC1* in human TM cell line total RNA

A 500bp fragment representing the 3' end of the human *FOXC1* coding region was PCR-amplified with the primers FOXC1-16F (5'CAAGCCATGAGCCTGTACG) and FOXC1-BEP (5'GGTTCGATTTAGTTCGGCT) in the presence of 25μCi α^{32}P-dCTP. This probe was used to probe an RNA blot of human trabecular meshwork cell line (HTM) RNA samples (provided by Dr. John Polanski), as well as a control lane containing porcine lymphoblast RNA. Both dexamethasone-treated and untreated HTM RNA samples were analysed to test for corticosteroid induction of *FOXC1*. The expected 4kb *FOXC1* transcript was found to be highly expressed in HTM cells in a steroid-independent fashion.

Conditions: Formaldehyde gel electrophoresis and transfer were performed as directed in (1). Blot was prehybridized in ExpressHyb (BD Biosciences) at 50°C for 90 minutes, after which it was hybridized to probe (17Mcpm in total) in 10mL ExpressHyb overnight at 50°C in a rotating bottle incubator. The probed blot was washed thrice in room-temperature 2xSSC solution containing 0.05% (w/v) SDS, for five minutes, followed by thrice in 60°C 0.2xSSC solution containing 0.1% (w/v) SDS. X-ray film was exposed to the blot for two days at room temperature.

1. (1996) Analysis of RNA by Northern and Slot-Blot Hybridization. In Ausubel, F., Brent, R., Kingston, R., Moore, D., Seidman, J., Smith, J. and Struhl, K. (eds.), *Current Protocols in Molecular Biology*. John Wiley and Sons, Vol. 1, p. 4.9.1.

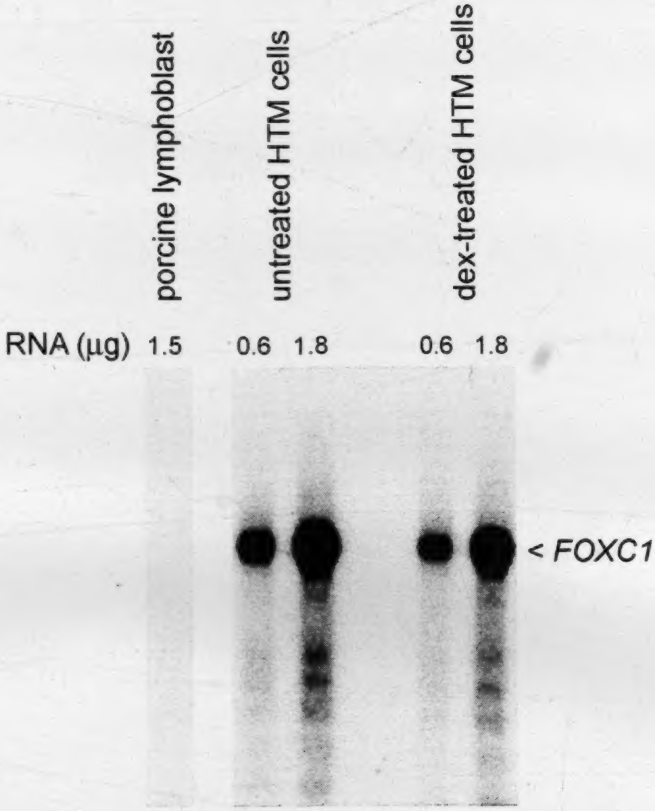
porcine lymphoblast
untreated HTM cells
dex-treated HTM cells
RNA (µg)
1.5
0.6
1.8
0.6
1.8
< FOXC1